Acoustic Resonance in Plate Evaporators

P. S. Hrnjak, N. R. Miller and E. Rodarte

ACRC CR-10 December 1997

For additional information:

Air Conditioning and Refrigeration Center
University of Illinois
Mechanical & Industrial Engineering Dept.
1206 West Green Street
Urbana, IL 61801

(217) 333-3115

The Air Conditioning and Refrigeration Center was founded in 1988 with a grant from the estate of Richard W. Kritzer, the founder of Peerless of America Inc. A State of Illinois Technology Challenge Grant helped build the laboratory facilities. The ACRC receives continuing support from the Richard W. Kritzer Endowment and the National Science Foundation. The following organizations have also become sponsors of the Center.

Amana Refrigeration, Inc.
Brazeway, Inc.
Carrier Corporation
Caterpillar, Inc.
Copeland Corporation
Dayton Thermal Products
Delphi Harrison Thermal Systems
Eaton Corporation
Ford Motor Company
Frigidaire Company
General Electric Company
Hydro Aluminum Adrian, Inc.
Indiana Tube Corporation
Lennox International, Inc.
Modine Manufacturing Co.
Peerless of America, Inc.
Redwood Microsystems, Inc.
The Trane Company
Whirlpool Corporation
York International, Inc.

For additional information:

Air Conditioning & Refrigeration Center
Mechanical & Industrial Engineering Dept.
University of Illinois
1206 West Green Street
Urbana IL 61801

217 333 3115

CONTENTS

CONTENTS (Continued).

0 EXECUTIVE SUMMARY

This report covers the results of work done under the purchase order number JPYAL02332-A (requisition number PYZ 1021300 D965) between Chrysler Corporation and the University of Illinois, dated 30 May, 1996 entitled, "Acoustic Resonance in Plate Evaporators". The purpose of this work was to investigate one possible source of a whistle observed during the start up phase of mobile air conditioners. It was hypothesized that the whistle might be due to flow induced noise. This phenomena has been observed in large tube bank heat exchangers used in the power generation industry.

In accord with the terms of the above mentioned purchase order, tests were conducted on more than six types of heat exchanger plates. Tests were also conducted on a specially modified plate containing a wire baffle. The range of pressures and flow rates were in accord with the statement of work.

In our laboratory tests, every evaporator plate geometry could be made to whistle under certain conditions. The conditions needed to support whistling include, single phase (vapor) flow and a critical range of flow velocities. The velocity at which whistling begins for each plate geometry is presented in this report.

Our results strongly support the flow induced noise hypothesis. This hypothesis states that resonance (whistling) occurs when the frequency of periodic flow instabilities (often vortex shedding) corresponds to a transverse acoustic natural frequency of the plate cavity. Once the excitation frequency matches the natural frequency the two periodic processes lock and the resonance is maintained over a wide range of flow velocities above the initial lockin velocity. Our results show a locked resonance over a considerable range of fluid (gas) flow rates for tests with both R134A and nitrogen. Further, the ratio of resonance frequencies for tests with R134A and nitrogen are related by the speeds of sound in the two fluids. Finally, our results showing the resonance frequency as a function of flow velocity bear a strong similarity to data reported for tube bank heat exchangers and other systems known to sustain flow induced resonance.

Investigators studying the phenomena in tube bank heat exchangers have discovered that the flow instabilities are a very complex and, as yet, poorly understood function of the obstruction shape, dimensions, transverse and longitudinal obstruction pitch, and packing arrangement (staggered or inline). In the case of heat exchanger plates, an added complication is the narrow thickness of the cavity and the potential for three dimensional flow over certain obstructions such as sausages. As a result, we are unable to drawn general conclusions in regard to the role of flow obstruction geometry on flow instability frequency.

In contrast, in general, we can predict the frequency of plate heat exchanger resonance. The resonance is simply the transverse acoustic natural frequency of the cavity computed using the speed of sound of the fluid corrected for the slowing effect of the flow obstructions. The literature shows similar good results for resonance prediction for tube bank heat exchangers.

As stated above, our results indicate that the phenomena only occurs under conditions of single phase vapor refrigerant flow through some portion of the evaporator. Such a refrigerant state in the evaporator normally only exists during system startup under hot or humid conditions. While we believe that the flow velocities used in our test may exist in the field, data to support the belief is not available to us.

The scope of the present project did not permit us to formulate more than a set of qualitative design guidelines for plate heat exchangers. In particular, we are unable to provide guidance on the design of the flow obstructions (dimples, hot dogs, sausages) beyond our observations for the plates tested. We can make recommendations on the geometry of the plate cavity. Our data points to the importance of avoiding cavities with parallel walls across the longer dimension in the longitudinal direction. Several alternative geometries are discussed in the report. We strongly feel that modification of cavity shape is the best approach to avoid whistling and that the modified geometry can furthermore yield heat transfer benefits. In order to provide quantitative design rules, more work must be done to further understand the role of flow obstruction geometry, cavity shape, and field operating conditions.

1 INTRODUCTION AND SUMMARY.

According to Chrysler's engineers [3], an evaporator whistle problem exists in the field during air conditioning system start up on hot and humid days. Many possible sources for this sound have been explored by Chrysler. After a discussion of the problem with faculty members at the Air Conditioning and Refrigeration Center at the University of Illinois, flow induced noise was suggested as a possible mechanism for the whistle. Preliminary calculations, (McDonough [5]), indicated that this is a plausible theory.

Flow induced noise in rectangular and cylindrical shell tube type heat exchangers due to acoustic resonance was documented as early as 1954 (Baird, Putman [1,2]). The common mechanism of flow induced noise in heat exchangers is due to a periodic flow instability in the wake of rigid cylinders inside the shell of the heat exchanger. When the shedding frequency of the flow instability formed in the wake of the flow behind the individual tubes happens to be near the natural frequency of the gas column perpendicular to the flow and the tube axis, a strong transverse acoustic oscillation of the gas column will be excited, Chen [6]. A similar mechanism is believed to occur in the plate evaporators studied in this investigation with the differences being the effects of the characteristic geometry in the formation of vortices and in the acoustic properties of the plate cavity. There is a lot of controversy regarding the different possible sources of the excitation in the heat exchanger acoustic resonance phenomena [13,15,17,18], this is in part complicated by the geometric characteristics which play a very important role in the type and form of possible periodic fluid instabilities, this is evidenced by the fact that even for simple geometries tested under laboratory conditions a clearly explained and understood mechanisms has not been established.

To the authors' knowledge, there have not been reports of flow induced noise problems in plate heat exchangers. Automotive air conditioning plate evaporators normally operate in the air/vaporizing liquid (two phase refrigerant) regime. In these heat exchangers, a phase change occurs on the refrigerant side, and in extreme cases even gas-gas operation can occur. It was theorized that flow induced noise could develop when gaseous refrigerant flows through the heat exchanger plates under certain operating conditions and for certain types of plate geometry.

This study was undertaken to confirm that flow induced noise can be produced in plate evaporators, to obtain a further understanding of the problem, to explore a wider range of evaporator geometries (plate types AS/PL, LH, JA, NSF 1, NSF 2, and NSF 3) in controlled refrigerant flow conditions, and finally to draw some conclusions useful to designers of automotive plate type evaporators.

As specified in the original proposal, the range of operating parameters to be studied were:

- Five flow rates.
- A pressure of 3.5 ± 0.7 bar (at the outlet).
- Refrigerant R134a.
- Superheated vapor (at about 20 ° C) at the inlet.

It was proposed that acceleration data be taken at least in three characteristic positions except for one set of more detailed experiments designed to verify trends registered in the DTP laboratory using air.

This report will:

- Describe the results of a set of tests which are significantly broader than those originally proposed.
- Support the hypotheses that evaporator whistling is caused by resonance induced by periodic flow fluctuations.
- Specify guidelines for designers to avoid the problem with recommendations for further study.

The range of test flow rates and refrigerant inlet states were not initially known. That is, data as to realistic inlet conditions were not available. Preliminary tests were carried out at a range of inlet conditions. It was discovered that significant evaporator whistle only occurs when single phase vapor exists somewhere in the evaporator plate and the flow rate is within a certain range. Approximate calculations indicate that these flow rates may exist in practice.

Tests using refrigerant in all plate geometries were carried out at more than three locations. Some data were taken with 1.5 plate evaporators (JA, LH, and AS/PL), 1.5 plate evaporators are evaporators in which a complete section plus half a section with an end plate are used. At the time these tests were carried out, we were not aware that there was flow through the half plate. As it turned out, this mistake was fortuitous since these tests clearly demonstrate the influence of a wire baffle on the shape of the acceleration spectrum (see section 8). All tests were rerun with the half plate closed in order to create a baseline for conclusions.

Additional tests were performed for these geometries:

- AS/PL modified.
- Two additional JA samples.
- One additional LH sample.

The AS/PL geometry was used to investigate the feasibility of baffling. Michael McDonough provided a modified AS/PL plate with a cylindrical steel wire inserted between the second and the third arrays of "hot dog" dimples.

Two additional JA evaporator plates were tested to check manufacturing variability and repeatability of our measurements. An additional LH evaporator plate was tested because the original specimen leaked. The actual tests performed are shown in Figure 6.

Our measurements were also extended to nitrogen flow tests. These tests were undertaken in an effort to develop a simpler and less costly measurement technique. Tests on the same plate samples were carried out using both R134a and nitrogen. All evaporator geometries were tested with nitrogen.

TABLE 1

TEST CODES AND FLOW RATES OF REFRIGERANT FOR THE DIFFERENT EVAPORATORS

Plate Type	Test Code	Flow Rates g/s R134a
AS/PL	A	14-25
LH	C	24-29
JA	D	17-29
NSF-1 Large Dimples	G	16-30
NSF-2 Large Sausages	E	15-29
NSF-3 Small Dimples	F	16-30

Even though refrigerant tests are more realistic and generate more powerful signals, nitrogen tests have the advantage of continuous and much simpler control of inlet pressure and flow rate for the fixed atmospheric exit pressure. In the end, nitrogen tests proved to be a better way to identify the flow velocity (and the resulting resonant frequency) at which the locking of the frequency of the flow periodicity with the first cavity natural frequency occurs.

Based on this study we have concluded:

1) The whistling phenomena only occurs when a threshold velocity is exceeded in a region of single phase vapor flow in an evaporator plate.

2) The results support the flow induced noise hypothesis.

3) Flow obstruction geometry is an important contribution to the phenomena. Our tests of a limited assortment of geometries do not permit us to draw general conclusions on how obstruction geometry affects the whistle phenomena.

4) The cavity geometry affects the whistle frequency in a predictable way. We feel strongly that details of cavity wall shape can greatly influence the likelihood of field whistle problems.

2 EXPERIMENTAL APPARATUS

Most evaporator testing was done using a single evaporator plate. The fluid (R-134a or N2) flowing inside the plates was controlled. This was done in order to duplicate, under steady state operation, conditions which exist only briefly in the field during air conditioning system startup. The measured variable was surface acceleration at different positions on the plate evaporator, plus all the relevant fluid information. Surface vibration is, of course, the generator of air radiated sound.

2-1 DESCRIPTION OF REFRIGERANT TEST SETUP

The main objective of the test loop is to maintain the desired state (pressure, temperature e.g. superheat or quality) at the inlet of the plate evaporator under testing. The continuous - flow system is designed using a diaphragm pump and two receivers: high pressure (H.P.) and low pressure (L.P.). The experimental setup is shown in (Figure 1.).

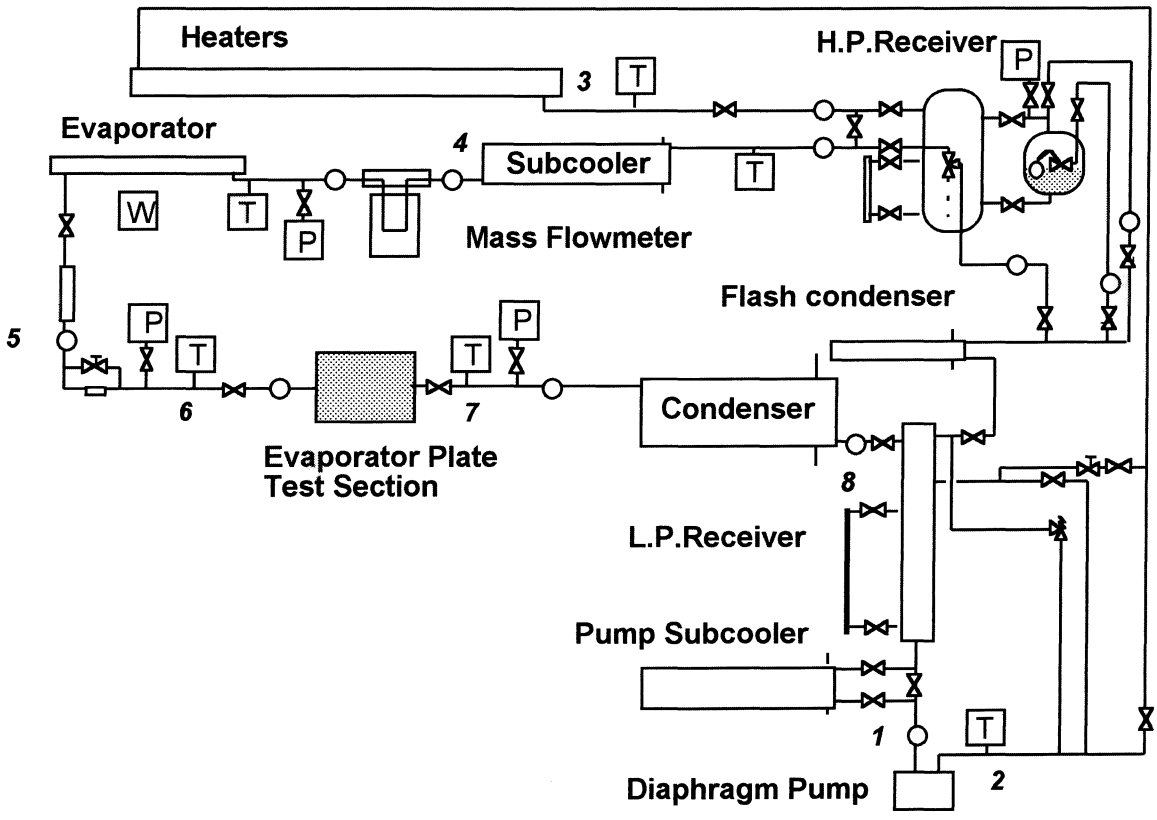

Figure 1. Refrigerant experimental setup - simplified.

Using a pump instead of a compressor ensures more freedom in choosing the refrigerant, the oil, and the oil concentration when needed. The diaphragm pump is found to fit requirements the best: relatively high inlet pressure (A/C and heat pump regime) and relatively low flow rates. The acknowledged possibility of pressure pulsation was minimized by using a high speed rate for the pump, proper setup design, cycle characteristics and installing a pressure absorbing vessel downstream of the pump (H.P. receiver) for the cases when needed. Regulation of the flow rate is made with the aid of a bypass to the main cycle.

Given the use of the diaphragm pump, an important design objective is to ensure stable pressures at the inlet of the plate evaporator during the test runs. The concept is to turn flow of in-compressible fluid (liquid in the diaphragm pump) into flow of a compressible fluid (to evaporate the liquid) before the orifice tube test section and to ensure sufficient vapor volume to buffer pulsations, the volume of the high pressure receiver was calculated to maintain pressure pulsations in the range of ±0.5% for the worst case (when the heater is filled with liquid and pressures are low). Fortunately, during the most of the test runs it is possible to achieve evaporation in the heater, resulting in negligible pressure pulsation even for the test runs when the H.P. receiver is bypassed.

The process path for the refrigerant is shown in Figure 2. It should be noted that the process is clockwise (evaporation occurs at high pressure and condensation at the low pressure).

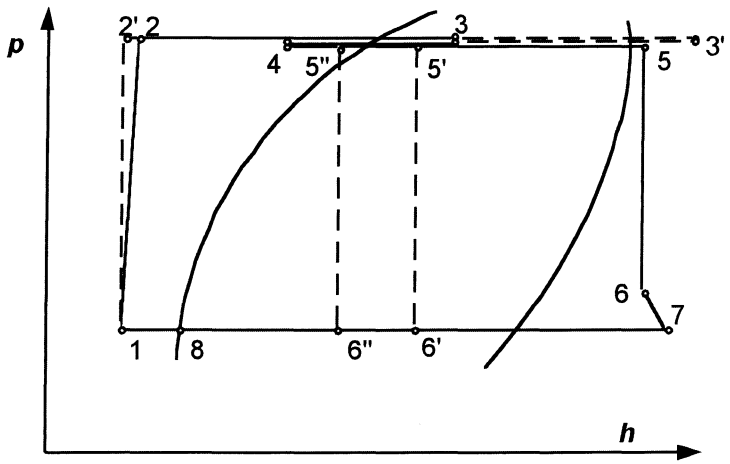

Figure 2.: Pressure enthalpy diagram of the test cycle.

The diaphragm pump pumps subcooled liquid from state 1 to 2 (state 2' represents an ideal, isenthalpic, process). Heaters then heat and partially evaporate refrigerant to state 3 (or fully evaporate and even superheat refrigerant up to 3'). The purpose of evaporation is, as explained earlier, to ensure enough vapor volume to absorb the pressure pulsations created by the diaphragm pump. Vapor is then condensed and sufficiently subcooled in the subcooler to ensure single phase liquid flow through the flow meter (state 4). In the evaporator refrigerant is heated (state 5) or even evaporated (state 5') in order to adjust desired conditions at the orifice tube inlet. Process 5-6 (or 5'-6', or 5" - 6") represents isenthalpic throttling in the expansion device. The process in the evaporator is shown with line 6 - 7 (or 6'-7): high pressure drop and some heat exchanged. Condensation in the condenser brings refrigerant to the state 8 (saturated liquid). Further subcooling is achieved in the pump subcooler (with slight pressure increase due to liquid column) which brings the refrigerant back to the state 1.

2-2 DESCRIPTION OF NITROGEN TEST SETUP

The nitrogen setup is shown in Figure 3. A tank of nitrogen is fitted with a pressure regulator. The pressure regulator is used to control the pressure upstream of the evaporator and thus the mass flow through the evaporator. After the pressure regulator the nitrogen is passed through a heat exchanger to maintain constant temperature after the expansion regardless of cylinder pressure. The evaporator follows the heat exchanger. Temperature and pressure can be read upstream and downstream of the evaporator. Finally nitrogen passes through a venturi were volumetric flow is measured. (see Figure 3).

Accelerometer locations are identical to those in refrigerant tests.

Limitations of the test setup prevented full evaporator testing due to the choked conditions in some parts of the apparatus, small modifications of the apparatus would permit full evaporator testing.

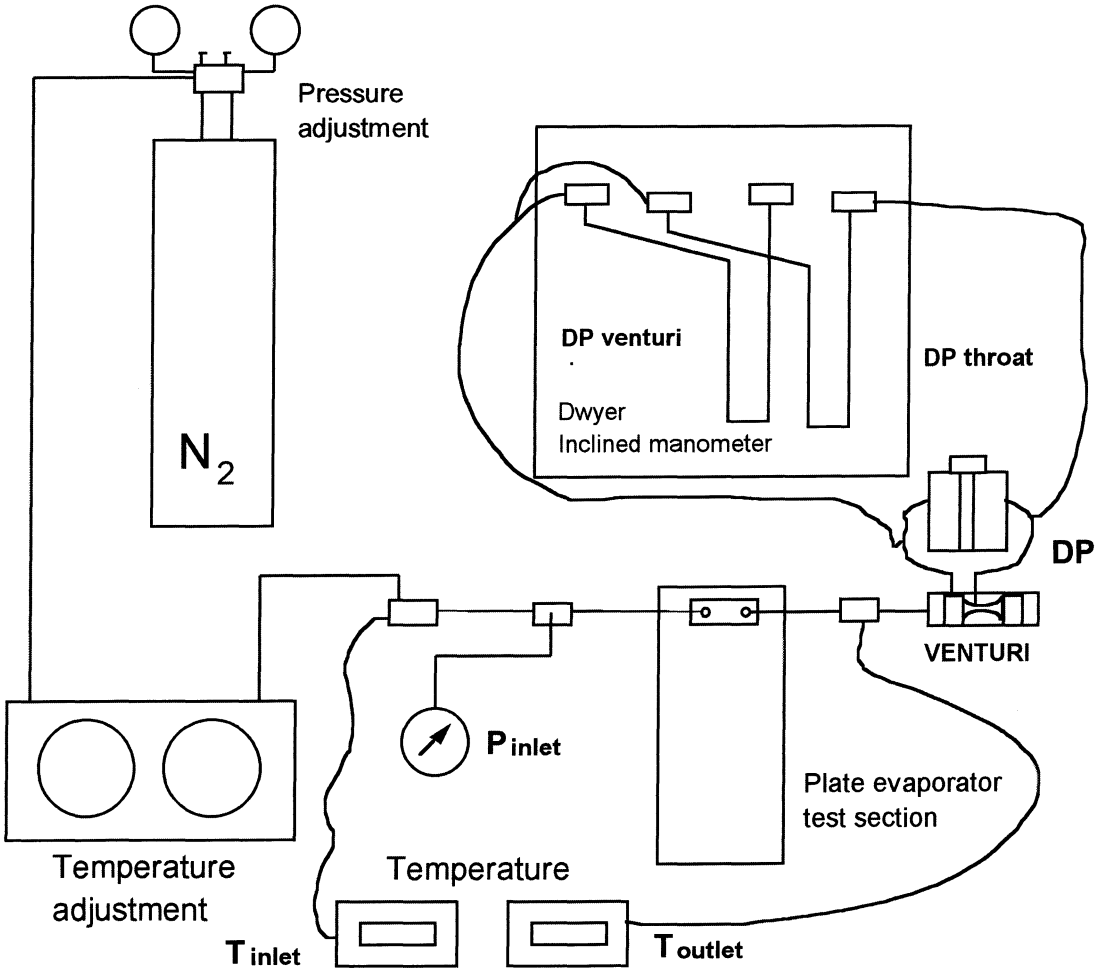

Figure 3. Nitrogen experimental setup.

3 DESCRIPTION OF TESTED PLATES AND TEST PROCEDURE

All evaporator plates tested are made of aluminum at DTP (Dayton Thermal Products) . They were made by cutting off all but the last one and a half plates of a full evaporator and removing the last fin array. As mentioned earlier, some tests were done with 1.5 plates and later all test were made with one plate open for flow. The headers (tanks) were sealed by welding at DTP and the half channel was sealed with epoxy in our laboratory.

Refrigerant connections are original, as used in full evaporators.

Pressure and temperature taps were located in the thermostatic expansion valve (TXV) block at the entrance and exit of the evaporator plate.

Evaporators were not insulated, but there was no significant heat exchange with the environment due to the operating temperatures and the lack of air flow.

Nuts were attached with epoxy to the plate surface to accommodate accelerometers during testing. Locations are shown in Figure 5.

Two types of locations were used. Locations on the plate are numbered and locations on the side are marked beginning with the letter S. The side locations are positioned on the edge of the evaporator plates as can be seen in a full evaporator.

The purpose of the accelerometer distribution is twofold:

a) Side locations are chosen because this is the most accessible position when the whole evaporator is tested.

b) Plate locations should indicate some signal distribution if it exists. The intention was to compare this distribution to results of some measurements done at Chrysler's Technical Center.

Numerous acceleration spectra results are available for further analysis (see appendices).

Our results demonstrate that side locations provide good readings. Values for frequencies at acceleration peaks measured at the side locations are identical to accelerations measured at plate face locations when resonance is present. No consistent relationship between acceleration amplitudes on the side and face of the plate evaporators was observed.

Figure 4 (attached sheet) shows the distribution of the acceleration signal for the AS/PL plate evaporator (Note different scales on y-axis). The largest accelerations are observed for measurement locations near the edges of the channel in the middle of the passage. For other plate evaporators geometries, no accurate acceleration measurements distributions could be established with certainty due to the limited resonance data taken with refrigerant and since nitrogen data was taken only at one location.

The amplitude of an individual acceleration measurements should be viewed with caution. Variation in plate stiffness due to the dimples undoubtledy causes the placement of the accelerometer to be very important. Differences in measured acceleration spectra amplitudes can be the result of minor differences in accelerometer placement on the evaporator plate.

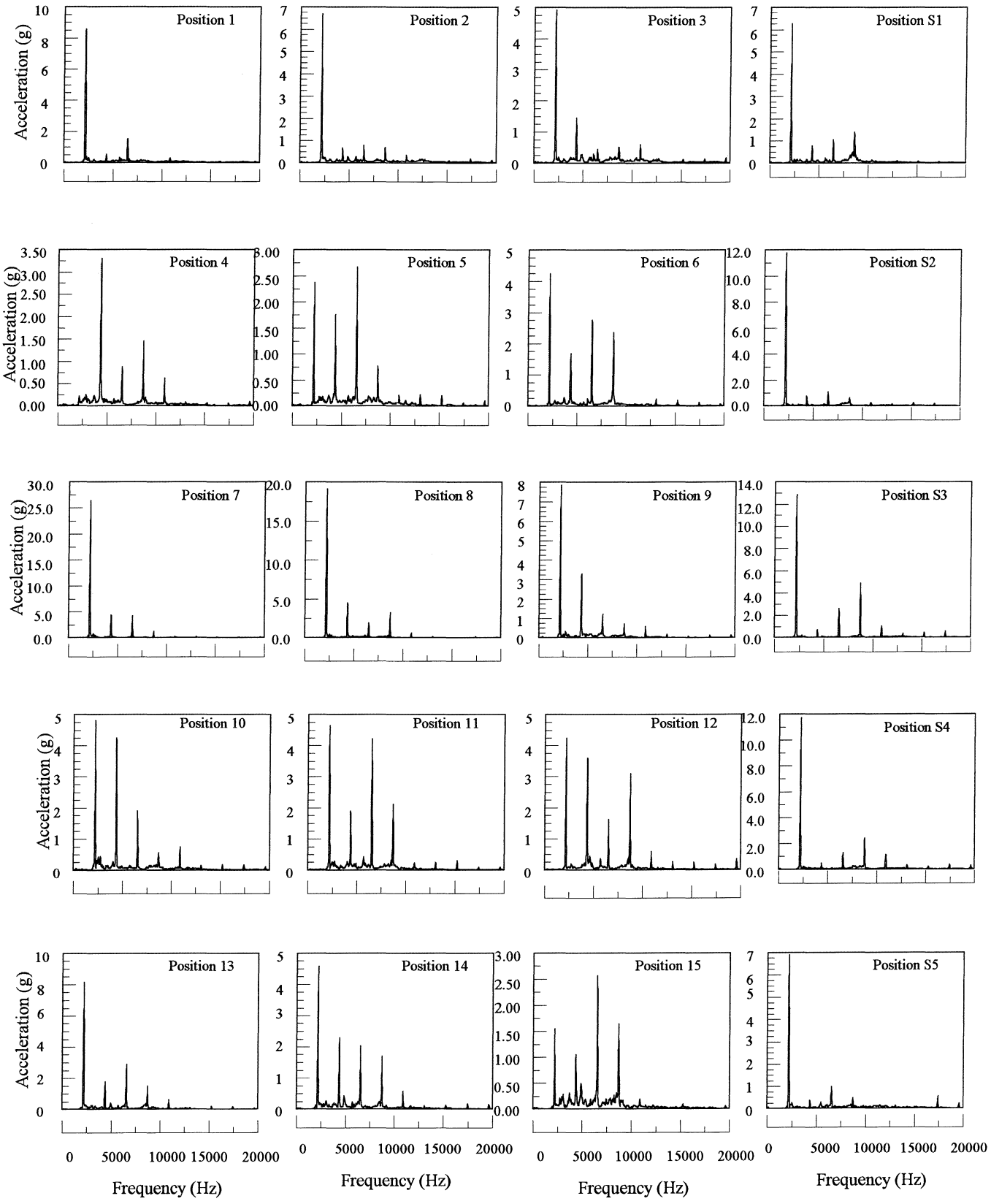

Figure 4. Acceleration power spectra, AS/PL plate evaporator, different positions.

Figure 5 shows the names of the plate evaporators and the position numbers where acceleration measurements were performed on each evaporator. These measurements were made using an HP3562A Dynamic Signal Analyzer and PCB Model M353B16 accelerometers. The accelerometer's range is 1-10000 Hz (+/- 5%) or 0.7-20000 Hz (+/- 10%).

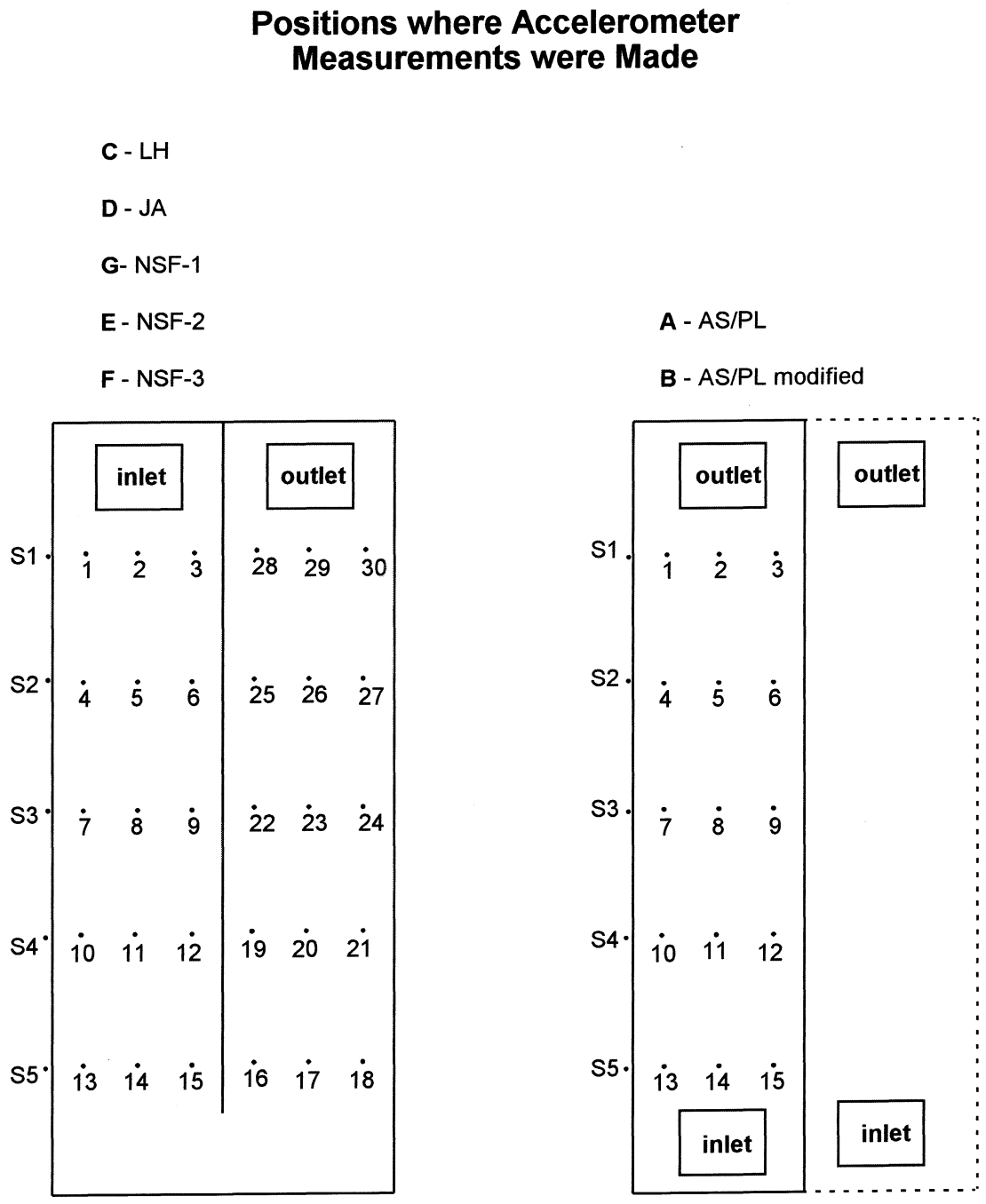

Figure 5. Numbering scheme during plate evaporator testing.

A diagram of the different tests which were performed on the 6 different plate evaporator geometries is shown in Figure 6.

Tests performed

Refrigerant	Nitrogen	Refrigerant	Nitrogen
A-AS/PL  **1.5 and 1 plate** each test 20 positions 10+5 flow rates	**one plate** one position 10 flow rates	F-NSF-3 small dimple **one plate** 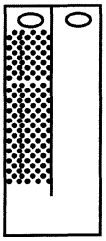 each test 15 positions 5 flow rates	**one plate** one position 18 flow rates
B-AS/PL mod 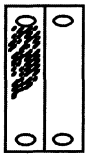 **1.5 and 1 plate** each test 20 positions 2+5 flow rates	one position 9 flow rates		
C-LH 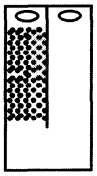 **1.5 and 1 plate** each test 35 positions 6+3 flow rates	**one plate** one position 20 flow rates	G-NSF-1 large dimple **one plate** 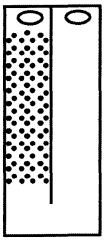 each test 15 positions 5 flow rates	**one plate** one position 10 flow rates
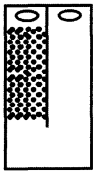 **one plate** each test 35 positions 0 flow rates	one position 20 flow rates		
D-JA  **1.5 and 1 plate** each test 30 positions 5 flow rates	**one plate** one position 27 flow rates	E-NSF-2 sausage **one plate** 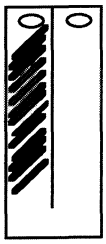 each test 15 positions 5 flow rates	**one plate** one position 19 flow rates
 **one plate** each test 30 positions 2 flow rates	one position 29 flow rates		
	one position 30 flow rates		

Figure 6. Tests performed in this project.

Typical acceleration spectra for a variety of plate evaporators are shown in figures 7 through 12, the graphs clearly show a resonant condition, in many cases accompanied by harmonics.

Graphs for both R134a and nitrogen present similar phenomena as can be seen for example in Fig. 7 and 8. The variations in the resonant frequency for both fluids is due to the difference in the speed of sound for the two cases. Table 2 presents the ratios of the frequencies at resonance for the acceleration spectra in Figures 7 through 12 and compares them with the ratios in the speed of sound for the two fluids.

TABLE 2

COMPARISON OF RESONANT FREQUENCY AND SPEED OF SOUND RATIOS FOR THREE EVAPORATORS

Evap.	R134a Freq. (Hz)	N2 Freq. (Hz)	Freq. Ratio	R134a C (m/s)	N2 C (m/s)	C ratio
AS/PL (A)	2078-2220	4831-5053	2.18-2.43	148.4-156.7	350	2.23-2.36
LH (C)	1787-1957	4140-4676	2.11-2.61	146.5-165	350	2.12-2.39
JA (D)	3415-3740	7707-8513	2.06-2.49	142.9-165.2	350	2.12-2.45
NSF-1 (G)	1937-2593	4312-5125	1.66-2.65	154.6-163	350	2.15-2.26
NSF-2 (E)	1443-2391	3320-3768	1.38-2.61	146.5-161	350	2.17-2.39

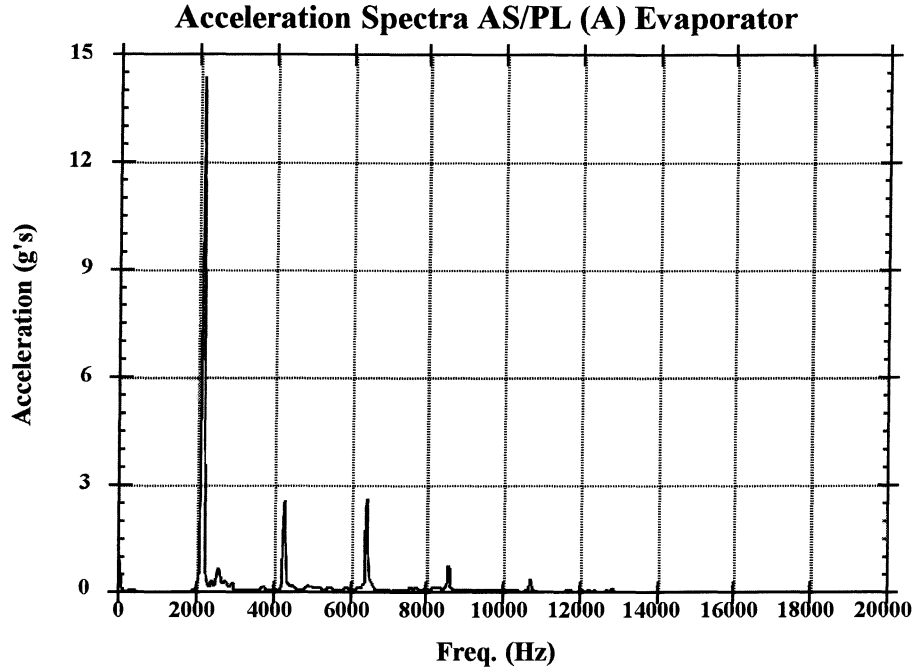

Figure. 7 Acceleration spectrum for AS/PL (A) evaporator at resonance (R134A , position 8, 18.6 g/s, Velocity at dimples = 23.8m/s, P evap inlet=6.31 bar, Tevap inlet=33.6 °C, Superheat at inlet = 10.4 °C.

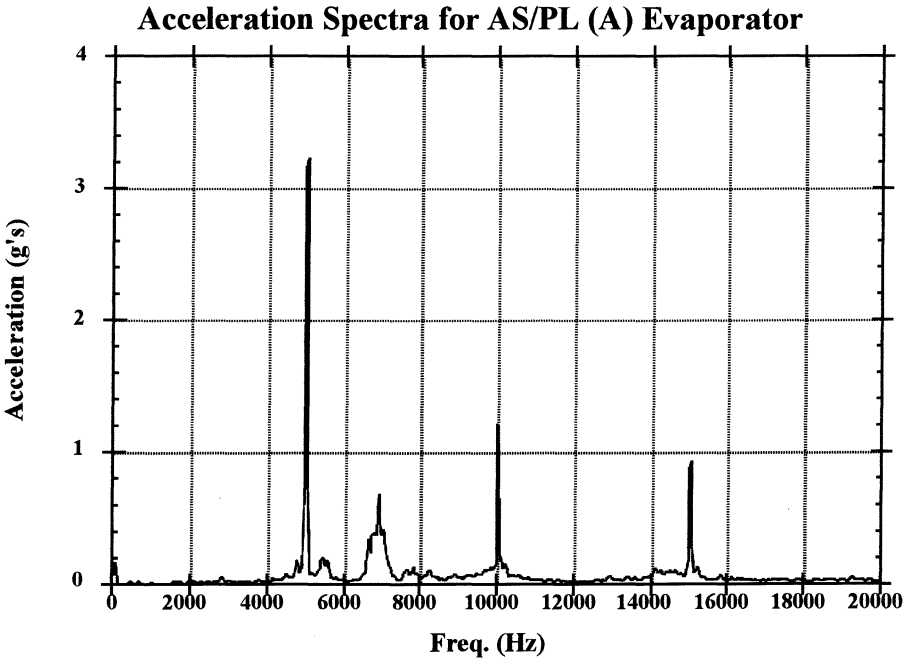

Figure 8. Acceleration spectrum for AS/PL (A) evaporator at resonance. (N2 Test, position 7, Velocity at dimples = 107 m/s,).

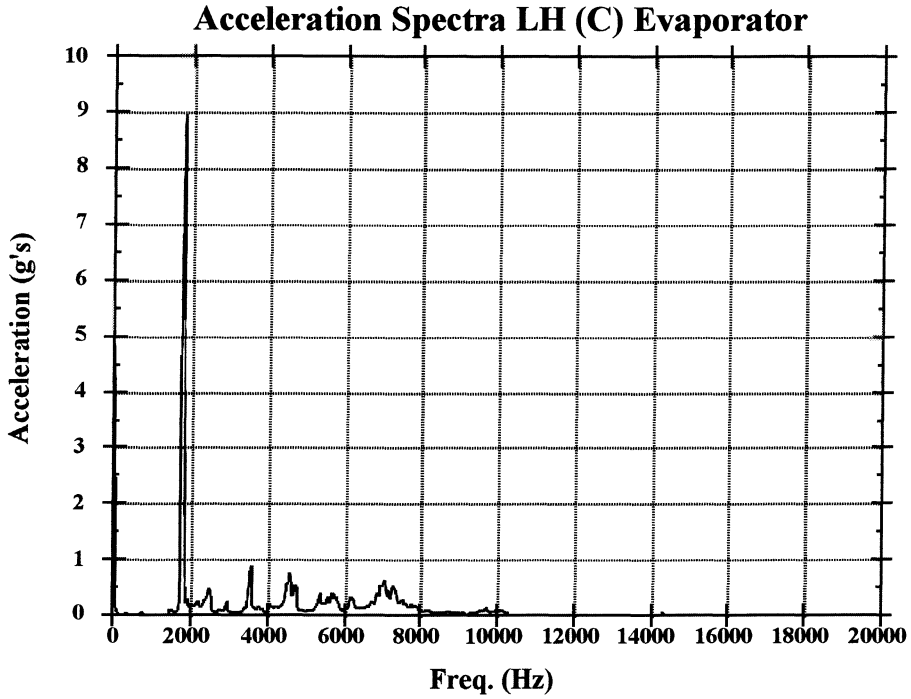

Figure 9. Acceleration spectrum for LH (C) evaporator at resonance.
(R134A Test, position 26,25.3 g/s, Velocity at dimples = 51 m/s, P inlet=6.88 bar, Tevap inlet=31 °C, Superheat at inlet =5 °C).

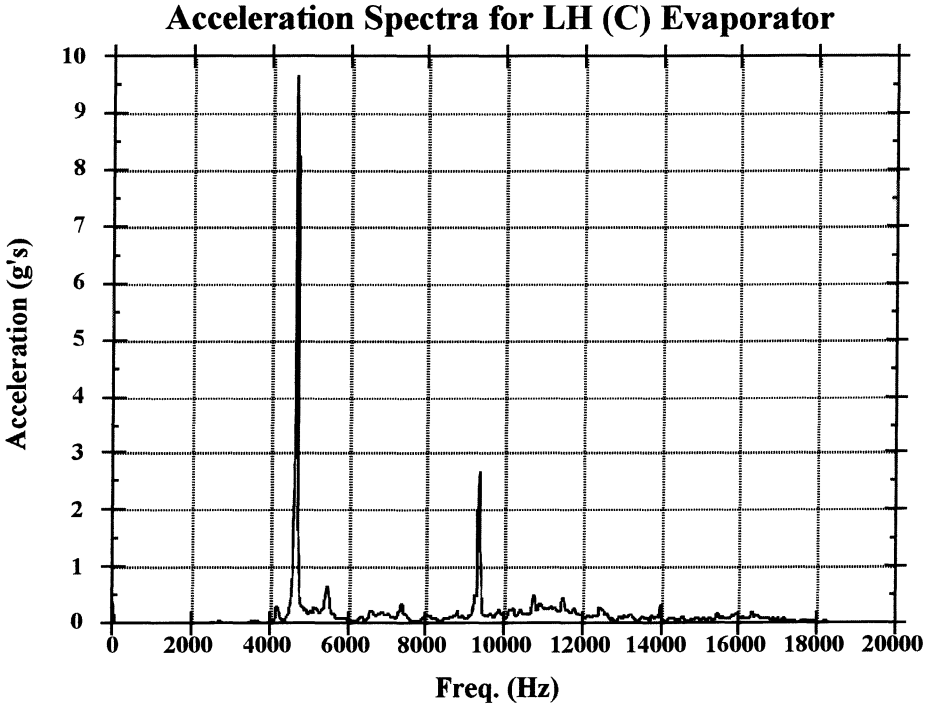

Figure 10. Acceleration spectrum for LH evaporator at resonance.
(N2 Test, position 23, Velocity at dimples = 178.5 m/s).

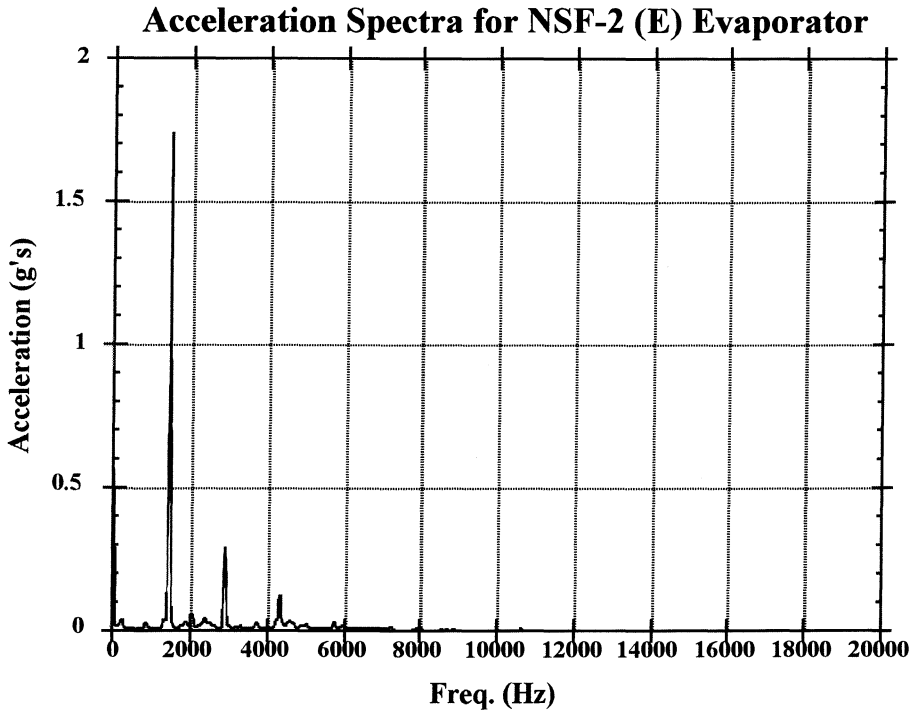

Figure 11. Acceleration spectra for NSF-2 (E) evaporator at resonance. (R134a Test, position 23, 18.4 g/s, Velocity at cross section = 11.98 m/s, P evap inlet = 6.9 bar, Tevap inlet = 32 °C, Superheat at inlet = 6.7 °C.

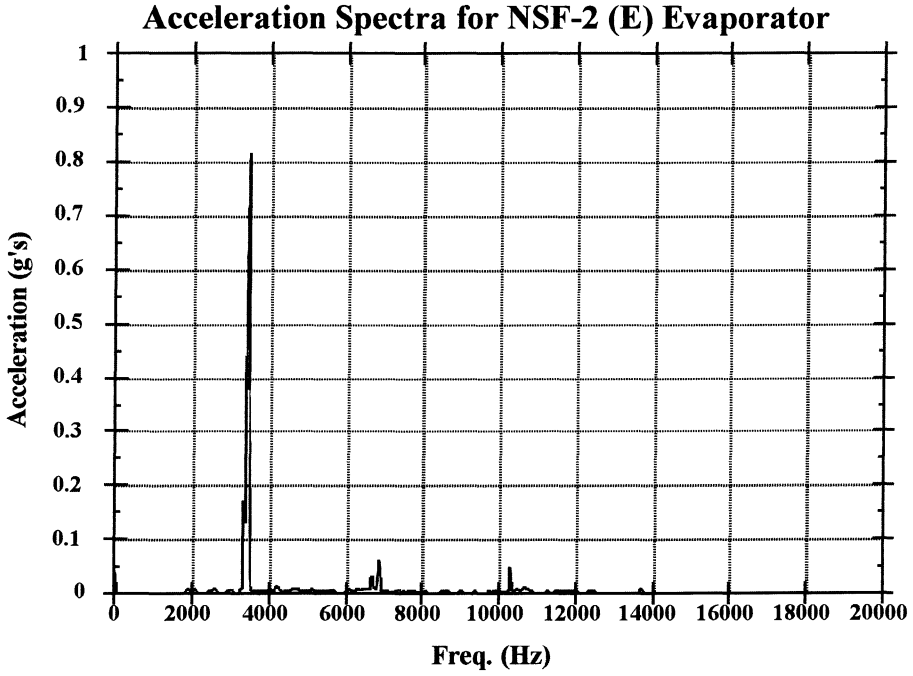

Figure 12. Acceleration spectrum for NSF-2 (E) evaporator at resonance. (N2 Test, position 23, Velocity at cross section = 27.4 m/s).

4 ESTIMATION OF RADIATED SOUND POWER

Sound power measurements are important in this study since they provide the means of comparing the different plate evaporators versus each other in a quantitative manner. Sound power estimation also helps in the evaluation of a resonant condition.

The sound power radiated from a machine surface can be estimated from the determination of the square surface velocity averaged over the surface area (Bies and Hansen, Chan and Anderton, Takatsubo, Ohno and Suzuki) [7,8,9]. This method is limited in its accuracy principally because of the complexities involved in the surface-fluid interactions. These interactions are represented by a radiation ratio factor σ which usually is a function of frequency. When the radiation ratio factor is not known the recommended practice is to A-weight the measured mean square surface velocity (Bies and Hansen) [7]. A-weighting a signal is a standard way of approximating the response of the human ear at low sound levels and in this way compensate for the variations in the subjective response of the ear at different frequencies.

The sound power radiated from a vibrating surface is given by:

$$W = \rho \cdot c \cdot Srad \cdot \sigma \cdot \bar{v}^2 \qquad (1)$$

Where:

ρ = Fluid density
c = Speed of sound in fluid
Srad = Surface area of vibrating structure
σ = Radiation ratio
$\bar{v}^2$ = Mean square surface velocity

When vibration measurements are made with an accelerometer, the velocity may be estimated with the following equation:

$$\bar{v}^2 = \bar{a}^2/(2 \cdot \pi \cdot f)^2 \qquad (2)$$

Where:

$\bar{a}^2$ = Mean squared acceleration
f = Band center frequency

In order to visualize and represent in a more convenient scale the results of equation (1) usually the base 10 logarithm is applied to it to obtain results in decibels relative to 1e-12 W.

$$Lw = 10 \cdot \log(\bar{v}^2) + 10 \cdot \log(Srad) + 10 \cdot \log(\sigma) + 146 \qquad (3)$$

Where:

Lw = Sound power level in dB relative to 1e-12 Watts

In order to use this method a recommended 5 to 10 measurements are needed distributed at random on the vibrating surface but not to close to the edges. The limitations in the accuracy of the absolute sound power determination from the equations above are significant, but based on the similarity of the different plate evaporator surfaces, this technique

can be used as a basis for comparison. A typical sound power graph as a function of frequency can be seen in Figure 13.

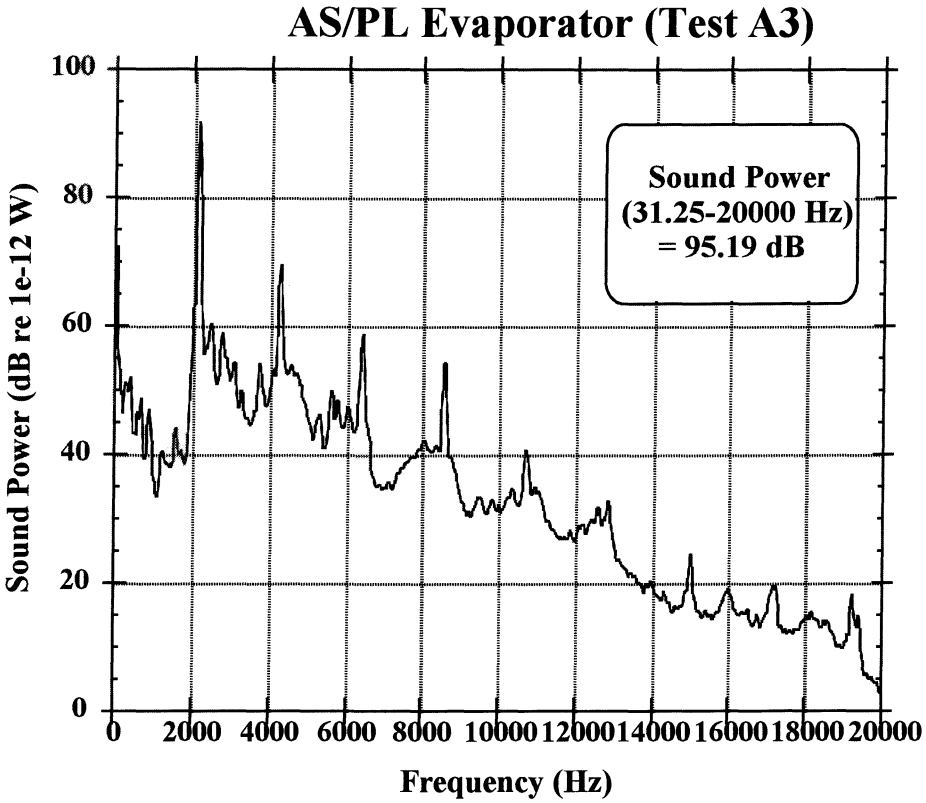

Figure 13. Sound power spectrum for AS/PL evaporator
R134a, velocity at dimples = 48.6 m/s, P at evaporator inlet = 6.9 bars
temp. at evaporator inlet = 25 °C, saturated vapor.

It is very important to note that average sound power is not a direct indication of the annoyance of a noise source since a pure tone is more disturbing than broad band noise of the same power level. Notice that almost all the sound power on Figure 13 is concentrated in the peak at about 2100 Hz. A better comparison can be made when a measurement of the distribution of the sound power is used. Two measurements that take into account the sound power distribution are:

a) The frequency band necessary to reach a predetermined percentage of sound power (say 95%) (Figure 14).

b) A percentage of the total sound power (say 95 %) divided by the total frequency band necessary to reach that percentage (Figure 15).

Measurement a) lacks information about how much sound power comprises 95% of the total sound power and therefore can only be used as an indication of a condition of resonance. A condition of resonance is determined when the sound power is concentrated in a narrow frequency band. Based on our tests we can conclude that a frequency band necessary to reach 95% of the total sound power of less than 500 indicates such a condition. Tests A1-A6, E3-E4 and C3 represent a test under resonant conditions. Measurement b), on the other hand, includes information about the level of sound power and therefore can be a more useful.

TABLE 3

RESULTS OF SOUND POWER ANALYSIS

Evaporator	Test number	Velocity at dimples (m/s)	Freq. band to get 95% sound power. (Hz)	95% of sound power divided by freq. band. (W/Hz)	Sound power dB re to 1e-12 W
AS/PL	A6	22.6	250	1.1434e-6	84.86
	A2	23.8	93.75	1.8436e-5	92.56
	A5	25.7	93.75	1.2011e-5	90.75
	A4	27.3	93.75	2.4573e-5	93.84
	A1	36.5	125	2.6995e-5	95.71
	A3	48.6	93.75	3.3387e-5	95.19
LH	C3	51.2	187.5	1.6532e-5	95.61
	C1	52.6	2812.25	3.1291e-7	90.03
	C2	59.0	1312.5	1.7119e-6	93.77
JA	D2	44.3	1500	8.6270e-8	82.92
	D5	48.7	2593.7	5.3074e-9	76.33
	D1	53.0	3312.5	4.0820e-8	84.21
	D3	62.3	3687.5	2.5932e-8	81.12
	D6	77.7	1593.8	2.8543e-7	87.44
NSF-1	G5	15.7	1375	1.9131e-8	74.52
	G3	17.9	1625	2.0804e-8	75.83
	G4	21.7	1156.3	1.3557e-7	82.20
	G2	24.3	1781.3	1.0641e-7	83.01
	G1	25.4	2375	8.0035e-8	83.03
NSF-2	E5	11.9	93.75	5.3535e-6	87.09
	E4	14.7	156.25	1.9404e-6	85.04
	E3	18.4	2718.7	9.2857e-9	74.82
	E2	23.6	1375	9.1529e-8	81.35
	E1	23.6	1937.5	5.7751e-8	80.83
NSF-3	F5	19.7	1281.3	4.2551e-8	77.60
	F3	24.2	2750	5.5326e-8	82.46
	F4	29.5	2125	1.4835e-7	85.26
	F2	32.6	2812.5	1.1353e-7	85.33
	F1	34.1	3843.7	1.3058e-7	87.28

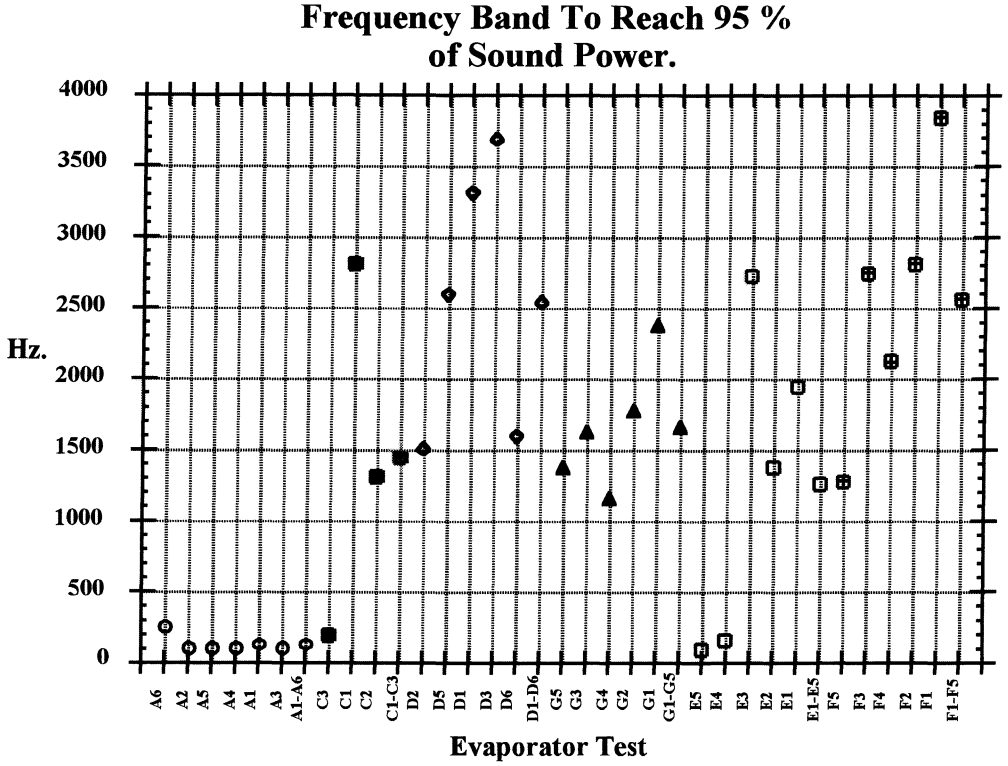

Figure 14. Diagram showing the frequency band required to get 95% of the total sound power.

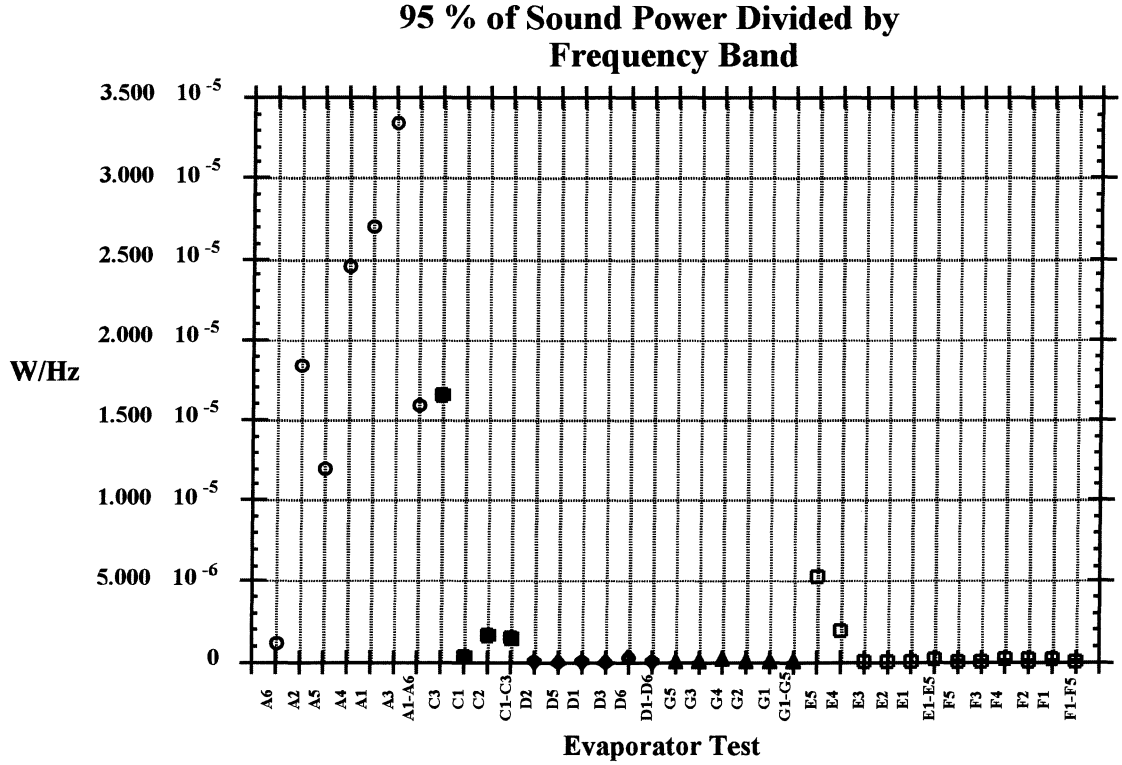

Figure 15. Diagram showing the relationship between sound power produced and frequency band necessary to produce it.

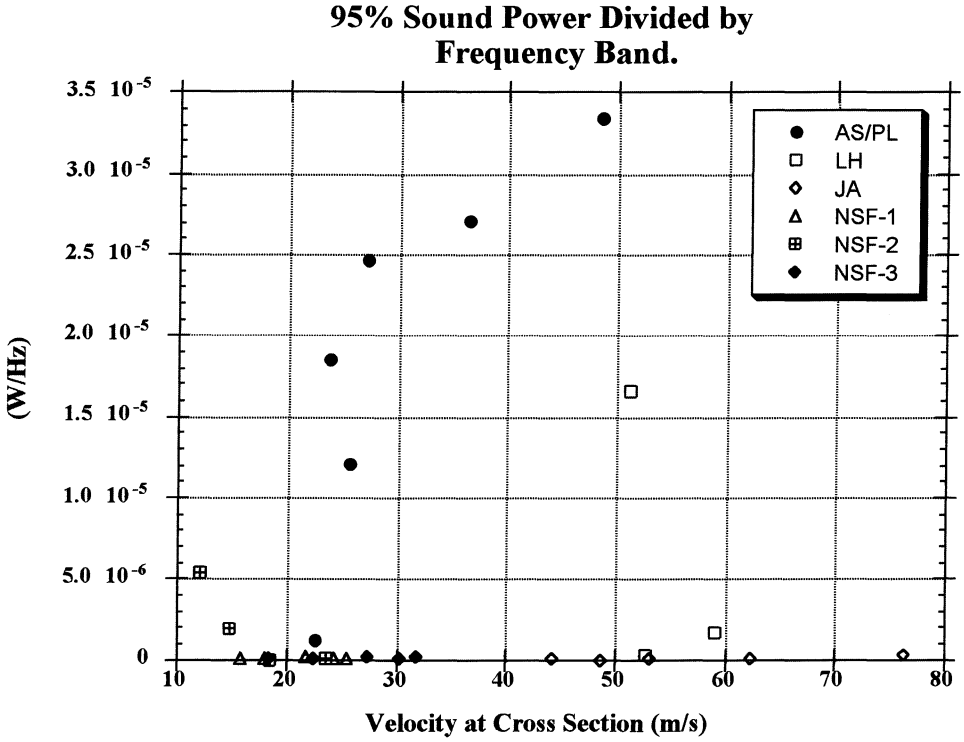

Figure 16. Diagram similar to Figure 15, where the velocity at the cross section is introduced to show its effects.

As can be seen in Figure 14, a plate evaporator at resonance can be clearly determined as one in which the frequency band to obtain the majority of the sound power is small (as explained previously). In Figure 15, resonance is indicated as a large value of W/Hz. Not all the tests performed on the plate evaporators were under resonant conditions. There were some tests {for example evaporators D, G and F (JA, NSF-1 and NSF-3) } that do not indicate resonance in figures 14 and 15 clearly even when the individual acceleration frequency graphs show some very distinct peaks at particular frequencies. That is, in some cases it appears that resonant conditions were reached in a limited region of the plate. Figures 17 and 18 show acceleration power spectra at two different positions during the same test for the NSF-1 evaporator plate which illustrates this conclusion. The surface averaging technique used here cannot show such effects. Figures 14 and 15 are made using averaging techniques, therefore the local effects cannot be appreciated . For plate evaporator F (NSF-3), Fig. 14 and 15 do not indicate a resonance, but as can be seen from the acceleration power spectra graphs for evaporator F during nitrogen testing in figures 19 and 20, there is a clear resonant condition. It is believed that this evaporator will whistle during refrigerant service if the flow velocity is high enough.

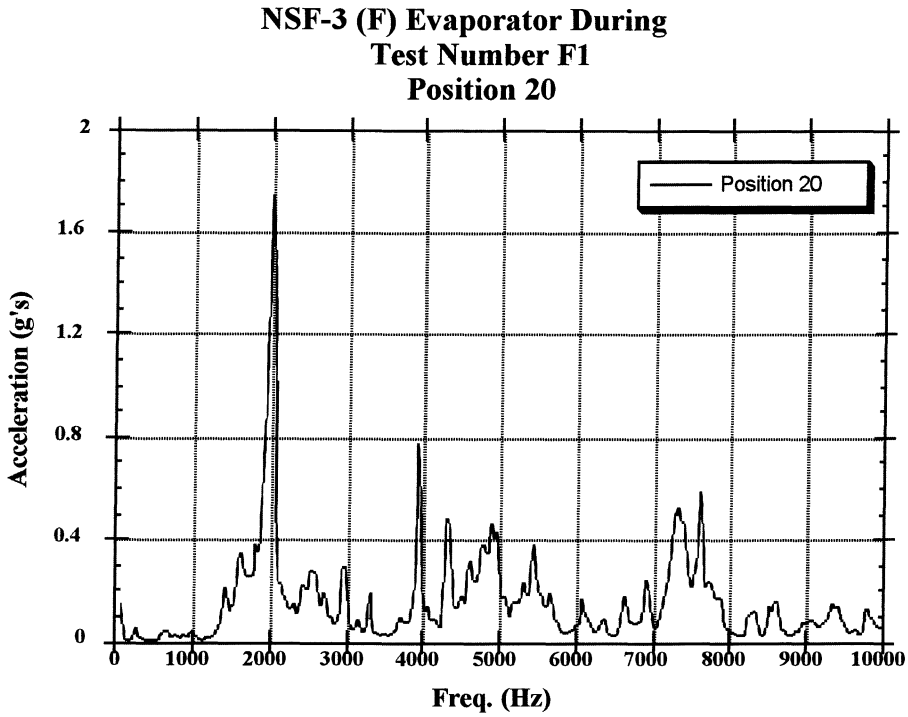

Figure 17. Acceleration Spectrum Position 20.

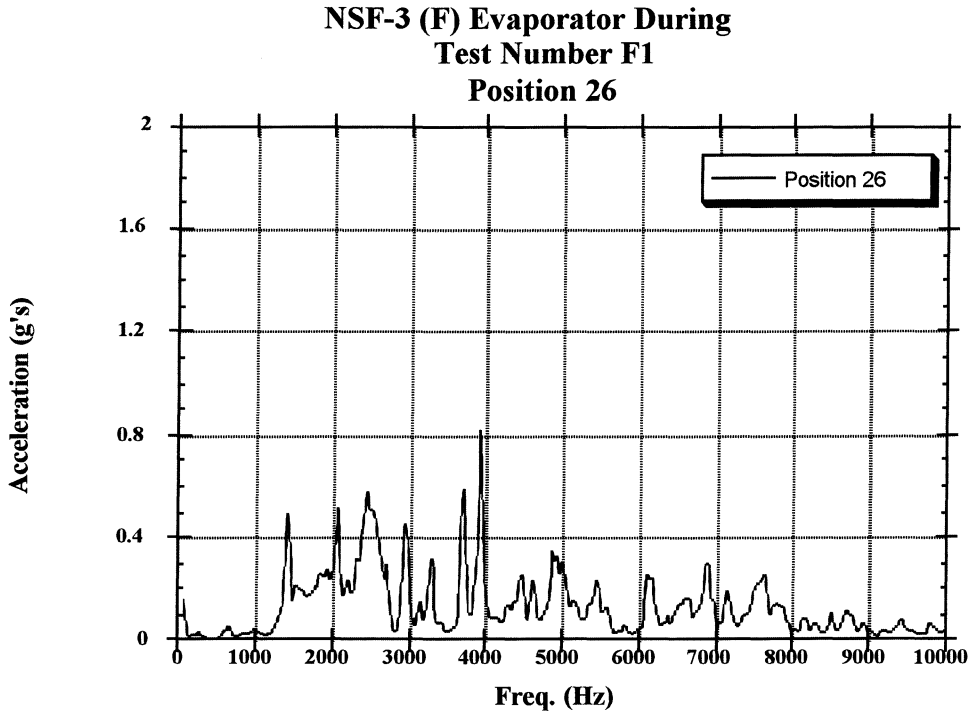

Figure 18. Acceleration Spectrum Position 26.

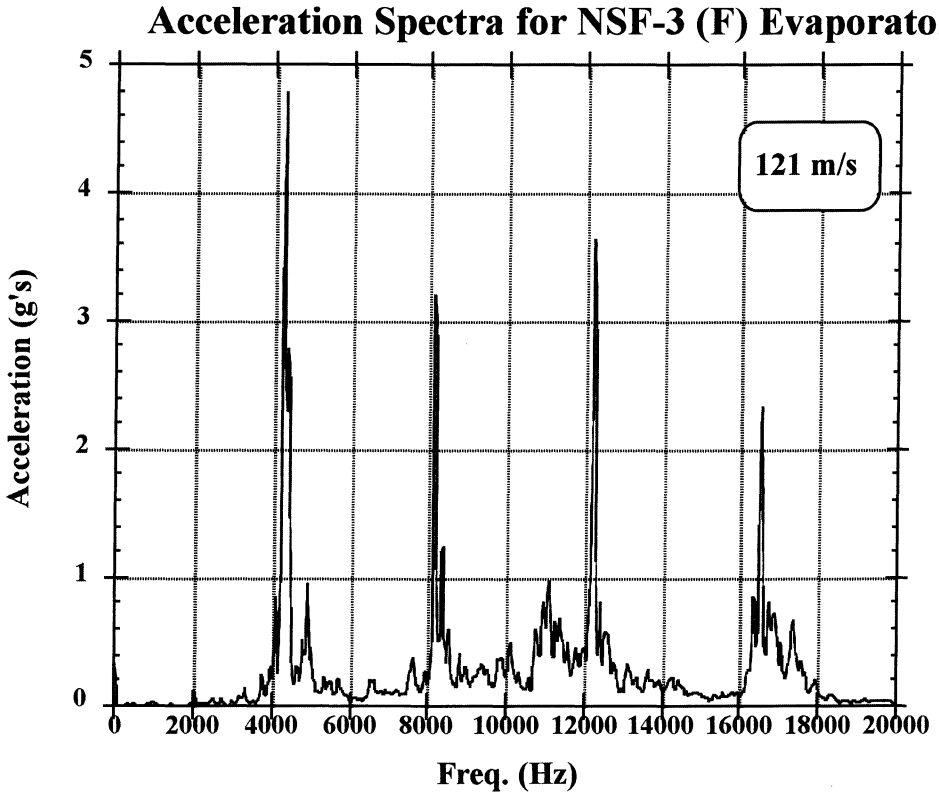

Figure 19. Acceleration spectrum for NSF-3 (F) evaporator plate at position 23, nitrogen test.

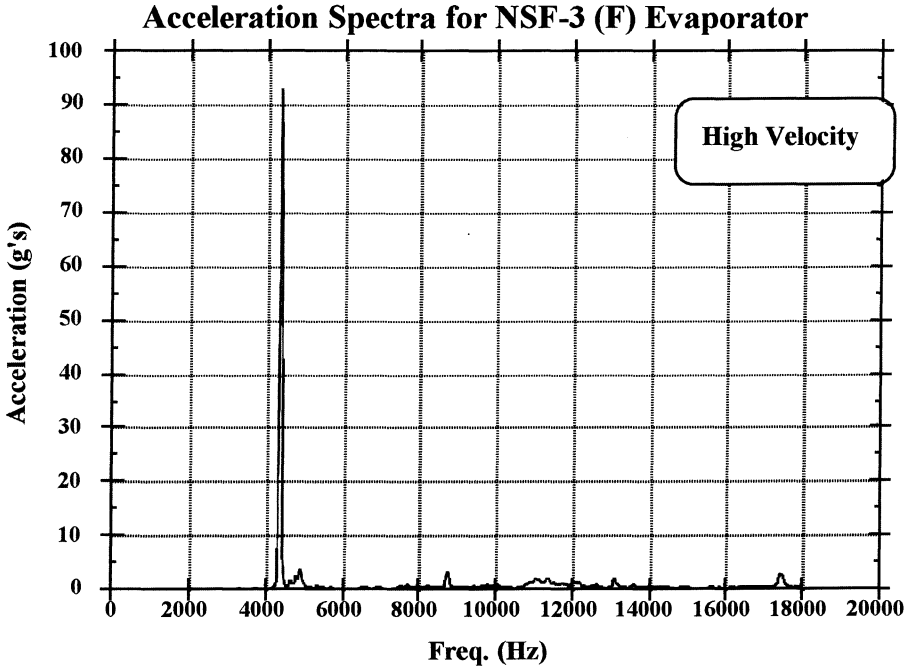

Figure 20. Acceleration spectrum for NSF-3 (F) evaporator at position 23, nitrogen test.

It is interesting to note that for the lower flow velocities in evaporators C and E (LH and NSF-2) the worst conditions develop. This can be explained if we assume an overshooting of the acoustic natural frequency by the excitation mechanism frequency. This phenomenon has been reported in the literature [10,17,18]. Further testing of these evaporators should be done before this hypothesis is confirmed. Figures 21 through 23 show this phenomenon occurred for a vibrating cylinder, a cylinder inside a duct, and a staggered in-line tube array.

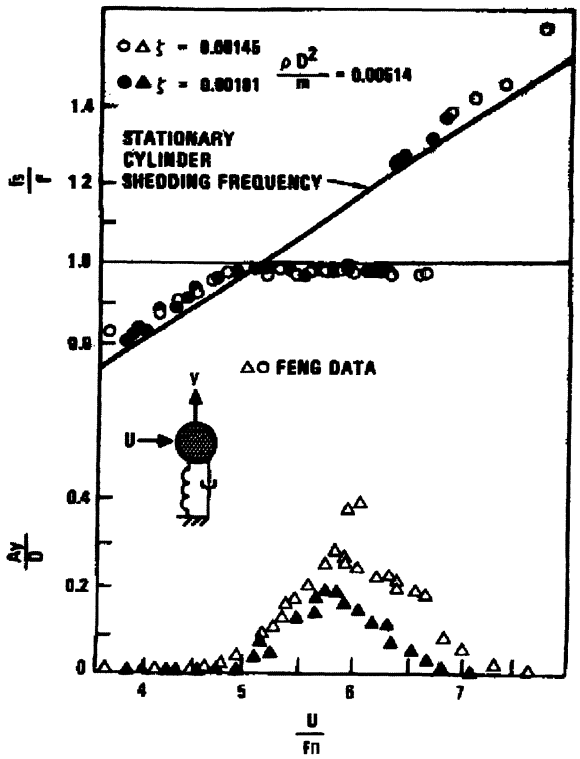

Figure 21. Vortex-induced vibration of a spring supported and damped circular cylinder; f is the natural frequency of the cylinder, (Blevins) [14].

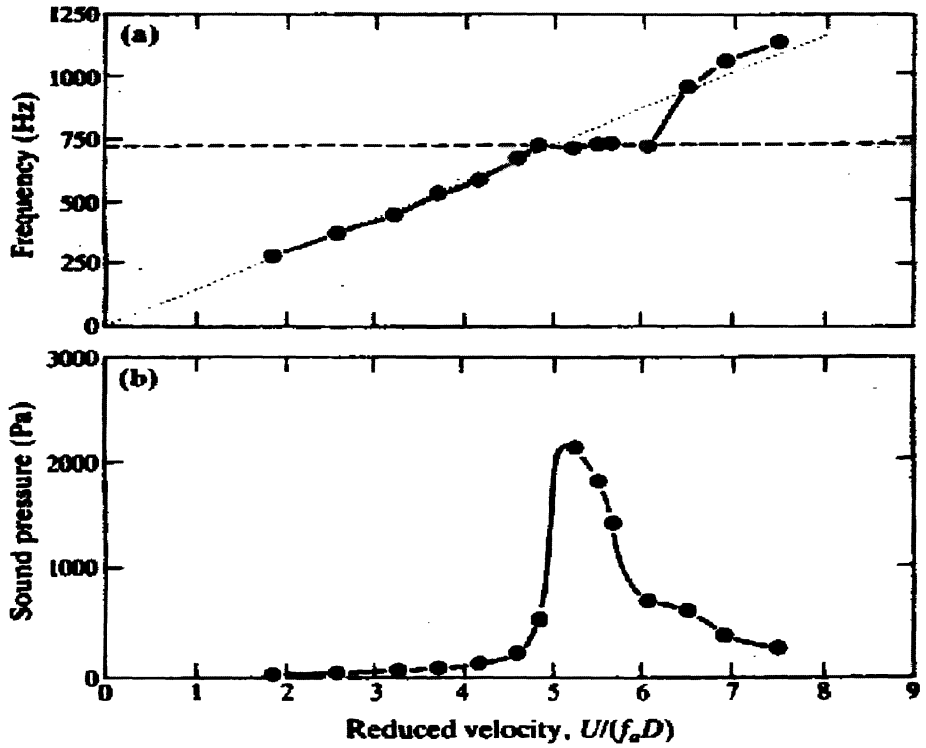

Figure 22. Sound pressure and frequency for single 25.4 mm diameter cylinder in 229 mm width duct. a) Frequency (first mode , fa=720Hz); b) Sound pressure. (Blevins and Bressler) [10].

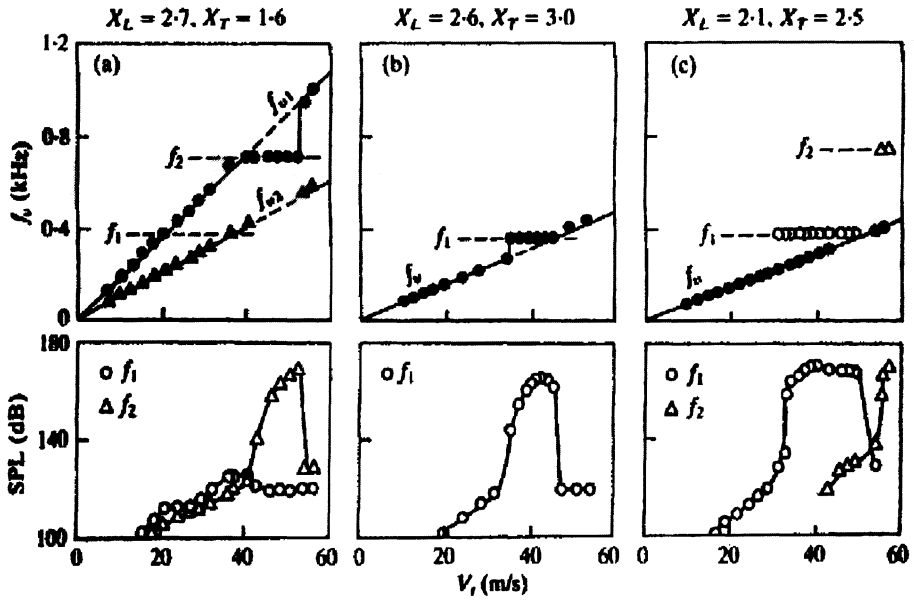

Figure 23. Frequency of vorticity shedding, fv, and sound pressure level, SPL, at the resonance frequencies, fl and f2, as a function of gap velocty, Vt. a) Staggered array, b) and c) In-line array. (from Ziada et al, [17]).

From Figure 24 it can be seen that evaporator D (JA) is tested at a relatively high flow velocity. This evaporator is known to be a "problem evaporator". Our testing does not confirm the problem. It is believed that the JA plate evaporator would most likely whistle at lower flow velocities. This is also believed true for evaporator C (LH), but further testing would be required to confirm these hypotheses.

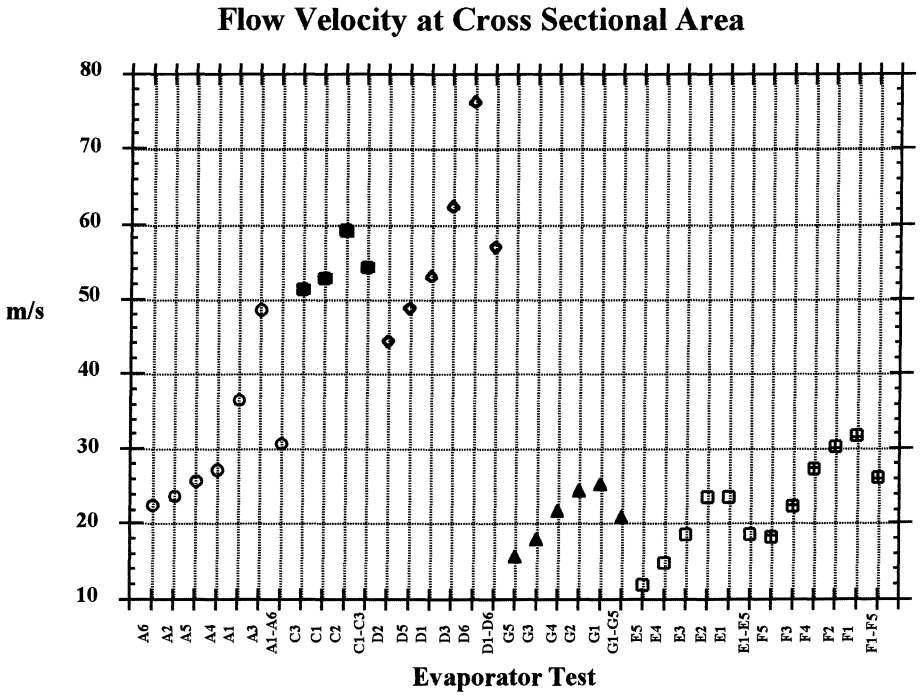

Figure 24. Diagram that shows the velocity of R134a at the cross section of the plate evaporators for the different tests performed.

5 PREDICTION OF ACOUSTIC NATURAL FREQUENCIES

In order to predict the acoustic natural frequencies of the evaporator flow passage for our case, two simplifications will be used. First, the refrigerant flow passage for the plate heat exchanger will be considered to be a rectangular volume for which the acoustic natural frequencies are presented in equation (4). Second, a correction for the speed of sound of the fluid will be used in the previously mentioned equation. This correction in the speed of sound has been used in previous studies and has been found to agree with experimental results made on large heat exchangers. (See Figure 24)

$$f_{ijk} = \frac{c_{eff}}{2}\left(\frac{i^2}{W^2} + \frac{j^2}{H^2} + \frac{k^2}{L^2}\right)^{\frac{1}{2}} \qquad i,j,k = 0,1,2,3... \qquad (4)$$

Where:

f_{ijk} = Acoustic natural frequencies
i,j,k = Eigenvalues that represent the different possible modes
W = Width
H = Height
L = Length
c_{eff} = Effective speed of sound in tube bundle

The mode of excitation is such that only the transverse mode is usually excited. Thus j and k are zero in equation (4), therefore equation (4) is simplified as shown in (5). The transverse mode corresponds to the mode perpendicular to both the fluid flow and the tubes in the bundle. In the present case (plate heat exchangers), the tubes are replaced by the evaporator plate dimples.

$$f = \frac{c_{eff}}{2W} \qquad (5)$$

The effective speed of sound of the fluid in the tube bundle is reduced by the presence of the tubes which scatter the sound waves. If the elements have dimensions which are a small fraction of the acoustic wavelength, the net result is a reduction in the speed of sound and an increase in dissipation (Blevins) [12]. The rationale behind the concept of effective speed of sound is that the travel time for a sound pressure front is lengthened by the scattering due to the obstructions of the tubes. This is why for our case in which relatively high frequencies are encountered in comparison with all the previous work for large heat exchangers there is a concern regarding the application of this concept, but it will be used in as a means of comparison. The effective speed of sound is determined based on the speed of sound of free space and corrected using the solidity parameter:

$$ceff = \frac{1}{\sqrt{1+\sigma}} \bullet c = \frac{c}{\sqrt{1+\sigma}} \qquad (6)$$

Where:

σ = Solidity or fraction of volume occupied by tubes
c = Speed of sound in fluid

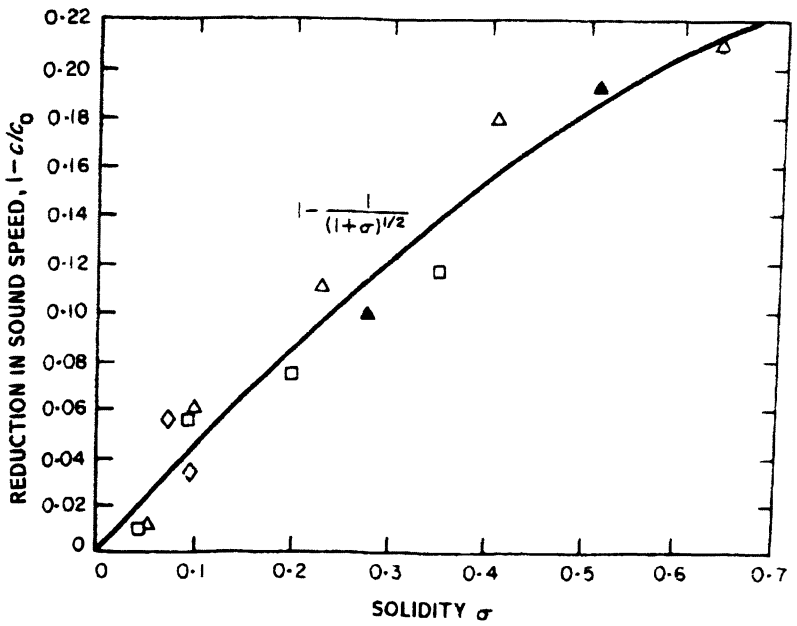

Figure 24. Reduction in sound speed as a function of solidity, from (Blevins) [12].

BASIC DATA USED TO CALCULATE ESTIMATED RESONANT FREQUENCIES

In order to estimate the natural frequency of the different evaporators given by equation 5, the speed of sound for the fluids of interest are needed:

$140 < c < 165$ m/s	For R134a
$c = 350$ m/s	For N2

The values for W and σ are now presented for each evaporator in the following table:

TABLE 4

GEOMETRIC CHARACTERISTICS OF TESTED PLATE EVAPORATORS

AS-PL (A)

1) W=31.4 mm (width) σ =0.356 (Chrysler)

LH (C)

2) W=37.5 mm (width) σ =0.404 (estimated at U of I)
3) W=29.5 mm(width between sausages)
4) W=80 mm (width bottom pass)

JA (D)

5) W=31 mm (width) σ =0.25 (estimated at U of I)
6) W=65.5 mm (width bottom pass)

NSF-1 (G-large dimples)

7) W=37.5 mm (width) σ =0.18 (Chrysler)
8) W=33.5 mm(width channel shorter section)
9) W=79 mm (width bottom pass)
10) W=75 mm (width bottom pass shorter section)

NSF-2 (E-large sausages)

11) W=35 mm (width small) σ =0.29 (Chrysler)
12) W=37 mm (width large)
13) W=74 mm (width bottom pass)
14) W=79 mm (width bottom pass between sausages)

NSF-3 (F-small dimples)

15) W=38 mm (width) σ =0.25 (Chrysler)
16) W=29 mm (width between sausages)
17) W=79 mm (width bottom pass)
18 W=71 mm (width bottom pass between sausages)

TABLE 5

ESTIMATED AND MEASURED NATURAL FREQUENCIES.

	Estimated		Experimental	
Evaporator	Refrigerant (R134a) (*)	N2 (*)	Refrigerant (R134a)	N2
AS-PL (A)				
1)	1914 < f < 2256	4786	2156	4840-5060
LH (C)				
2)	1575 < f < 1857	3938	1969	4170-4640
3)	2003 < f < 2360	5006		
4)	738 < f < 870	1846		
JA (D)				
5)	2020 < f < 2380	5049	3770	7610-8300
6)	956 < f < 1127	2390		
NSF-1 (G-large d.)				
7)	1718 < f < 2025	4296	1935	4200-4800
8)	1924 < f < 2267	4809		
9)	816 < f < 961	2039		
10)	859 < f < 1013	2148		
NSF-2 (E-large S.)				
11)	1761 < f < 2075	4402	1430	3310
12)	1666 < f < 1963	4164		7070-7320
13)	833 < f < 982	2082		
14)	780 < f < 919	1950		
NSF-3 (F-small d.)				
15)	1648 < f < 1942	4119	2000	3970-4375
16)	2159 < f < 2544	5397		
17)	793 < f < 934	1981		
18)	882 < f < 1039	2205		

(*) Estimates of acoustic natural frequencies based on a range of possible characteristic dimensions and range of speeds of sound for R134a. Effective speed of sound estimated based on equation 6.

6 ESTIMATES OF STROUHAL NUMBERS BASED ON EXPERIMENTAL DATA

Table 6 presents Strouhal number estimations using the slope of the frequency-velocity diagrams, figures 28 to 39, and specifying a characteristic dimension D.

Strouhal Number

Strouhal numbers can be determined for the tested evaporator from the velocity-frequency graphs (Figures 29-40) using the relation:

$$S = \frac{fD}{U} \qquad (7)$$

Where:

S = Strouhal number
f = Resonating frequency (Hz)
U = Velocity at start of resonance (m/s)
D = Characteristic dimension (m)

TABLE 6

STROUHAL NUMBERS CALCULATED FROM NITROGEN EXPERIMENTAL DATA

Evaporator	frequency (Hz)	U start (m/s)	D (m) 10^-3	Strouhal #
AS-PL (A)	4831.4	48.062	5	0.503
AS-PL mod (B)	6860	70.06	5	0.490
LH (C)	4171.2	109.33	3.5	0.134
JA (D)	7606.8	128.21	3	0.178
NSF-1 (G)	4482.0	40.439	4.5	0.499
NSF-2 (E)	7073.7	61.169	4	0.463
NSF-3 (F)	4387.1	50.362	4.5	0.392

7 COMPARISON OF EXPERIMENTALLY DETERMINED STROUHAL NUMBERS VERSUS PUBLISHED STROUHAL MAPS FOR TUBE ARRAYS

TABLE 7

STROUHAL NUMBER AND VORTEX SHEDDING FREQUENCY USING RESULTS FROM THE LITERATURE FOR DIFFERENT EVAPORATORS

Evaporator	Strouhal # from (Blevins) [14]	Dimple diameter (m)	Exp. deter. Vel. at cross section (m/s) to begin resonance	Estimates of Frequency (Hz) using Strouhal number.	Actual Observed frequency Hz.
AS/PL (A) T/D = 1.6 L/D = 1.3	0.46 (very close to 0.18 and 0.31)	0.005	48	4416	4840-5060
LH (C) T/D = 2 L/D = 3.5	0.23	0.0035	109.3	7182	4170-4640
NSF-1 (G) T/D = 1.8 L/D = 2.7	0.23	0.0045	40.4	2065	4200-4800
NSF-3 (F) T/D = 1.5 L/D = 2.9	0.23	0.0045	50.4	2576	3970-4375

Note: T/D is the transversal spacing between tubes divided by the tube diameter.
L/D is the longitudinal spacing between tubes divided by tube diameter.

Table 7 was made as follows: the first column of the table was obtained by direct measurements from the plate evaporators. This information was used to get a Strouhal number from the maps shown in figures 25 and 26 (Maps by Fitz-Hugh as mentioned in [14]), the next step is to find the flow velocity for each evaporator when a resonant conditions begins to develop. A characteristic dimension usually the tube diameter is also needed, in this case the dimple base diameter. With this information an estimate of the frequency predicted by the maps to make the evaporator resonate is found. The last column of the table shows the acoustic frequencies found experimentally. This table clearly indicates the inaccuracies of this maps for our case.

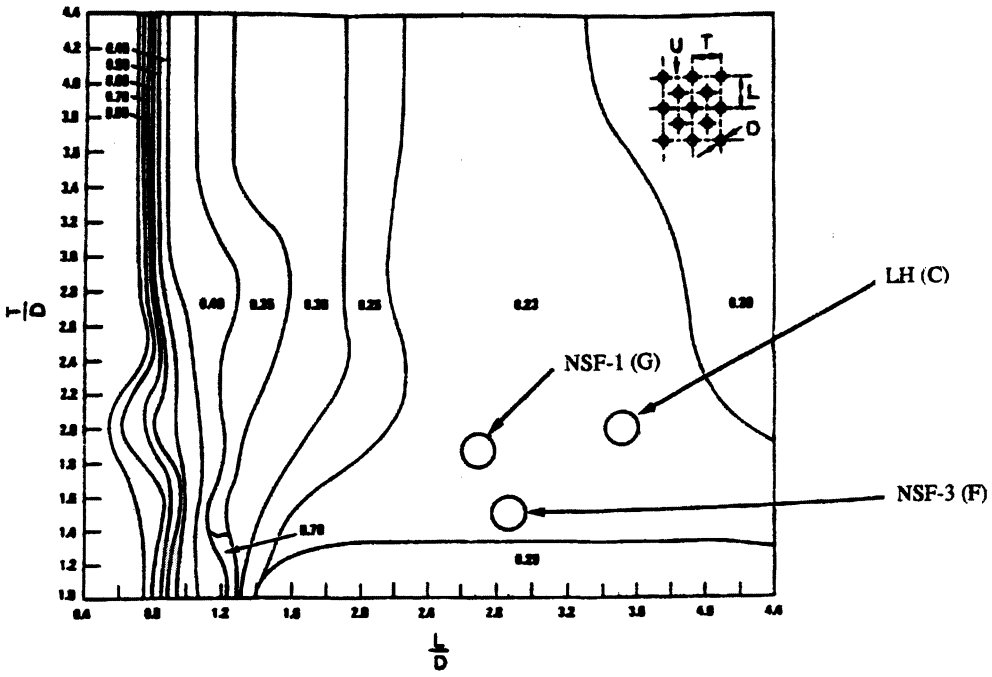

Figure 25. Strouhal number map for staggered tube arrays by Fitz-Hugh as presented in Blevins [14]. The difficulties of Strouhal number prediction are emphasized by our estimations shown in the diagram.

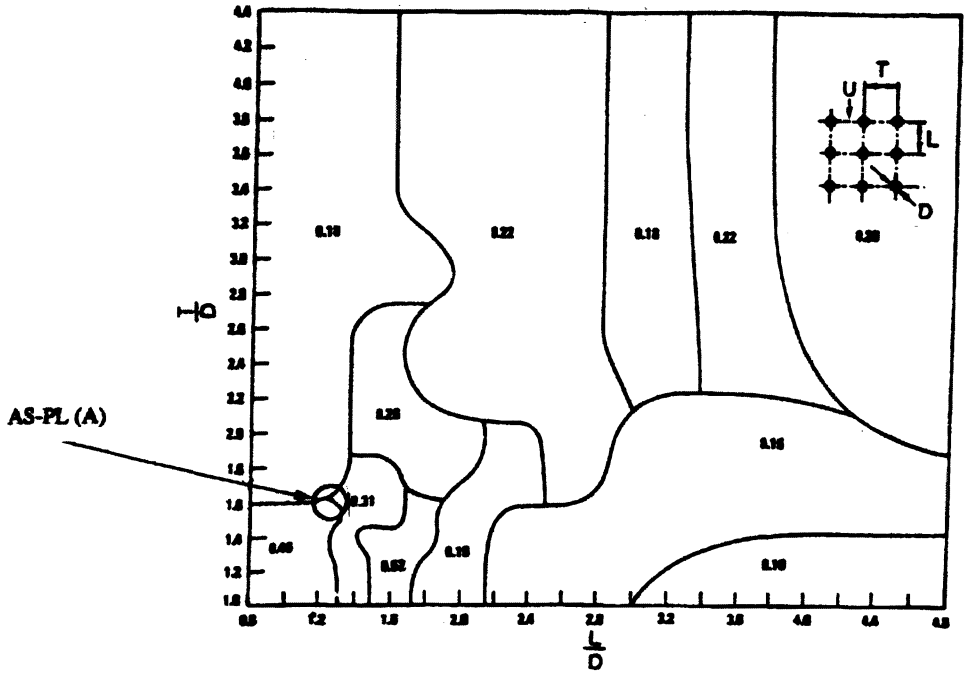

Figure 26. Strouhal number map for inline tube arrays by Fitz-Hugh as presented in Blevins [14]. The difficulties of Strouhal number prediction are emphasized by our estimations shown in the diagram.

8 EXPERIMENTAL RESULTS SUPPORTING THE VORTEX SHEDDING RESONANCE PHENOMENA.

The vortex shedding behavior of a cylinder is a well known and studied phenomena. There are diagrams showing the variations in Strouhal number as a function of Reynolds number [16], in which it can be seen that for a large range of Reynolds numbers the Strouhal number is approximately constant. Since the Strouhal number is constant as well as the reference diameter, a graph of vortex shedding frequency vs. flow velocity is a straight line. Even much more complicated structures such as tube heat exchangers have large periodic eddies in their closely spaced tube arrays. (These periodic eddies have been demonstrated by flow visualization and turbulence measurements as mentioned in [15].). In staggered tube arrays a linear relation is also maintained between the vortex shedding frequency and the velocity of the fluid. Figure 27, for a staggered tube type heat exchanger (from [15]), shows the linear relation between velocity and frequency before the acoustic natural frequency of the cavity is reached. At this point there is a "lock in" phenomena in which the vortex shedding frequency couples to the acoustic natural frequency. As the flow velocity increases further, the shedding frequency abruptly leaps upward when the second transverse mode is excited.

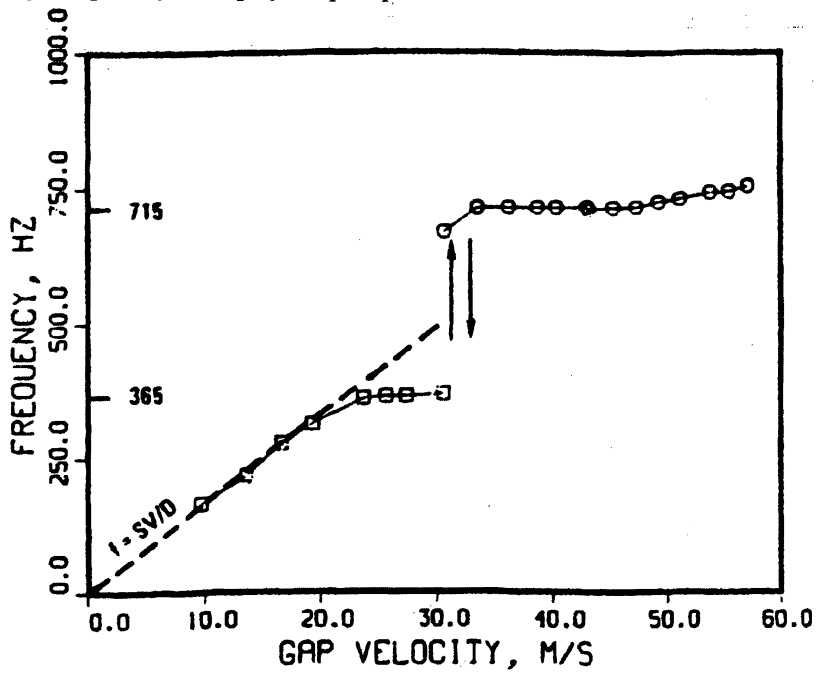

Figure 27. Vortex Shedding as a function of velocity in which the "lock in" effect is shown once resonance begins [15].

The measurements described above were made on large heat exchangers or models of exchanges using microphones or hot wire anemometers to measure the acoustic phenomena. In the case of the plate evaporators which are the subject of this report, measurement difficulties and the original scope of this project, limited measurements to acceleration measurements taken from the surface of the evaporator plates. Measurements of acceleration of the outside plate vibrations are not sensitive enough to separate periodic flow generated vibrations from the random white noise type vibrations generated by turbulence. Our measurement techniques limit our observations to resonant conditions only, since it is here where a measurable acceleration spectrum can be obtained. An extension to this project could explore the flow characteristics inside the plate evaporators using some technique such as hot wire anemometry. By doing inside measurements an accurate method of

determining the Strouhal number could be developed which could help to understand and predict the behavior of different plates geometries, in particular 3-D geometries.

A representative graph for the AS/PL evaporator (which was the easiest tested plate to excite into resonance) is shown in Figure 29. As can be seen, it is of the same form as Figure 27. The Strouhal number for this evaporator can be calculated as the slope of the line drawn on the plot multiplied by a characteristic dimension. In the case of this evaporator the frontal length of the small sausage was chosen as a characteristic dimension. A complete set of frequency-velocity graphs is presented in Figures 28 to 39 along with the schematic diagrams that show the different geometries of each plate heat exchanger.

The frequency-velocity diagrams were made by picking the frequencies in which the highest peak in the values of acceleration were detected in the acceleration-frequency diagrams.

AS/PL Plate Evaporator

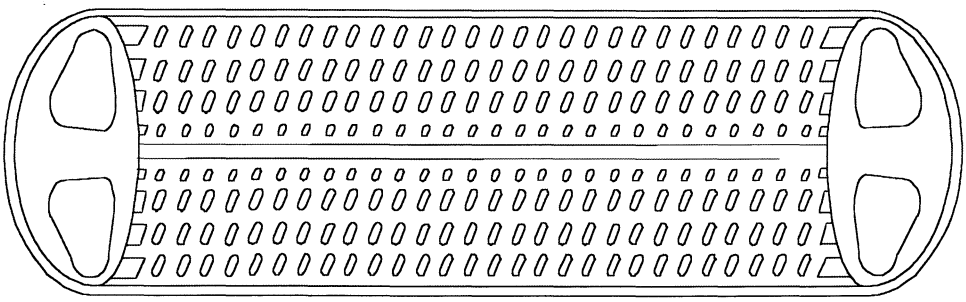

Figure 28.Schematic drawing of AS/PL plate to show details of flow obstructions. The flow enters one side and exits the other side. The two passages are not connected. For our testing only one passage was used.

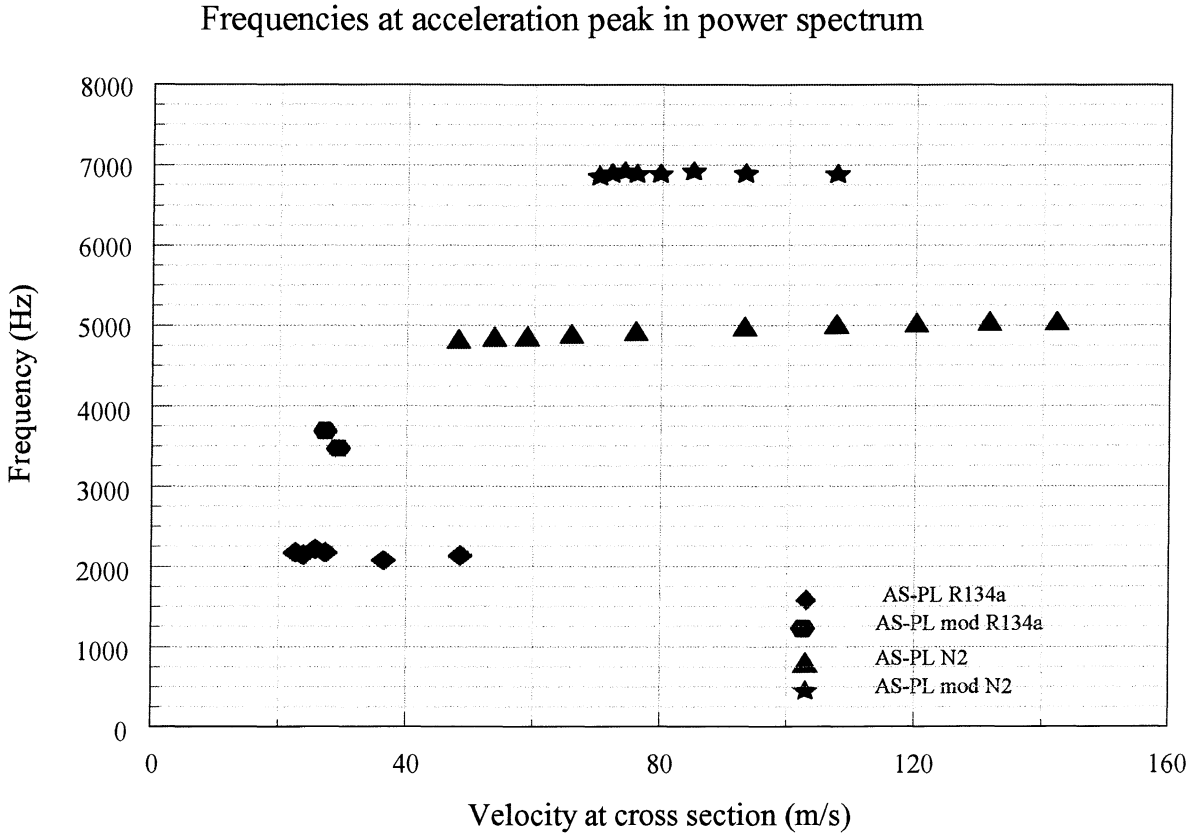

Figure 29. This diagram contains the frequencies at which the peaks in acceleration were found in the power spectra of the different tests. The differences in the frequencies are explained due to a variation in the channel width by the introduction of a wire in the center of the modified AS/PL plate evaporator and also to the change in speed of sound of the different fluids.

JA Plate Evaporator

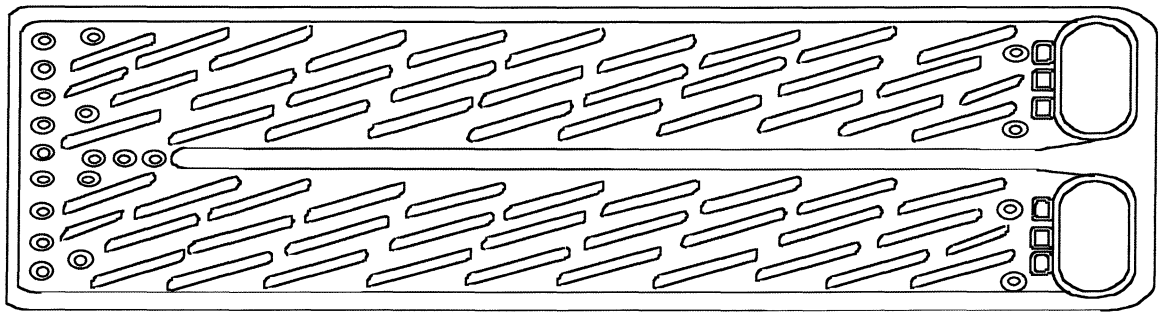

Figure 30. Schematic drawing of JA plate to show details of flow obstructions.

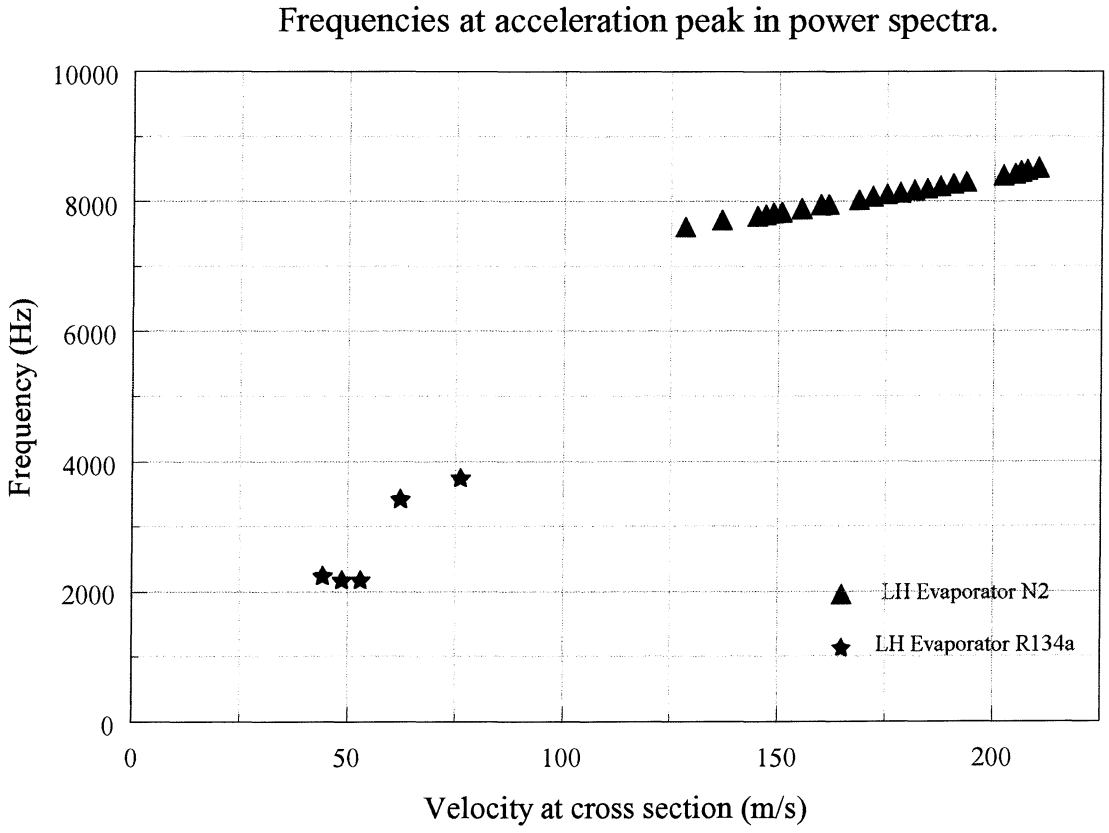

Figure 31. This diagram contains the frequencies at which the peaks in acceleration were found in the power spectra of the different tests.

LH Plate Evaporator

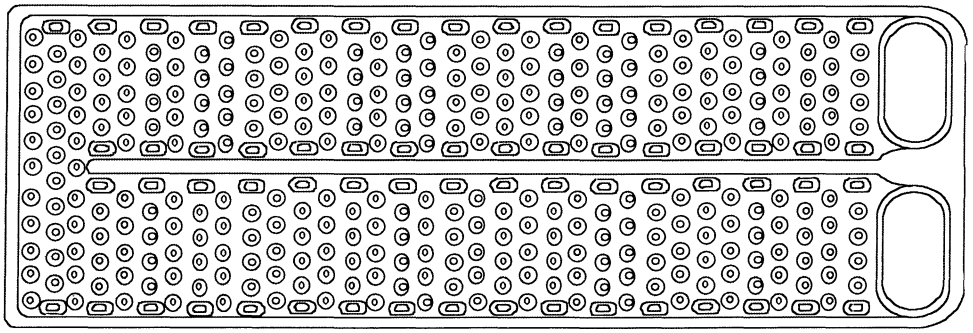

Figure 32. Schematic drawing of LH plate to show details of flow obstructions.

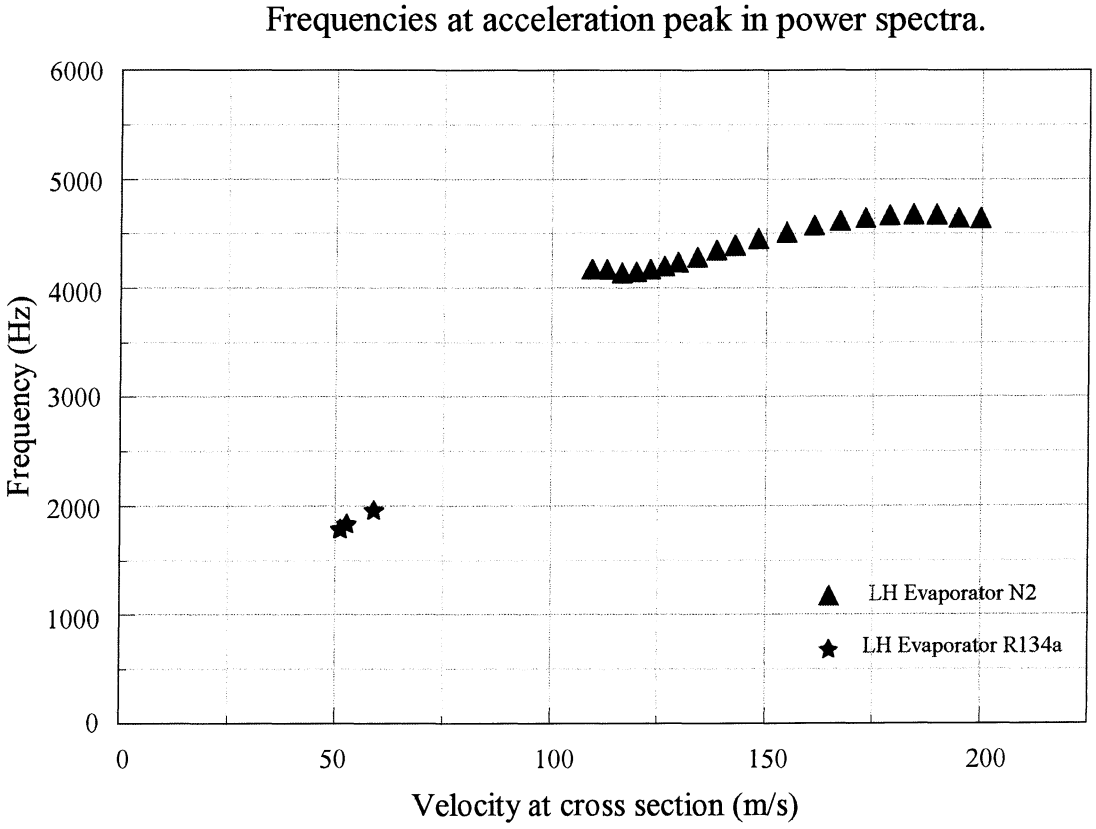

Figure 33. This diagram contains the frequencies at which the peaks in acceleration were found in the power spectra of the different tests.

NSF-1 Plate Evaporator

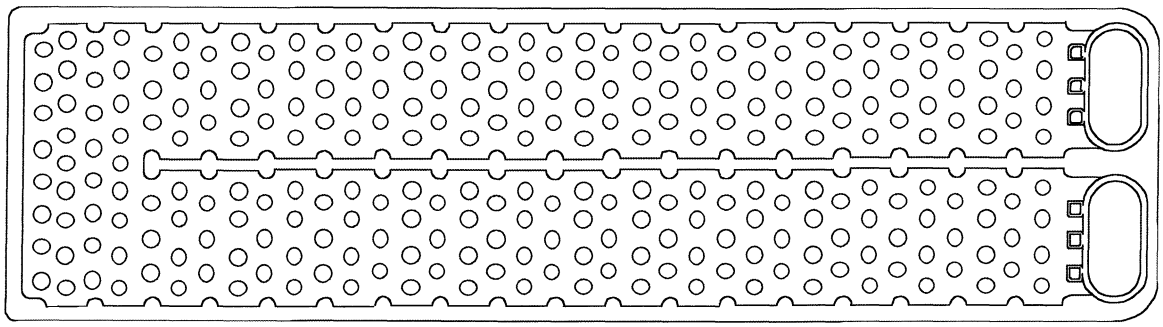

Figure 34. Schematic drawing of NSF-1 plate to show details of flow obstructions.

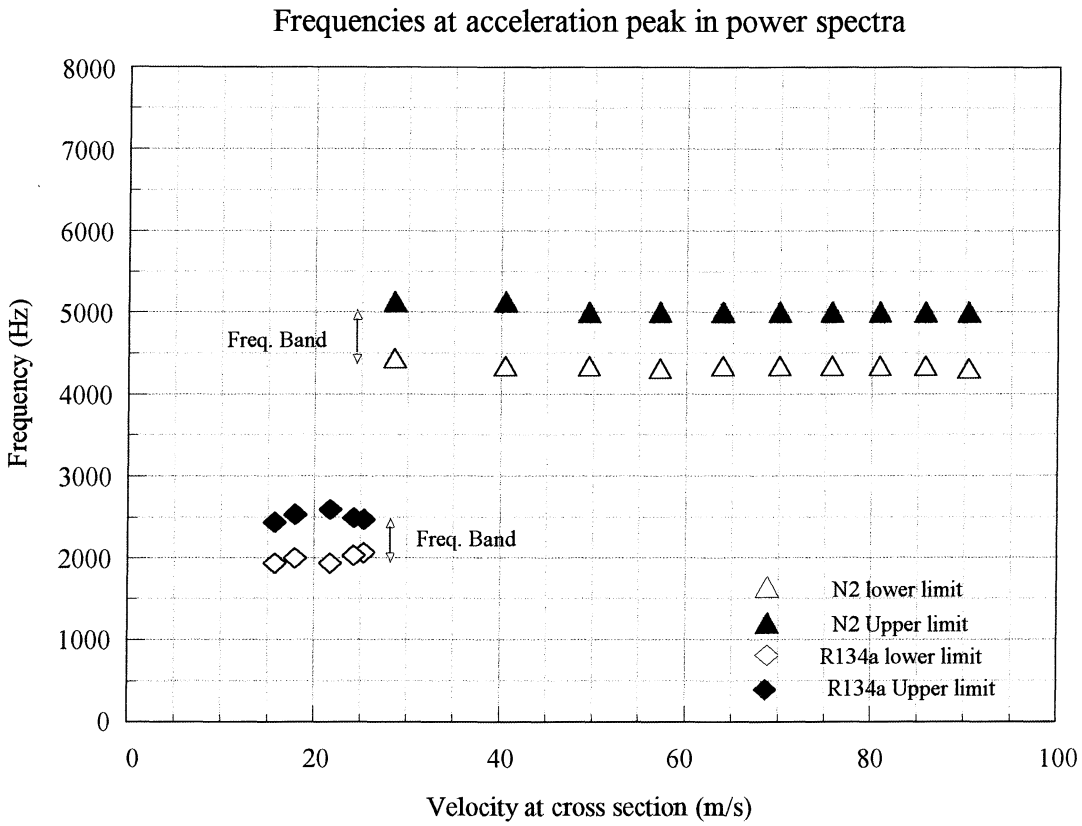

Figure 35. This diagram contains the frequencies at which the peaks in acceleration were found in the power spectra of the different tests. The spectra exhibit closely spaced peaks indicated as "frequency bands" in figure above.

NSF-2 Plate Evaporator

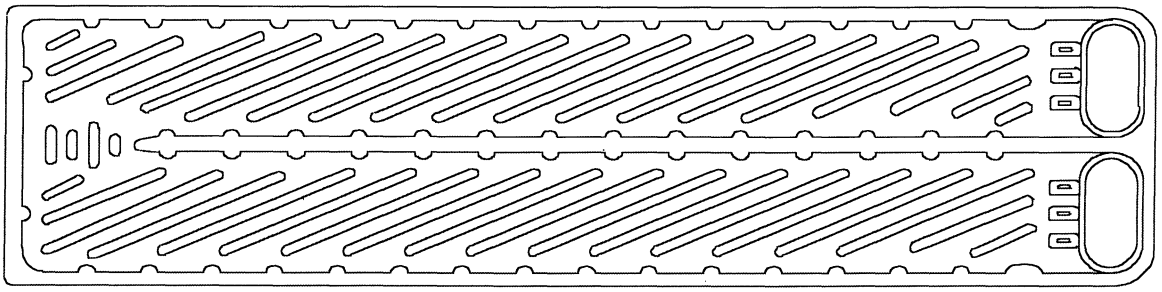

Figure 36. Schematic drawing of NSF-2 plate to show details of flow obstructions.

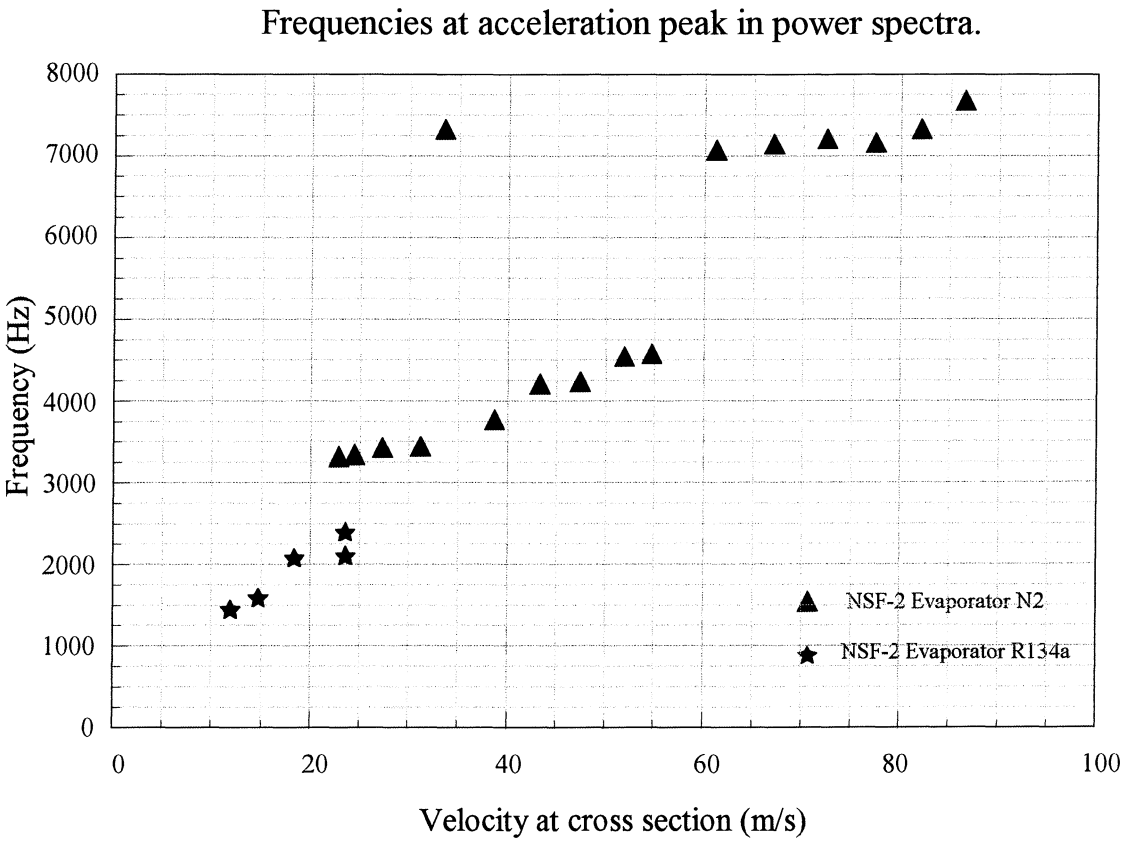

Figure 37. This diagram contains the frequencies at which the peaks in acceleration were found in the power spectra of the different tests.

NSF-3 Plate Evaporator

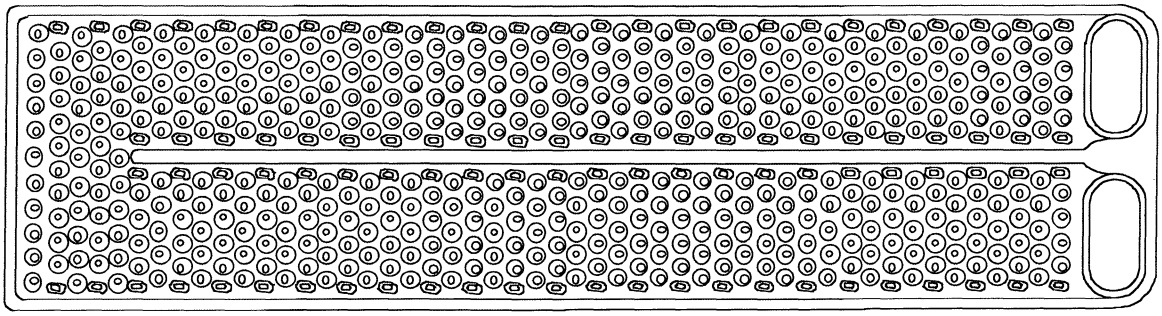

Figure 38. Schematic drawing of NSF-3 plate to show details of flow obstructions.

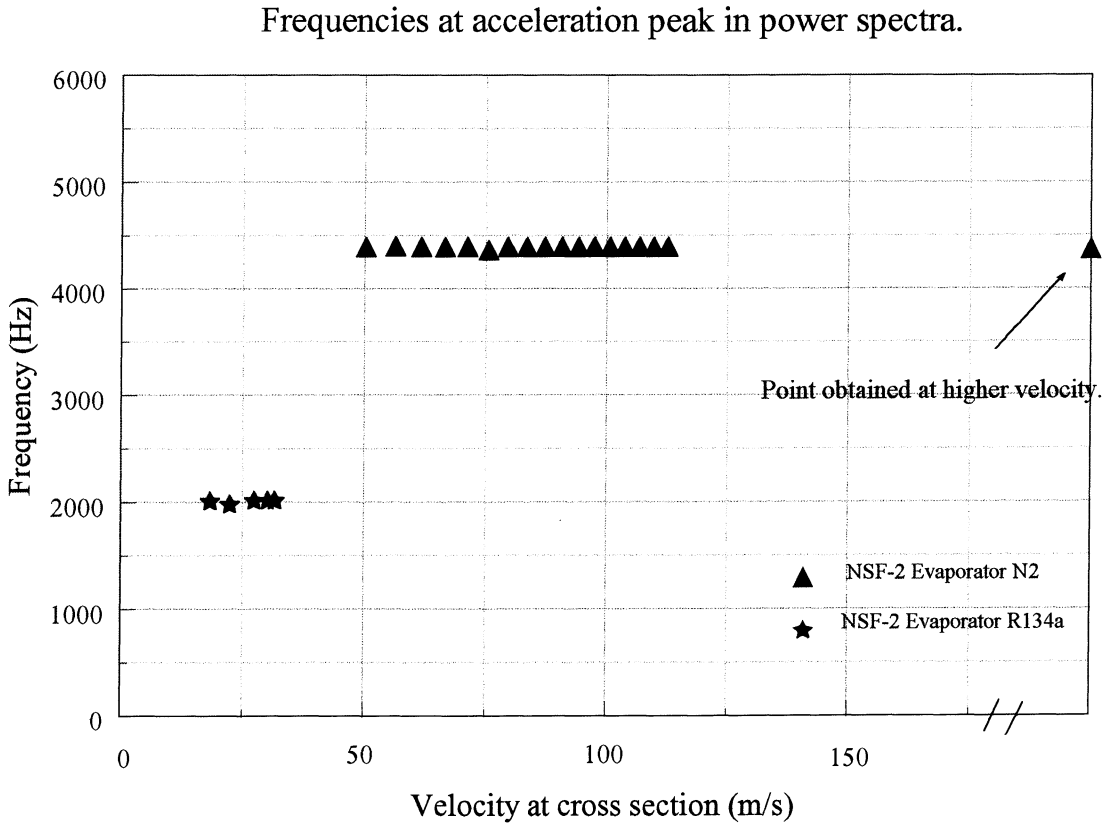

Figure 39. This diagram contains the frequencies at which the peaks in acceleration were found in the power spectra of the different tests.

A very important result of Figures 28-39 (frequency-velocity diagrams) is that nitrogen test data falls in line with refrigerant data. Using the Strouhal number as the proportionality constant to relate the frequency against the velocity over the diameter, it can be seen that the onset of resonance does not depend on the fluid and that the periodic flow disturbance appears to follow a linear relationship between these parameters. A single dominant Strouhal number appears to exist over the typical operating range of a given heat exchanger. This result supports the vortex shedding induced acoustic resonance theory since the measurements of the accelerations produced on the surface of the plate evaporators at resonance for the two fluids agree (see Figure 29 for example). This also demonstrates the usefulness of the much simpler, faster and cheaper nitrogen tests. However, due to the different damping characteristics of the two fluids our acceleration data does not allow us to compare the actual magnitude of the sound power produced by each fluid. It has also been reported in the literature (Ziada [17,18]) that sometimes, due to damping, the first mode is not excited, but higher modes are. This is explained by the reduction in damping for higher modes as reported by Blevins [12]. This later fact makes some actual refrigerant tests a requirement.

Another fact that supports the vortex induced acoustic resonance hypothesis is that the resonant frequency ratios are in agreement with the speed of sound ratios of the two fluids as can be seen in Table 2 (pp. 16).

It is interesting to note the frequency bands in Figure 35. These frequency bands are believed to be the result of resonances occurring at different frequencies due to the variations in transverse dimensions. Figure 34 shows that the side walls of this plate heat exchanger have "speed bumps" on the sides, this continuous variation in the transverse dimension which supports the resonance produces a continues band of possible resonance frequencies. This type of reflecting walls, in other words, seems to spread the resonant frequency, and by doing this, the response in the form of large accelerations in the plate walls, which leads to large sound power generation, is limited. Further the generated sound is broadband instead of harmonic. (A hiss rather than a whistle.) This behavior supports the concept of modifying the side walls of the heat exchanger to influence the acoustic character of the heat exchanger. The frequency band can also be seen in the nitrogen tests. A representative spectrum showing the frequency band appears in Figure 40. Additional spectra can be seen in the refrigerant acceleration spectra graphs for NSF-1 plate evaporator G1 to G5 tests in Appendix I and the NSF-1 N2 Test in Appendix II.

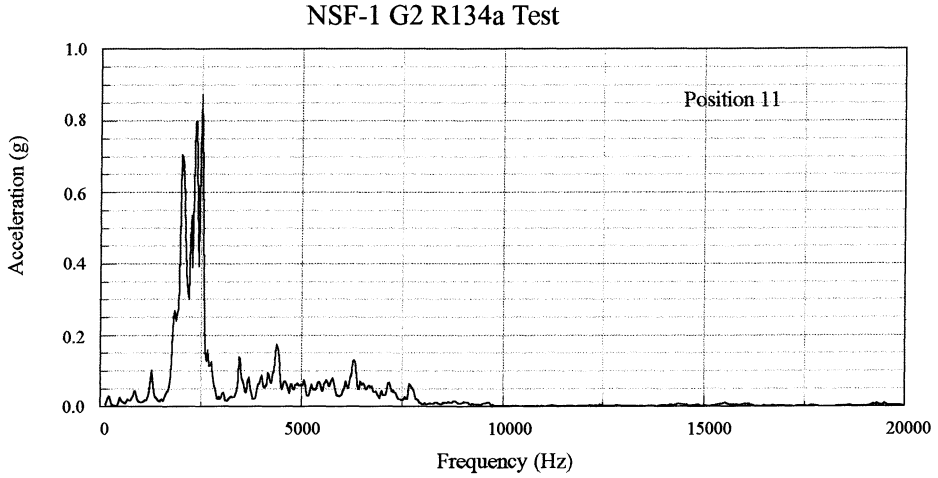

Figure 40. Acceleration power spectrum showing a resonance frequency band.

Other frequency bands are formed as shown in Figure 41. Figure 41 is the acceleration power spectrum of an early test of the AS/PL modified plate evaporator in which the flow moves through a complete channel with a wire in the middle and also through a half channel made with a regular plate joined with a flat plate making what was defined as a half plate (1.5 test sections). Here, we could see the combined effects of the half plate behaving as a regular AS/PL heat exchanger and the section with the wire in the middle behaving as an AS/PL modified evaporator. It was found that the sharp resonance peaks in the spectrum at about 2000 Hz agree exactly with the single plate AS/PL evaporator tests done later and the frequency behavior of the peak which has the broader base near 3500 Hz agrees with the AS/PL modified evaporator. It is believed that this broadening of the frequency band is due to the curvature of the wire, possibly also due to the leakage of fluid past the wire increasing the system damping, and perhaps the fact that the two sections of the plate cavity created by the wire are not of equal width (see below).

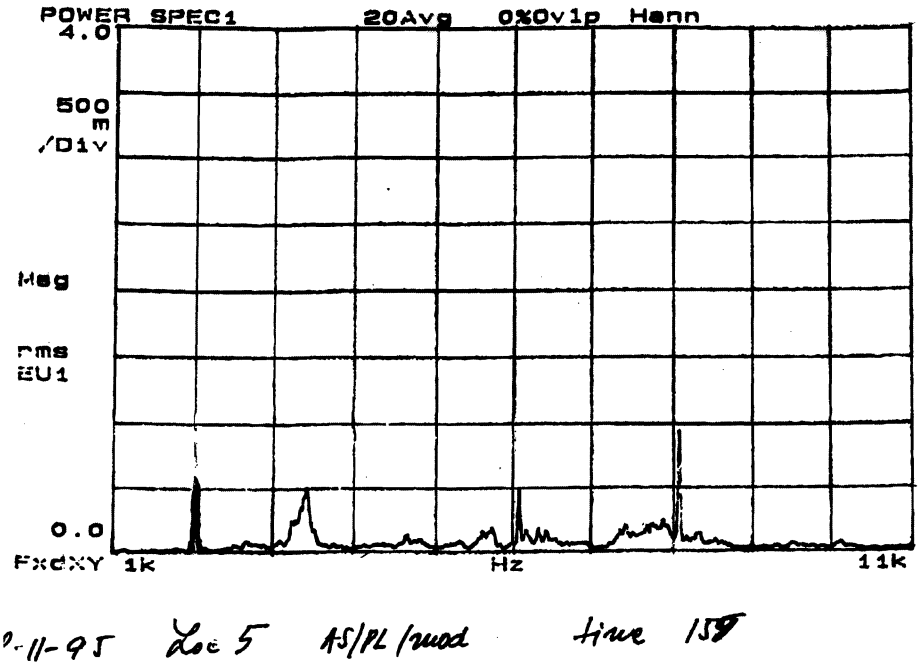

Figure 41. Acceleration power spectrum of 1.5 plate AS/PL modified evaporator.

Figure 29 shows the behavior of plate evaporators AS/PL and AS/PL modified. One fact to notice here is that the frequency of the modified plate is not exactly double the frequency of the unmodified AS/PL. This could be explained by the fact that when the wire is introduced, the position of this wire does not divide the chamber into symmetrical halves, and therefore the natural acoustic frequency of this cavity should not be twice the other. Another important fact to note is that since the wire does not introduce a solid wall to divide the chamber, it is believed that the fluid inside can be exchanged between chambers producing a very significant source for damping which is known to affect the amplitude and the frequency of resonance. Finally, even though four refrigerant tests were made for the modified AS/PL, only two points are shown in the diagram (Figure 29). This is due to the fact that a distinctive peak is hard to detect, see Appendix I, AS/PL modified refrigerant acceleration power spectra graphs B1 to B4 tests.

Figure 37 shows the very complicated behavior of the NSF-2 "E - Large sausages" plate evaporator. For this plate heat exchanger a clear resonant condition is shown in tests E4 and E5 (see Appendix I, NSF-2 refrigeration acceleration power spectra diagrams) and these resonance conditions do not agree with any of the predicted resonances for this case as shown in Table 5. This fact implies that either the effective speed of sound estimate is not accurate or that the resonance in this particular case has a different characteristic dimension. This is possible since the large sausages may act as walls that support a resonance between them. Another important concern in this case is the excitation mechanism. For this geometry a more strongly three dimensional flow is established due to the cross pattern. In addition, the "speed bumps" on the side walls are staggered instead of in line as in the case of the NSF-1 plate evaporator (Figure 34). Since for this geometry a three dimensional flow is experienced, it is not understood at this point how this flow periodicity acts. This idea is strongly supported by the fact that even for two dimensional geometries there is controversy about the excitation mechanisms, as is described for example in Ziada [17,18], in which some discrepencies are described between in-line and staggered tube arrays regarding their resonance behavior in conjunction with the excitation mechanism or flow periodicities.

9 FACTORS WHICH MAY REDUCE THE WHISTLING PHENOMENA - GUIDELINES FOR DESIGN

The whistling phenomena in an evaporator plate is the result of the frequency of the flow periodicities that result when the fluid passes through the flow obstructions in the plate cavity (dimples, hot dogs, etc.) matching one of the transverse acoustic natural frequencies of the evaporator cavity. It is known that vortex shedding is one possible mode of flow periodicity and that the frequency of this type of flow phenomena is a linear function of flow velocity. There is still controversy about the exact mechanism of excitation, but if vortex shedding is assumed as some evidence shows, then if the flow rate is increased from zero, resonance will only begin when the vortex shedding frequency reaches the first transverse natural frequency of the cavity. Once this resonance is established, it persists as the flow velocity is increased due to the "locking" of the shedding frequency to the cavity resonance frequency.

There are cases when this straight forward approach does not apply as seen for example in Ziada et al [17,18]. The difficulties are due to the fact that sometimes the first mode of resonance does not seem to be excited and resonance is produced when the flow periodicity matches the second mode; this is believed to be caused by the different damping for each mode which vary significantly [17]. Other difficulties are due to the fact that sometimes several excitation frequencies are created by flow periodicities. Thus a unique excitation frequency does not exist for each flow velocity through a given heat exchanger geometry. In order to investigate this phenomena, measurements of flow velocity and or sound pressure inside the heat exchanger are needed to determine the behavior of the flow periodicities.

According to the vortex shedding excitation induced whistling theory, whistling can be avoided in two ways.

- By keeping the vortex shedding frequency below the first transverse acoustic natural frequency of the plate cavity.
- By reducing the strength of or completely eliminating the acoustic natural frequencies, or moving them to higher frequencies.

9-1 METHODS FOR KEEPING THE VORTEX SHEDDING FREQUENCY BELOW THE ACOUSTIC NATURAL FREQUENCY OF THE PLATE CAVITY

For a given refrigerant mass flow rate, the vortex shedding frequency can be reduced by:

- Increasing the channel cross sectional area so that the flow velocity is reduced.
- Adding more plates to reduce the flow velocity in each channel.
- Modifying the geometry of the flow obstructions (dimples, etc.) in such a fashion that the rate of increase of shedding frequency with refrigerant flow rate is reduced, maybe by trying random dimple patterns.

None of these alternatives are very attractive. Increasing the channel cross section or number of plates will probably produce a reduction in heat transfer capacity. We know very little about how changes in the geometry of the flow obstructions will change the relationship between vortex shedding frequency and flow velocity. We will discuss how a better understanding of these relationships might be developed below.

9-2 METHODS FOR MODIFYING THE ACOUSTIC NATURAL FREQUENCY OF THE EVAPORATOR CAVITY

The cavity natural frequency is well understood and can be manipulated in many ways.

- The cavity width could be reduced (and its height increased to maintain cross sectional area) so that the first natural frequency of the cavity would be increased.

- The shape of the reflecting walls of the cavity could be modified to make them more concave or convex so as to avoid flat, perpendicular, walls which are classic requirements for standing acoustic waves.

- The channel width could be made to vary in the direction of refrigerant flow. This would reduce the length of the channel which would be subject to resonance at any particular natural frequency. The concept is to reduce the volume of refrigerant supporting a standing acoustic wave. This in turn would reduce the surface area of the plate vibrating at the whistle frequency and hence the total sound power radiated to the environment.

All these techniques could be successful, but the latter two seem less likely to reduce the capacity of the heat exchanger.

One final possibility might involve manipulating the effective speed of sound to change the cavity natural frequency. This technique is not very attractive since it would effect the plate structure and the shedding frequency, flow velocity relationship.

10 DIRECTIONS FOR FUTURE WORK

The focus of this study was to understand the nature of the whistling phenomena and to attempt to formulate some guidelines for evaporator plate design. We feel that the flow induced noise hypothesis for evaporator whistling has been adequately supported. We have supplied some design guidelines, but the goals and resources available for this study did not permit us to gather the data and formulate the theory necessary for quantitative design rules for evaporator plates.

Two general areas merit further study:

- The geometry of the evaporator plate. This includes the shape and distribution of flow obstructions, the shape of the evaporator walls, and the variation of channel cross section along the direction of the refrigerant flow.

- System considerations. This includes the design of the evaporator as well as the influence of the expansion valve, compressor, etc.

10-1 INFLUENCE OF GEOMETRY ON THE PERIODIC FLOW FREQUENCY-FLOW VELOCITY RELATIONSHIP

10-1-1 INVESTIGATION OF THE SHAPE OF THE FLOW OBSTRUCTIONS.

It has been demonstrated that the relationship between periodic flow frequency at a given refrigerant flow rate and the size, shape and packing of the flow obstructions (dimples, hot dogs, etc.) is poorly understood at best. It is felt that an understanding of the geometric factors affecting this relationship could be developed economically through a series of tests on models. It is felt that these model studies could use nitrogen as the fluid. This would greatly simplify the models since they would not need to be pressure vessels. Characteristics of the flow obstructions which could be studied include:

- shape of the support (dimple, sausage, hot dog, other...)

- packing pattern.

- packing density

10-1-2 INVESTIGATION OF THE REFLECTING WALL GEOMETRY

A careful study of the effect of the wall geometry on cavity resonance could be conducted. Concave or convex walls (such as shown in the cavity cross section below) could be studied using models and nitrogen as the fluid.

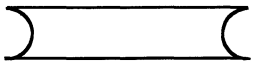

10-1-3 INVESTIGATION OF THE INFLUENCE OF VARIATION OF CHANNEL CROSS SECTION ALONG THE DIRECTION OF THE REFRIGERANT FLOW

It is felt that the width of the plate channel could be continuously varied in the direction of refrigerant flow. It is felt that there must exist some optimum geometry which would maximize heat transfer while keeping the whistling phenomena within acceptable limits.

Once again, it is felt that model studies using nitrogen as the fluid could be profitably employed. The position, angle and the shape of the separating baffle, and channel geometry could all be studied and their influence quantified. Some examples of proposed geometries appear below.

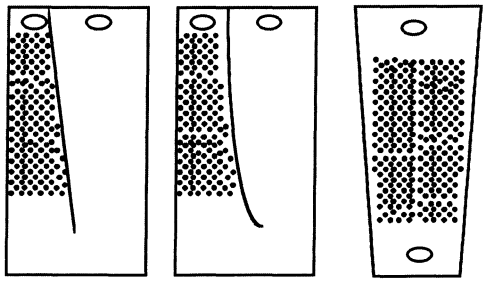

Note: This proposed design has been disclosed to the University of Illinois and to Chrysler Corporation for review for possible patenting.

10-2 SYSTEM APPROACH

In addition to investigations of the details of plate design, an investigation of the various system aspects could provide insight into the nature of acoustic problems. In particular, the design of the evaporator may well effect the nature of the flow through individual plates. Situations may develop in service in which the flow of refrigerant is poorly distributed and may result in a condition of acoustic resonance in one or more plates.

The interaction of the evaporator with system components such as the compressor, condenser, evaporator, and TEV / orifice tube merit more investigation.

10-3 SOUND POWER

The customer is not concerned with how a refrigeration system produces an objectionable whistling sound. He or she is interested only in the sound pressure which reaches their ears. In this report, we have demonstrated how surface evaporator plate acceleration measurements can be used to estimate the sound power radiated from the plate. It would be valuable to make system sound intensity measurements (from whole evaporators and from evaporators mounted in production enclosures), and to relate those measurements to an empirically based theory of sound generation by the evaporator and other system components.

Appendix I

Acceleration Power Spectra, Refrigerant Tests

AS/PL A1 R134a Test

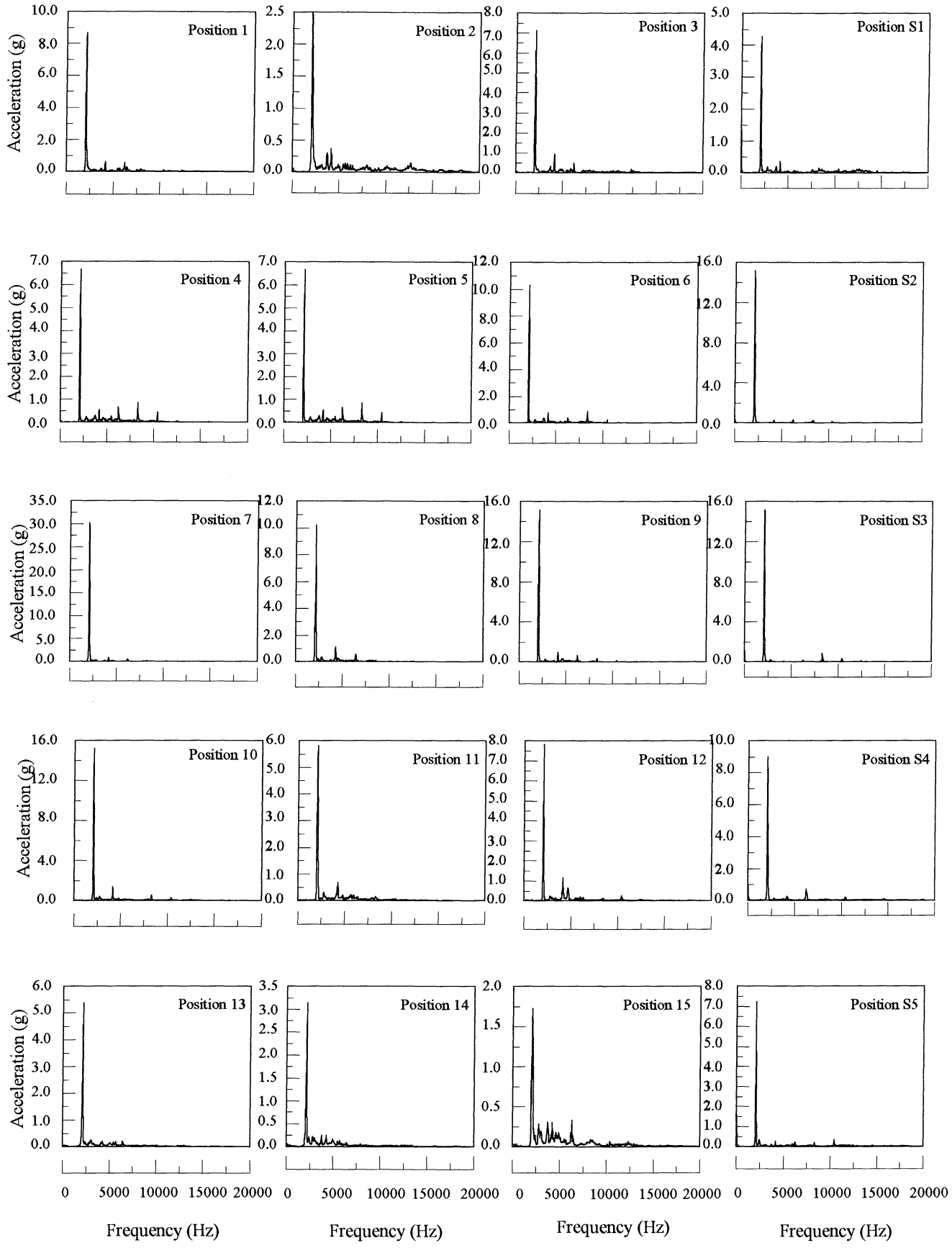

AS/PL A2 R134a Test

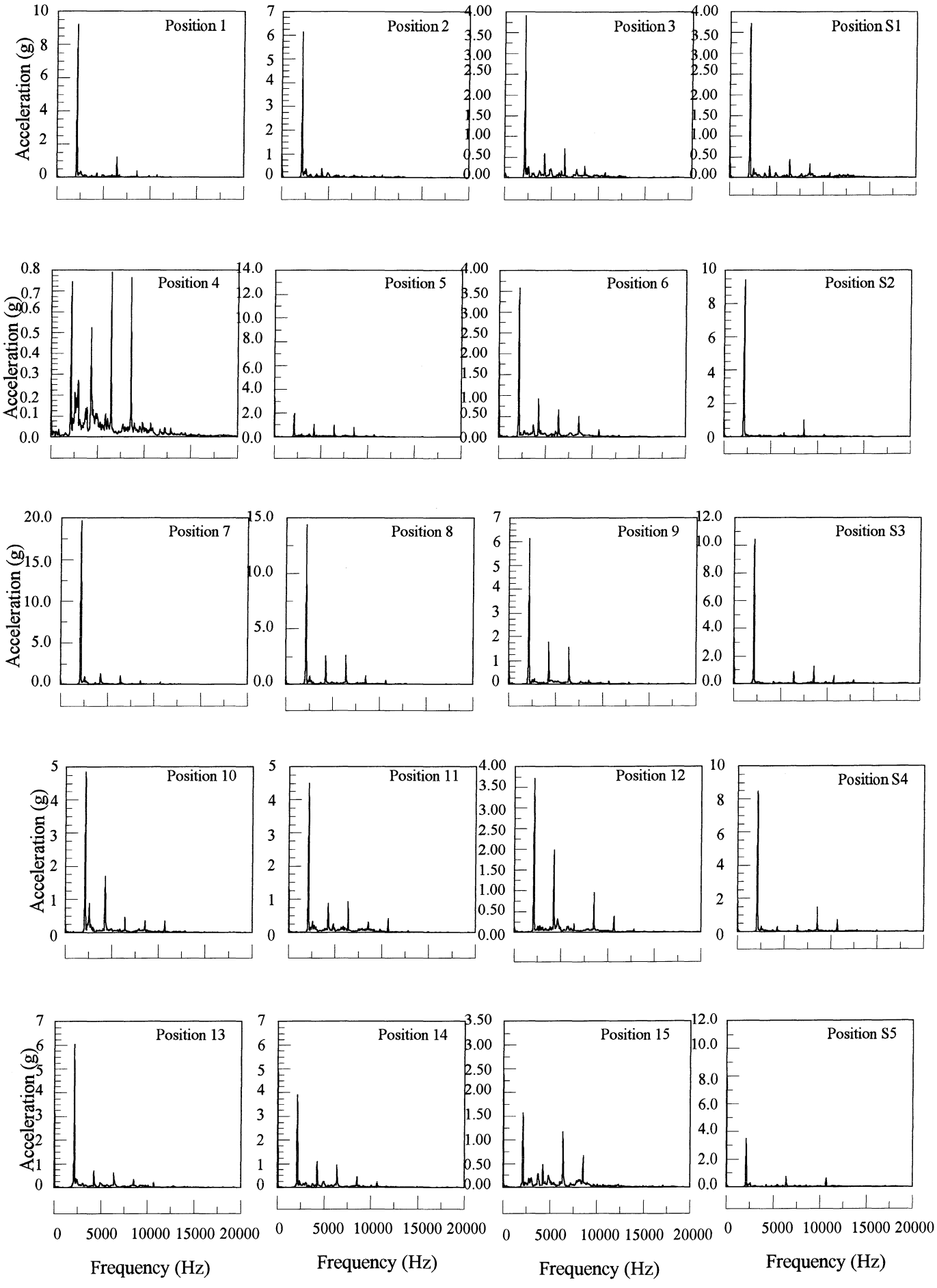

AS/PL A3 R134a Test

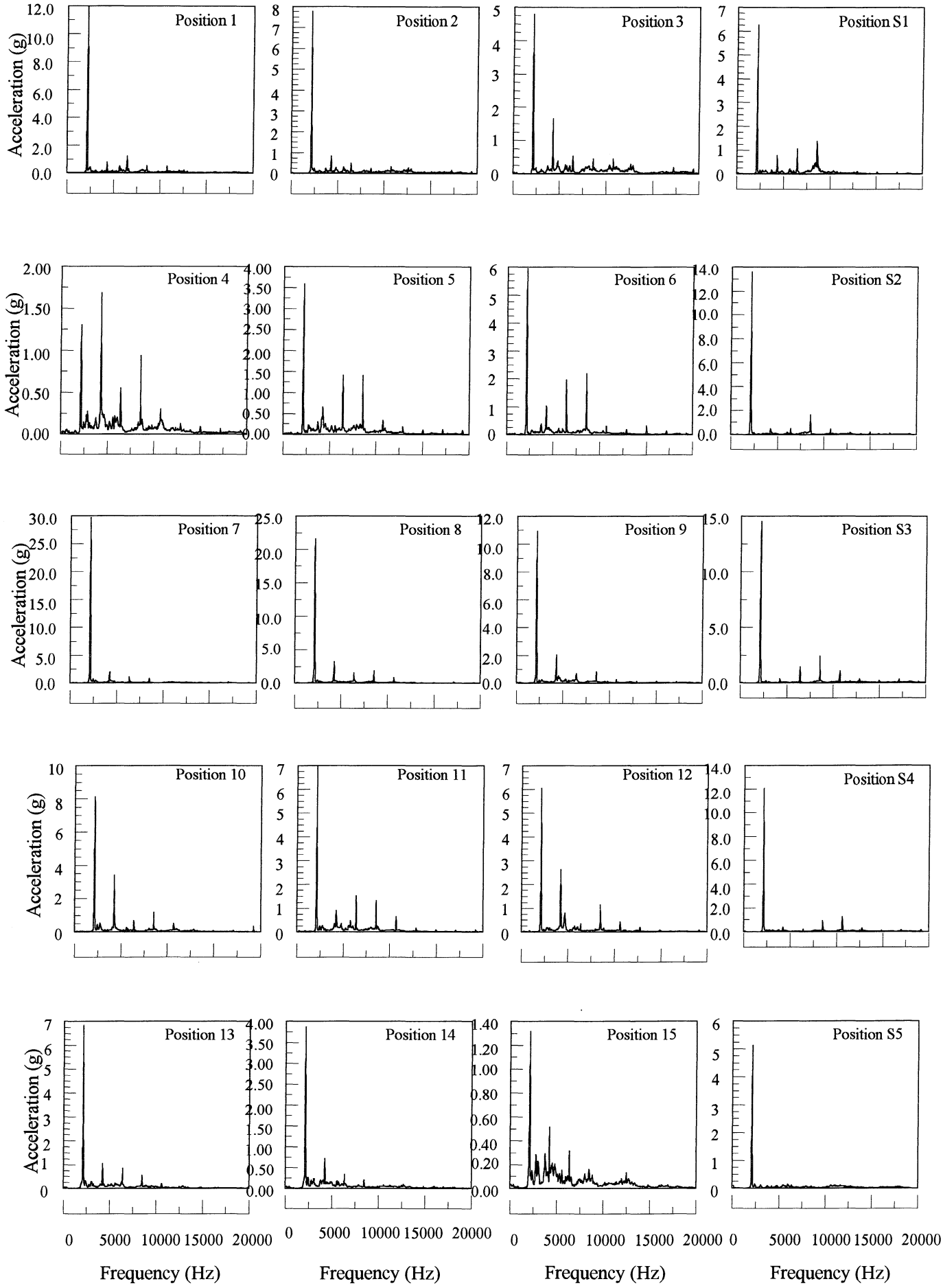

AS/PL A4 R134a Test

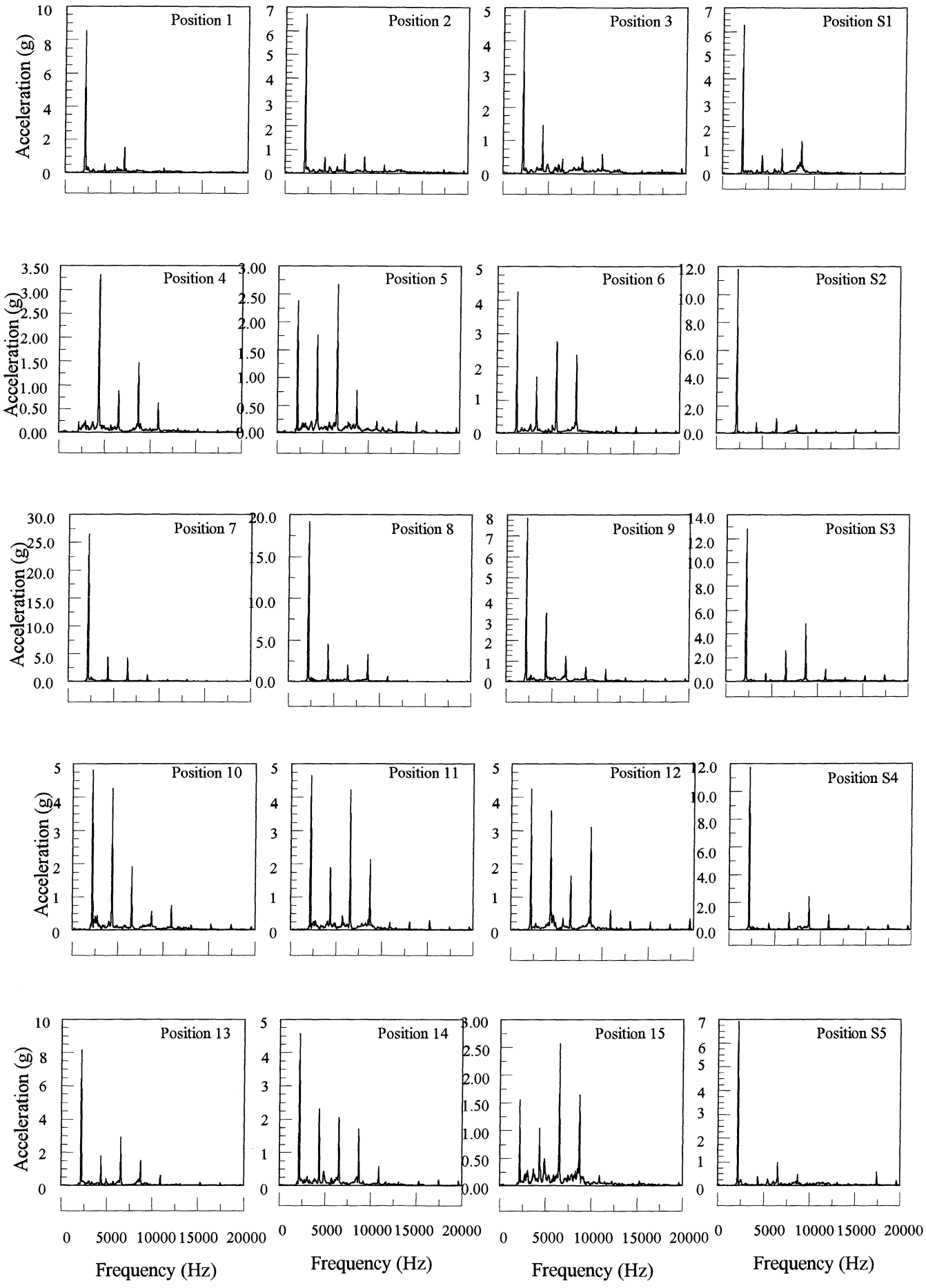

AS/PL A5 R134a Test

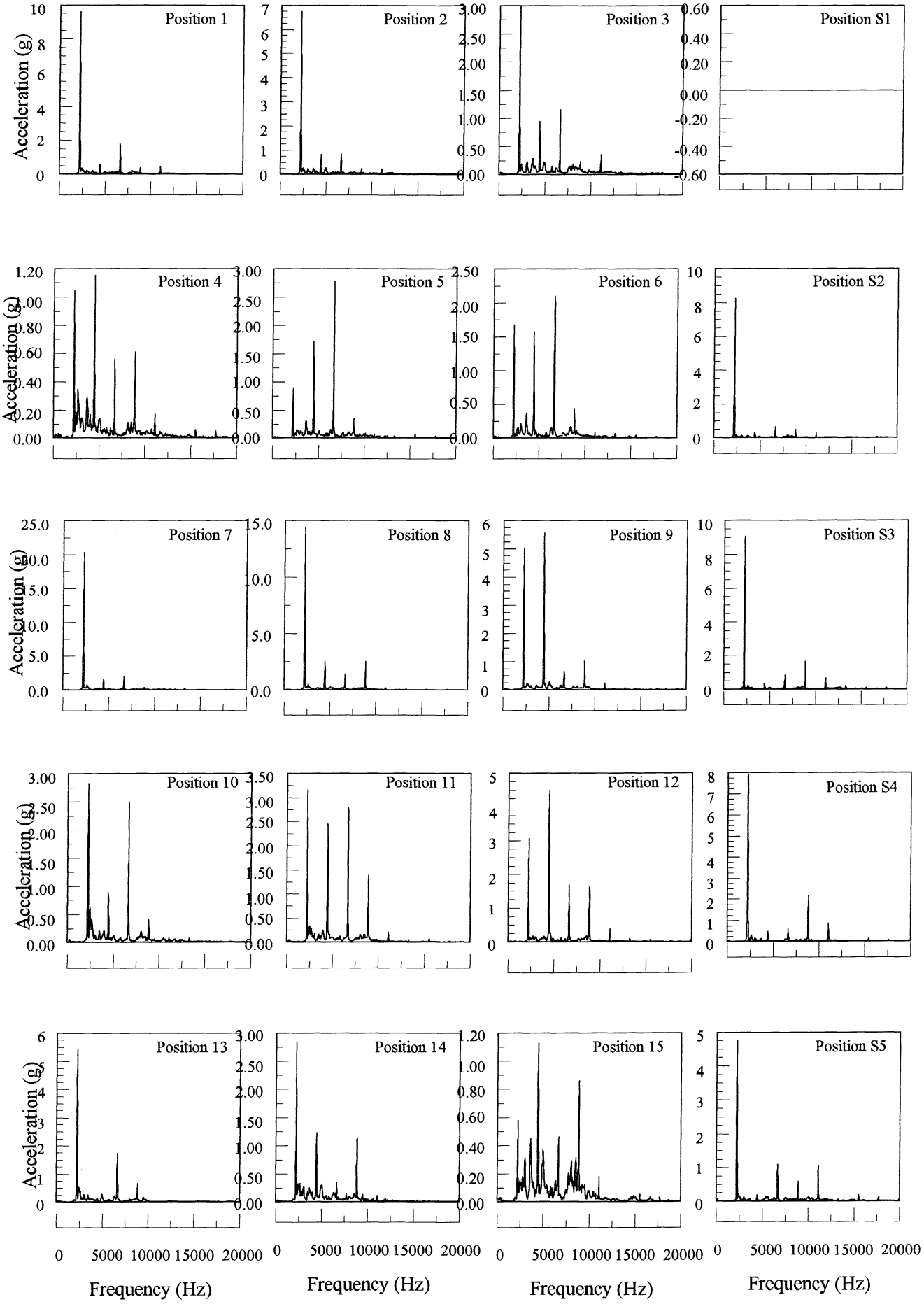

AS/PL A6 R134a Test

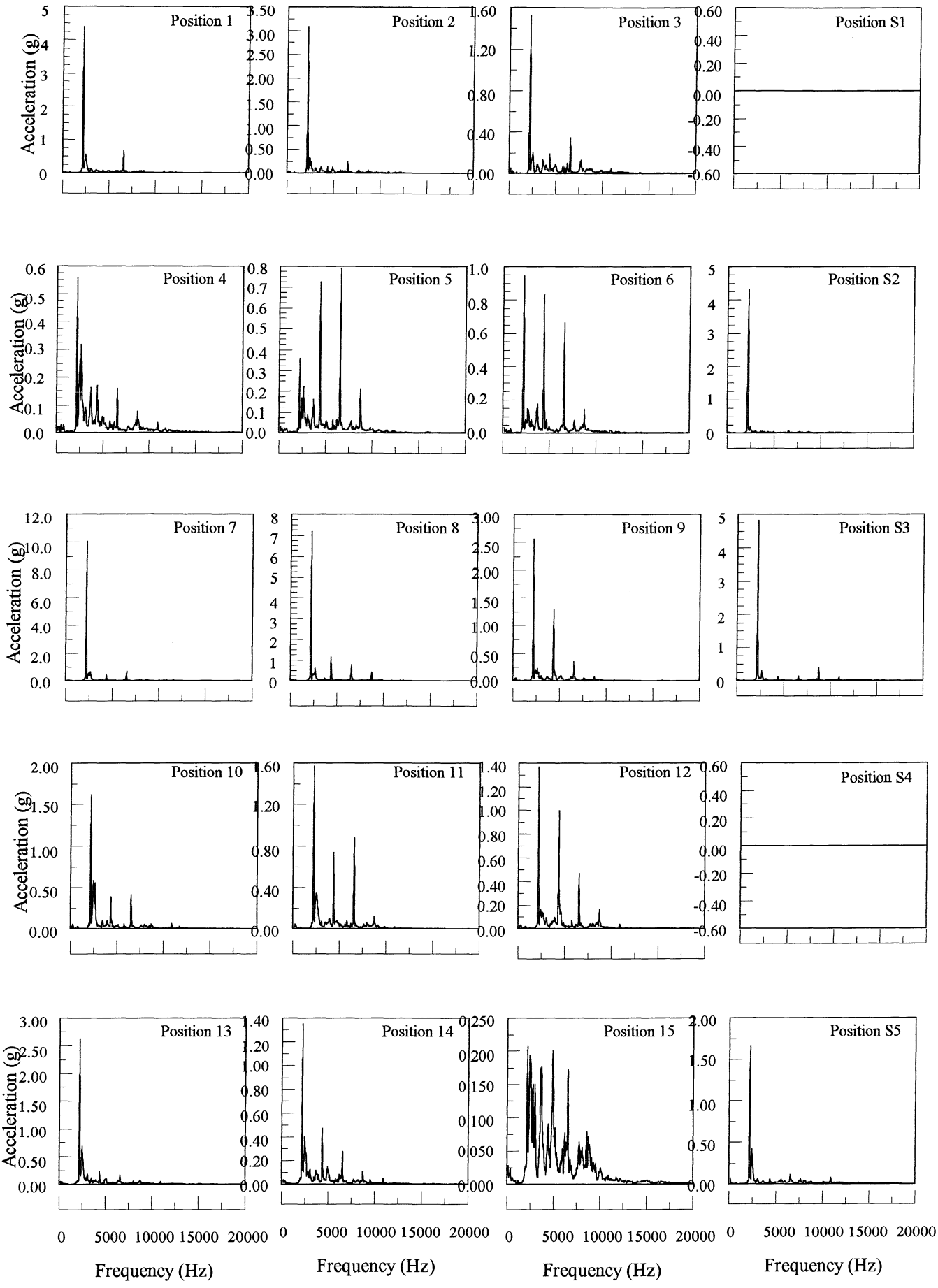

AS/PL mod B1 R134a Test

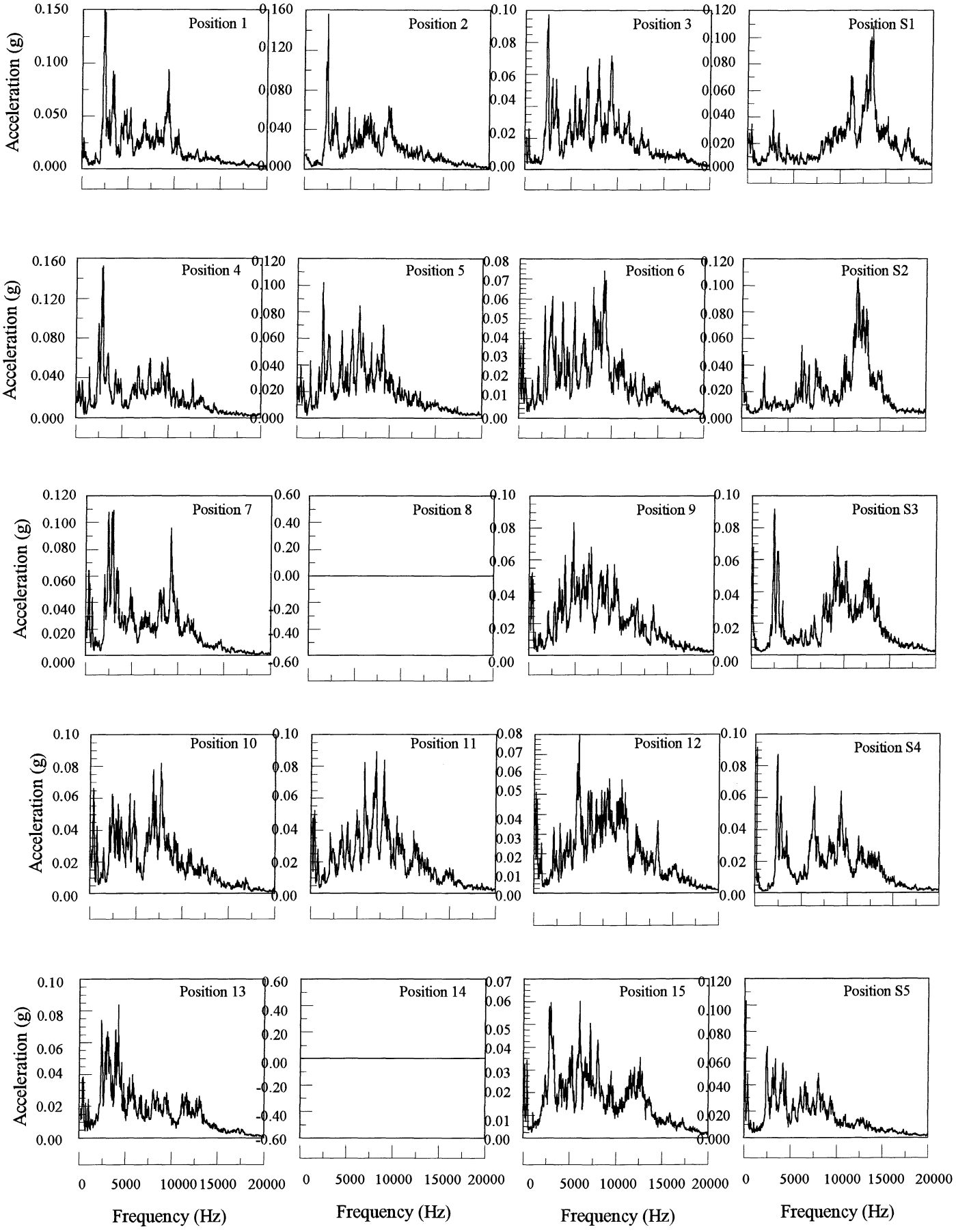

AS/PL mod B2 R134a Test

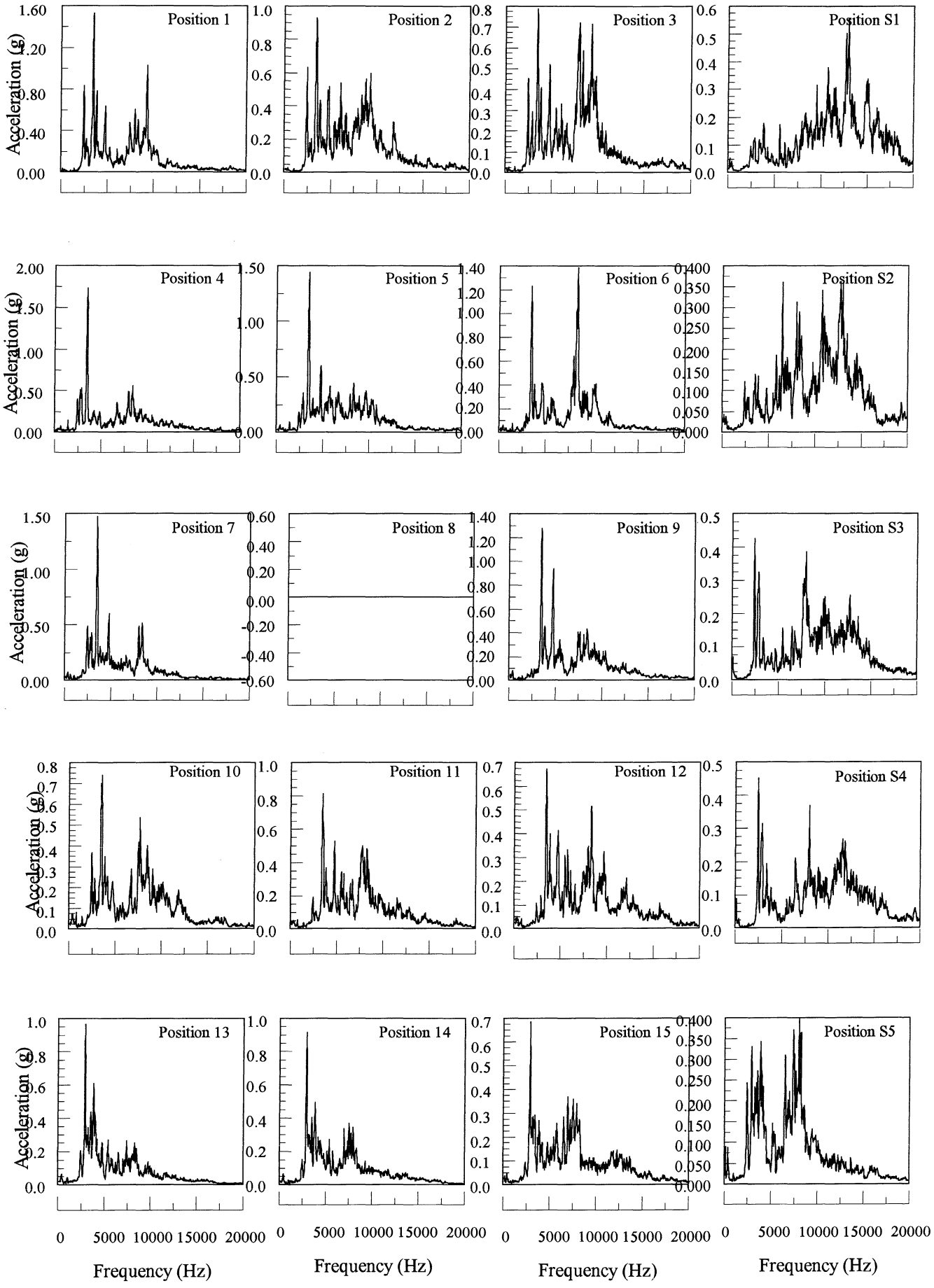

AS/PL mod B3 R134a Test

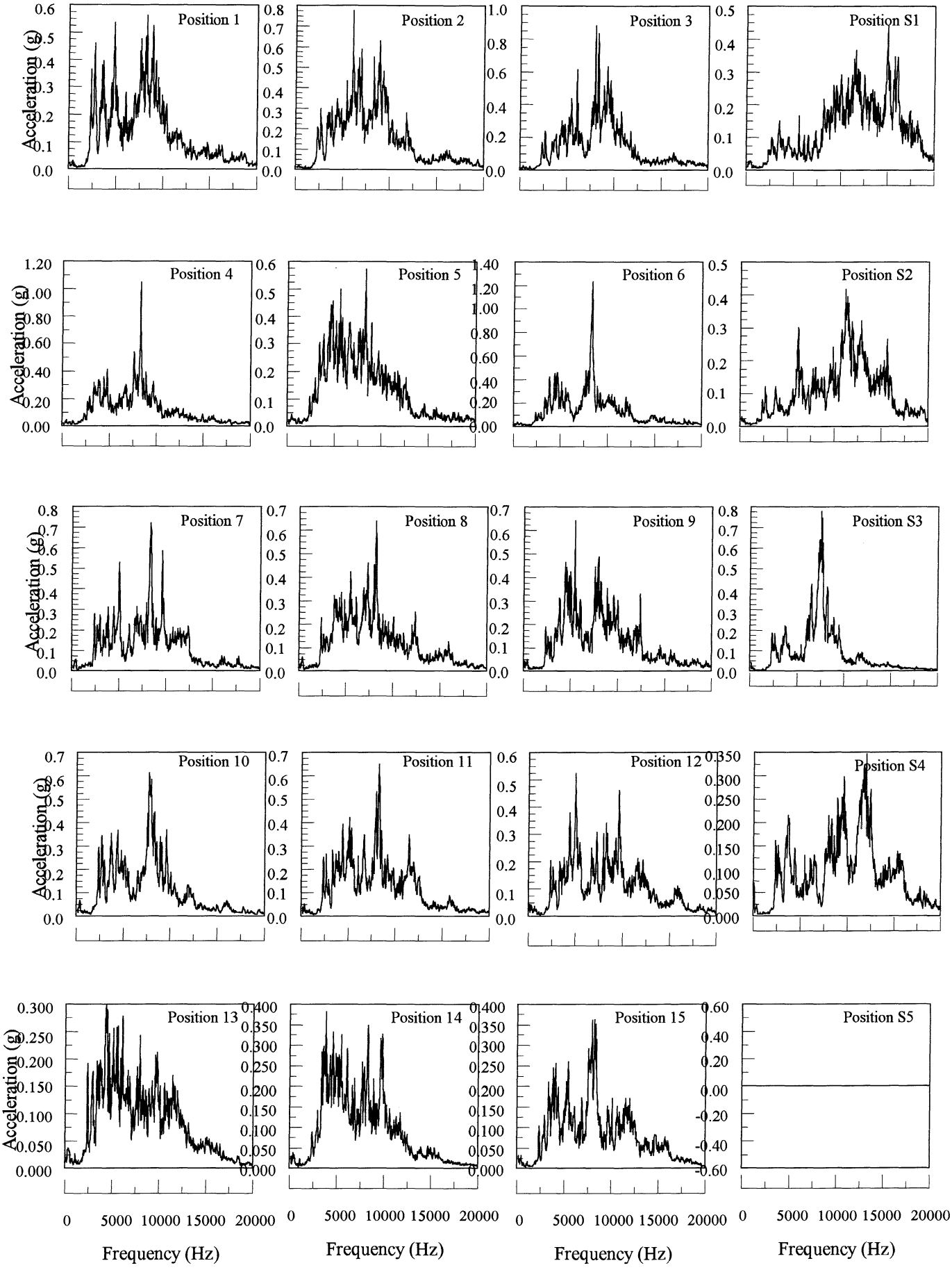

AS/PL mod B4 R134a Test

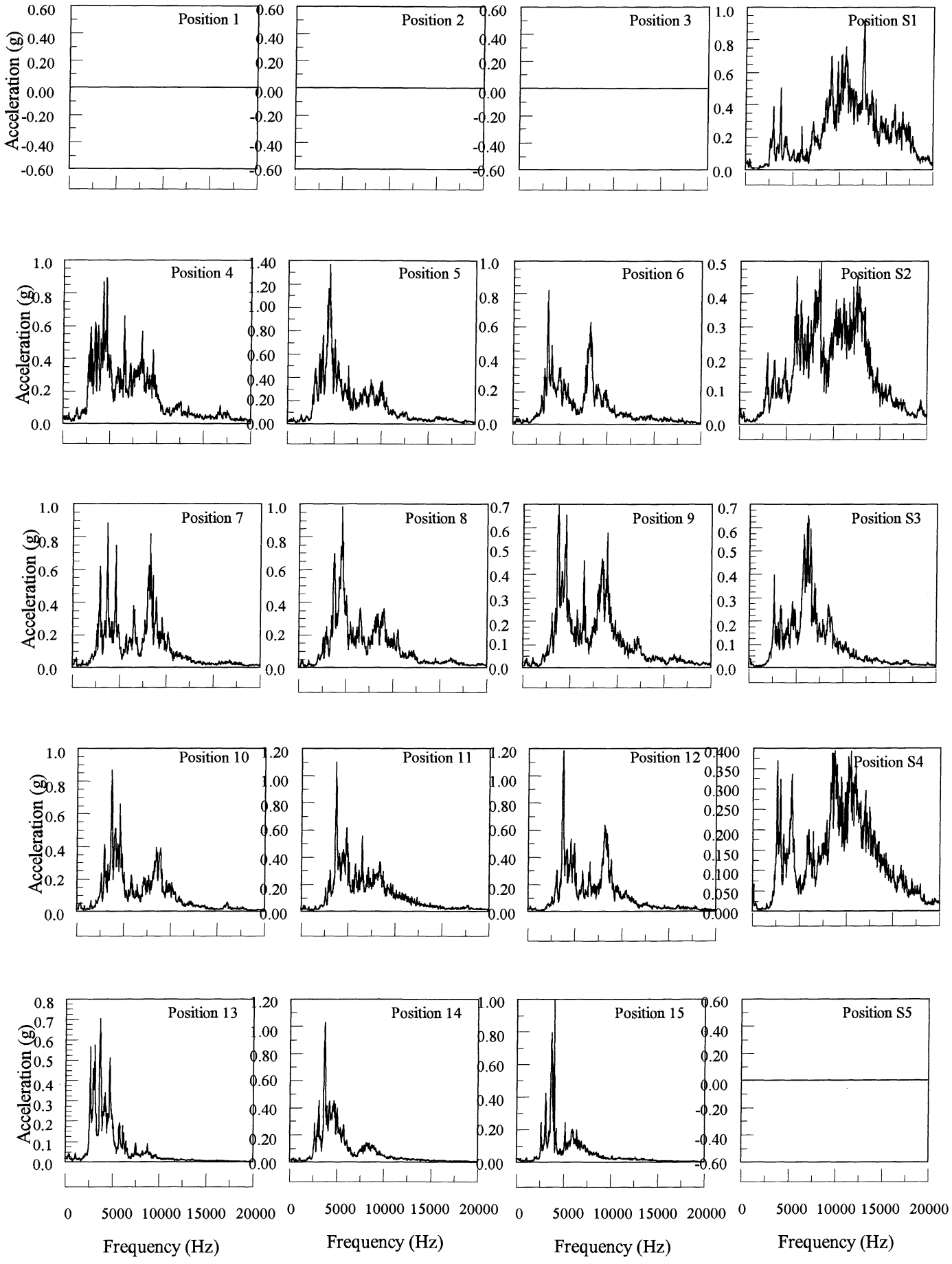

LH C1 R134a Test

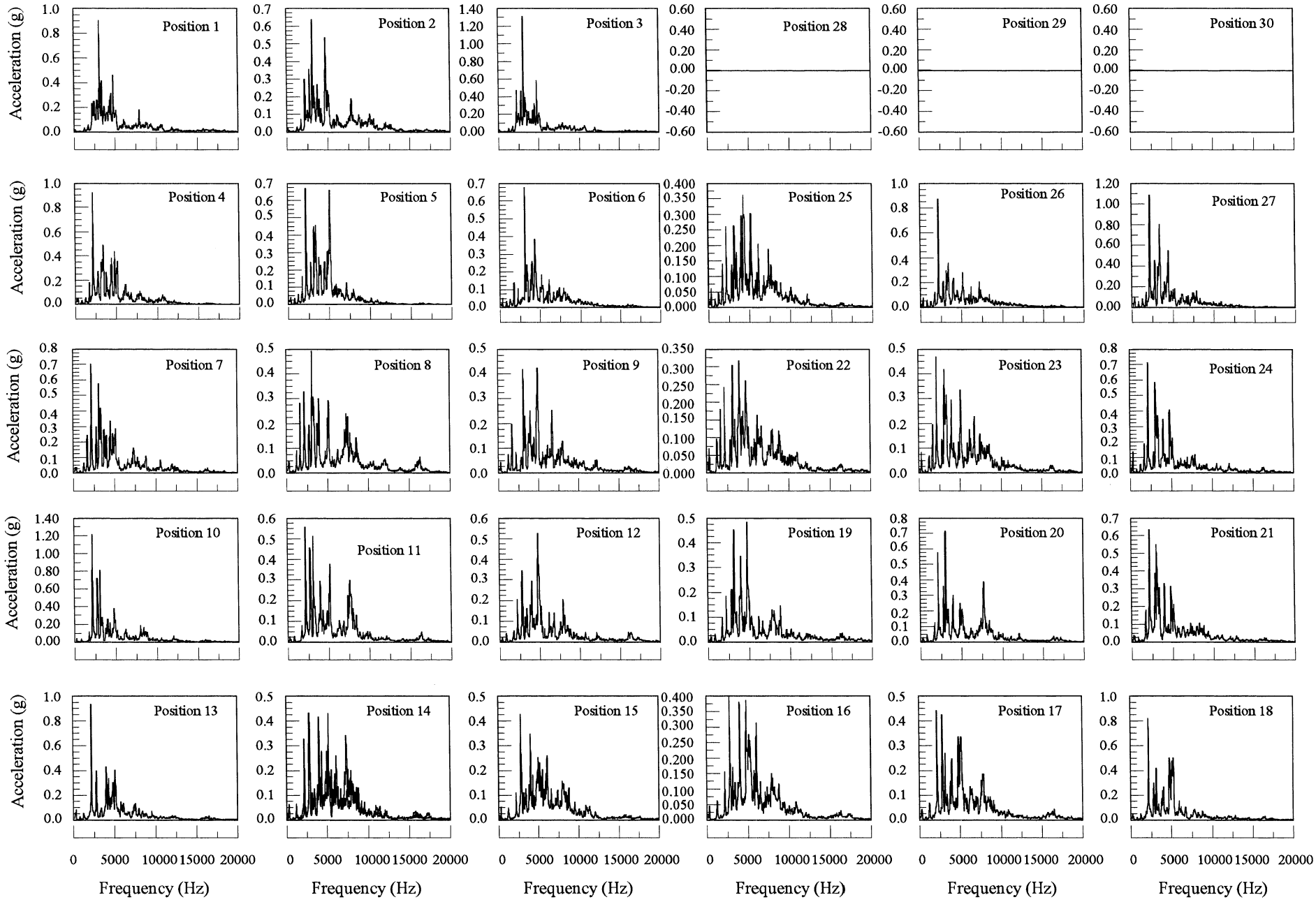

LH C2 R134a Test

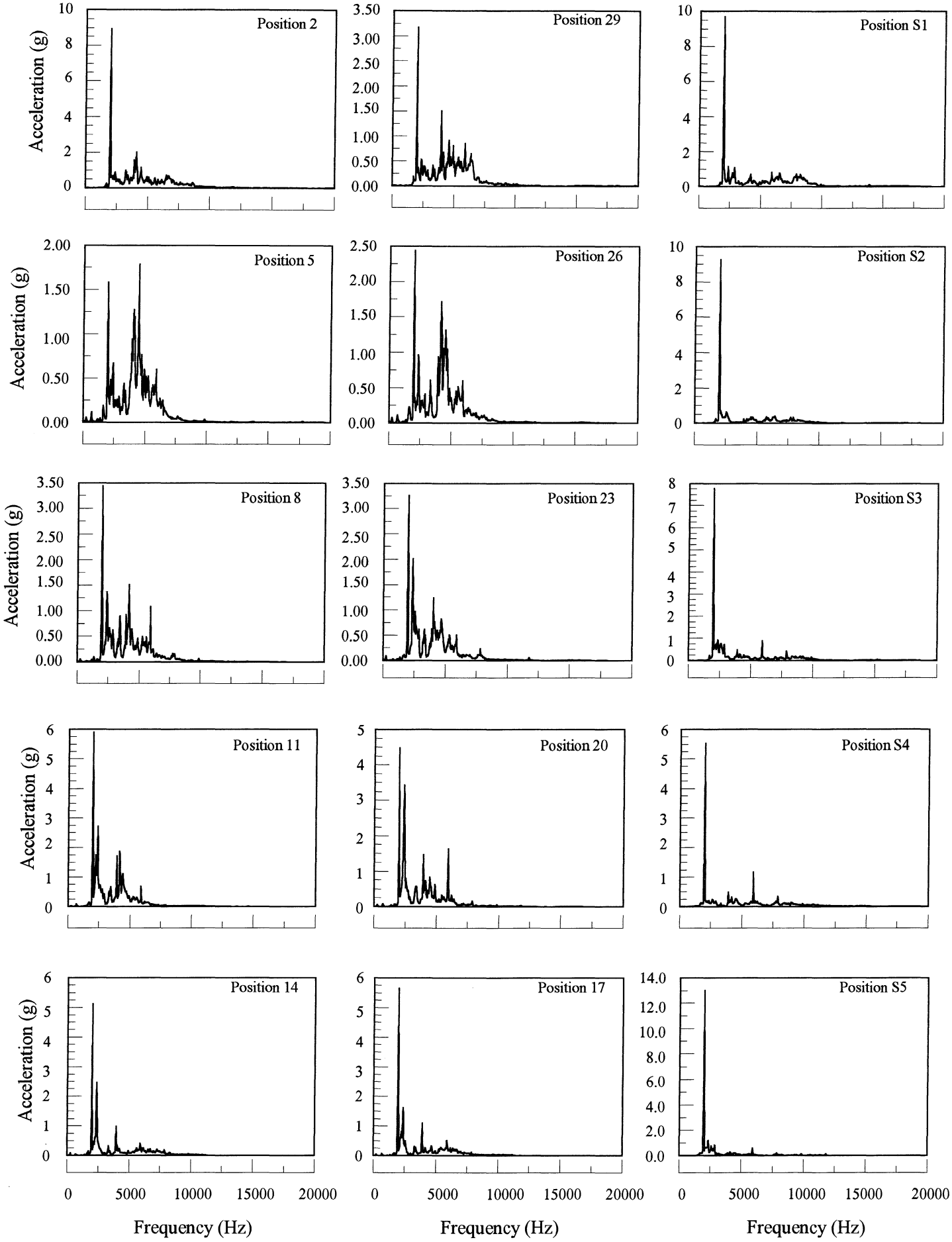

LH C3 b R134a Test

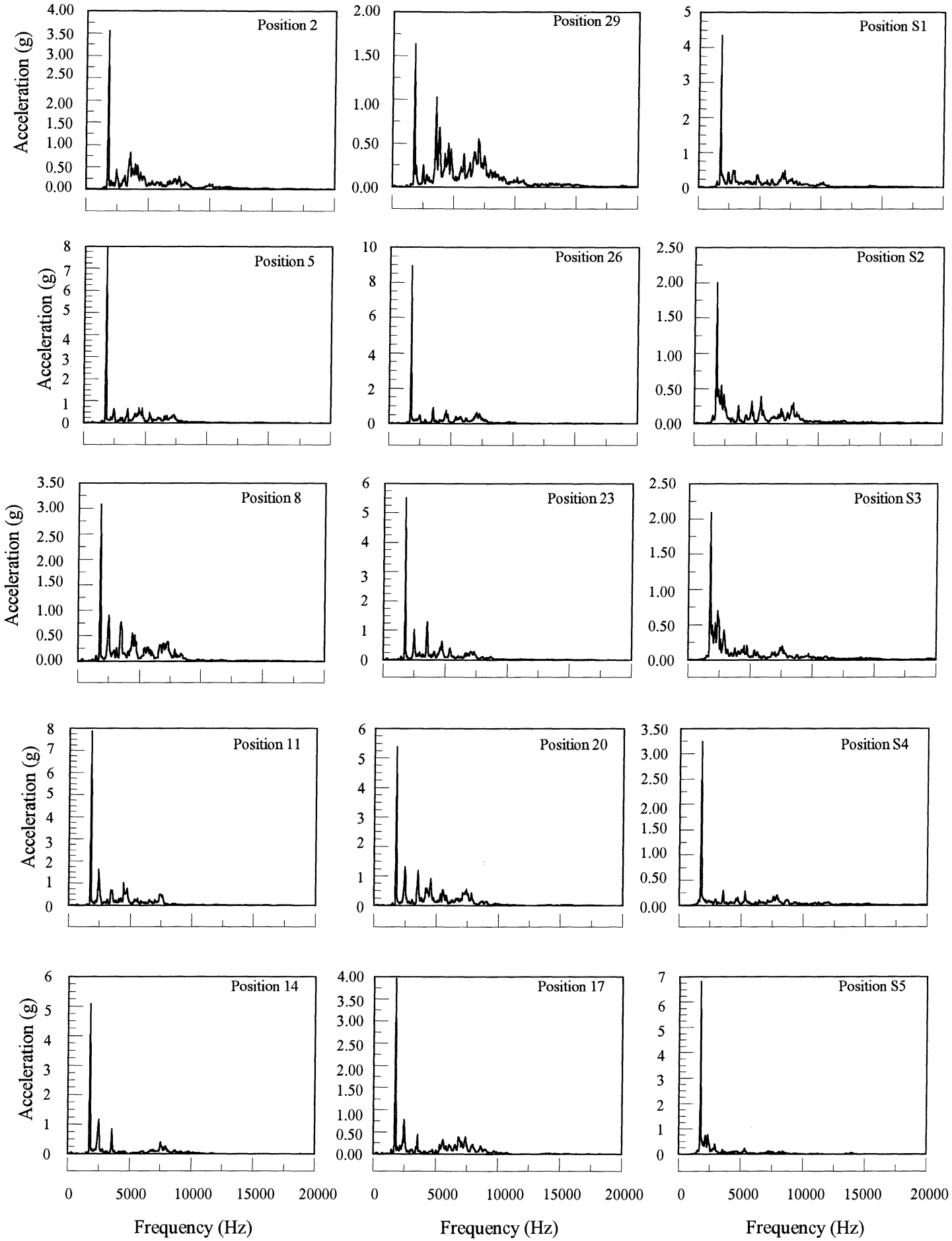

JA D1 R134a Test

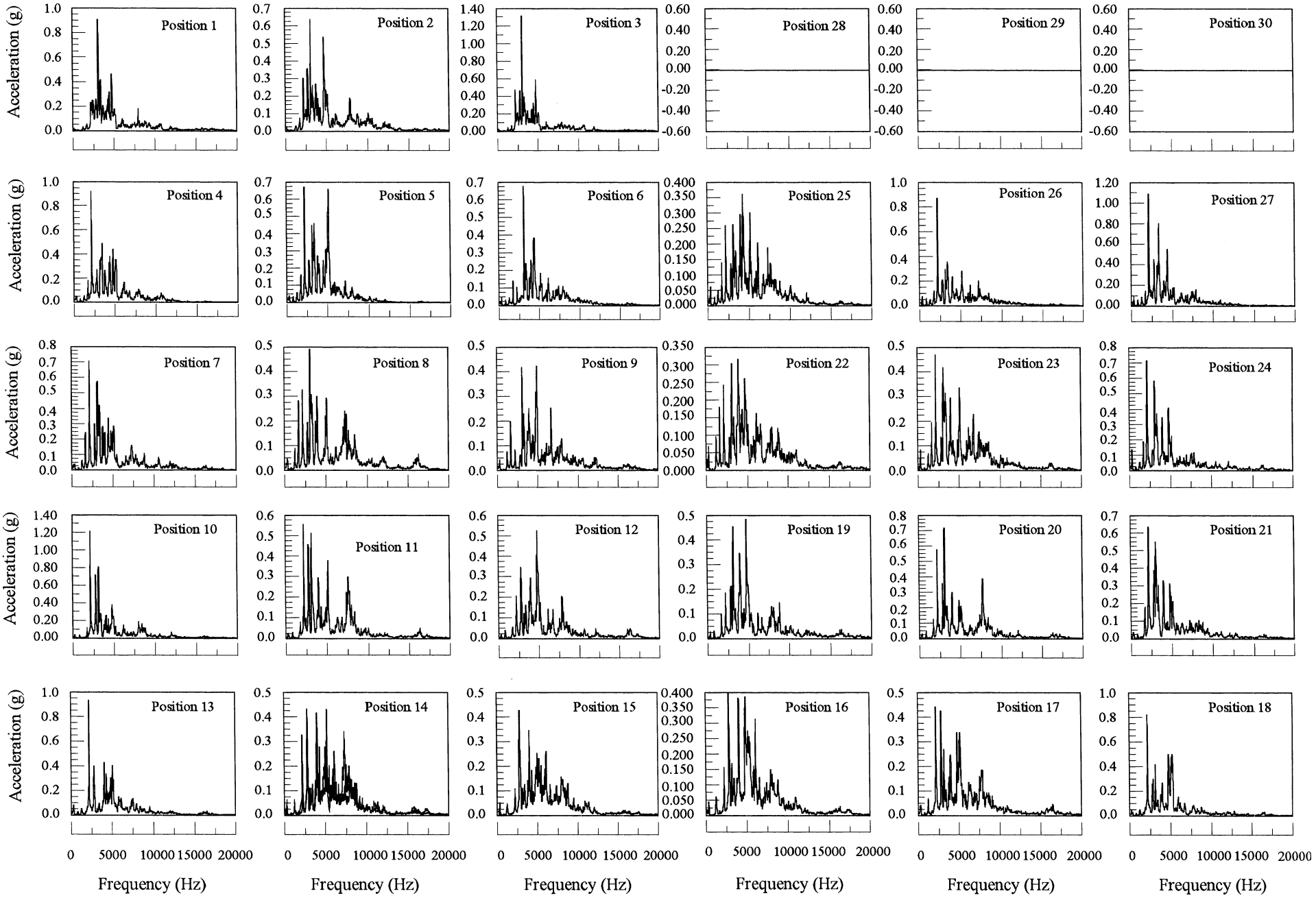

JA D2 R134a Test

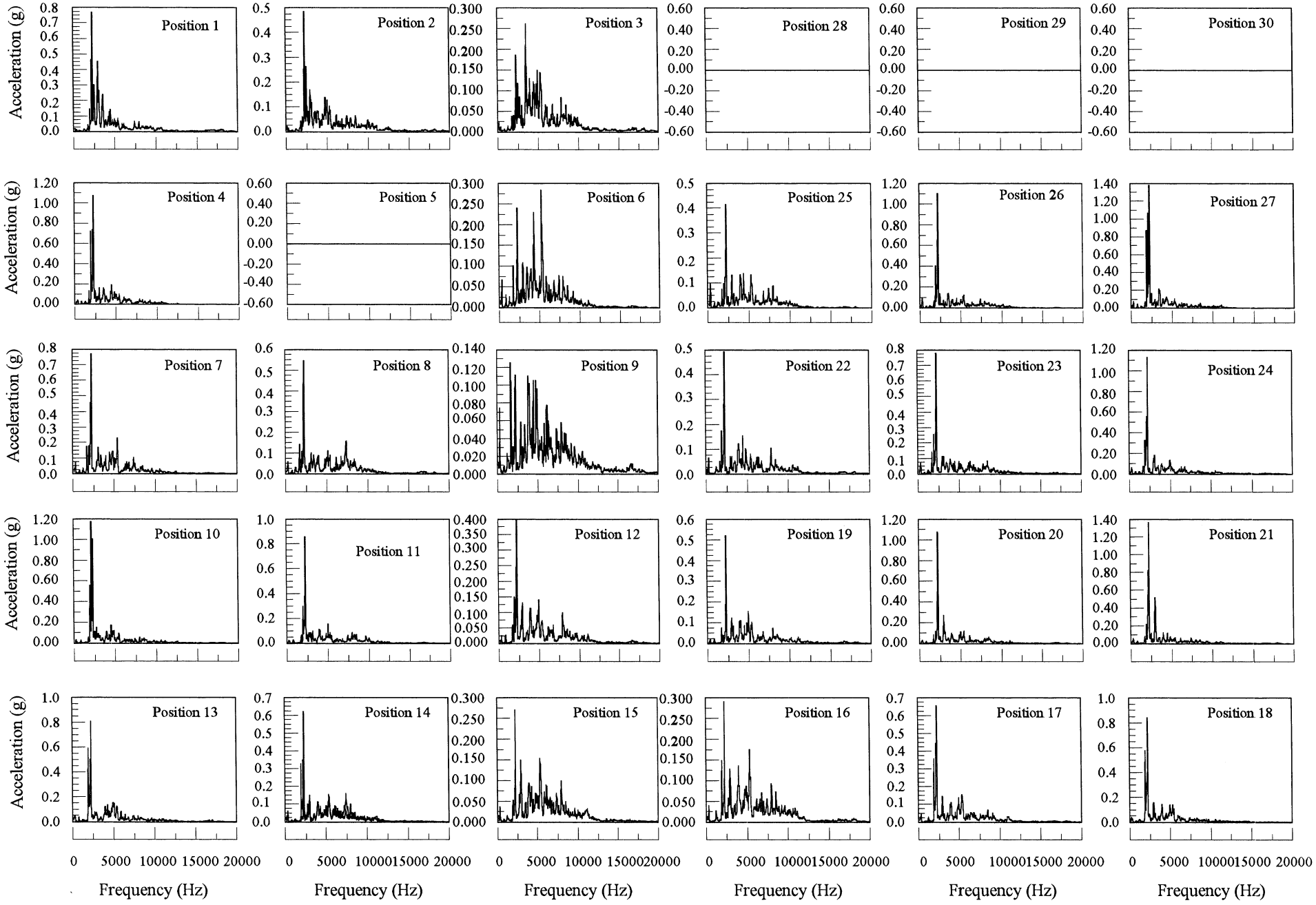

JA D3 R134a Test

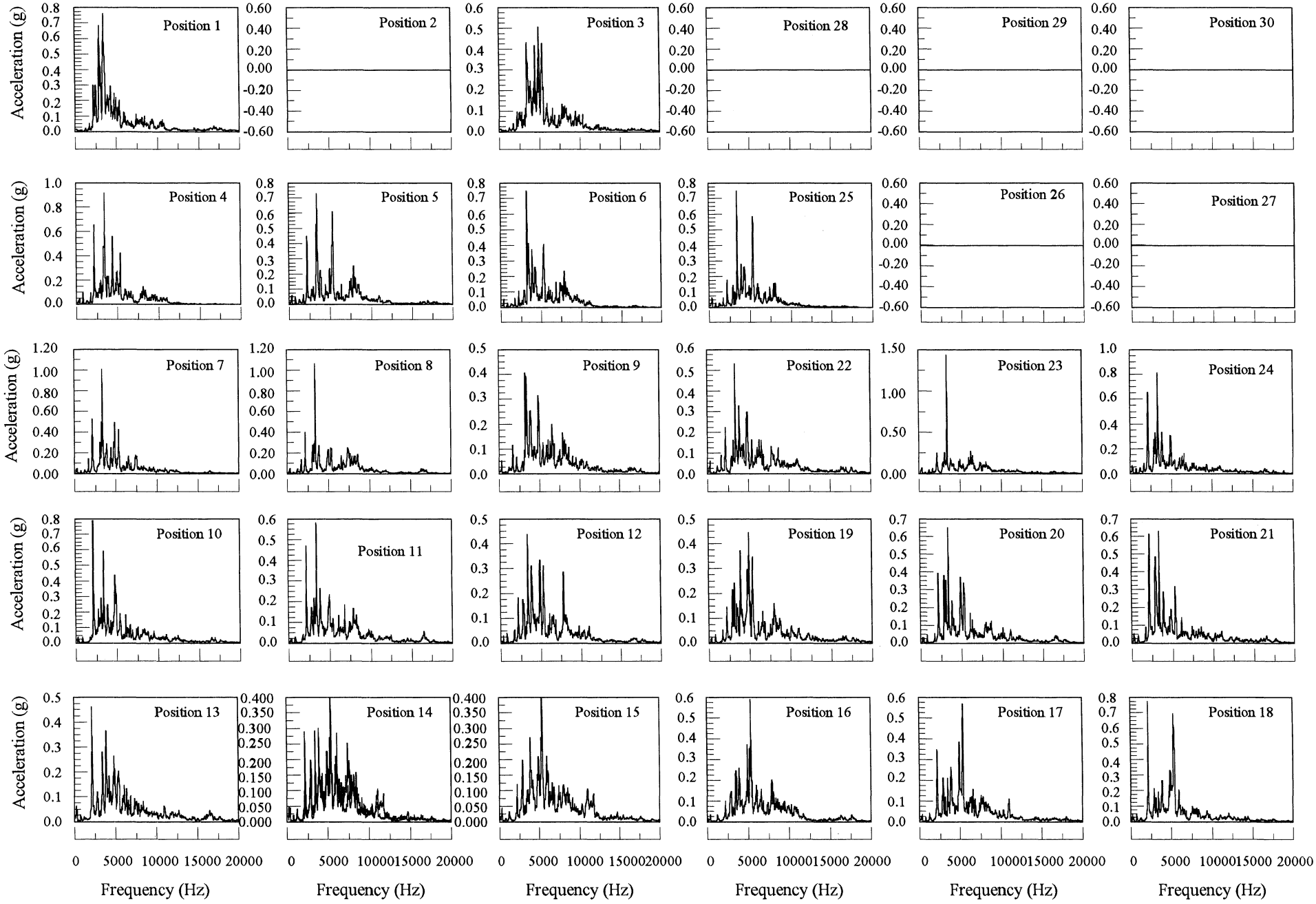

JA D5 R134a Test

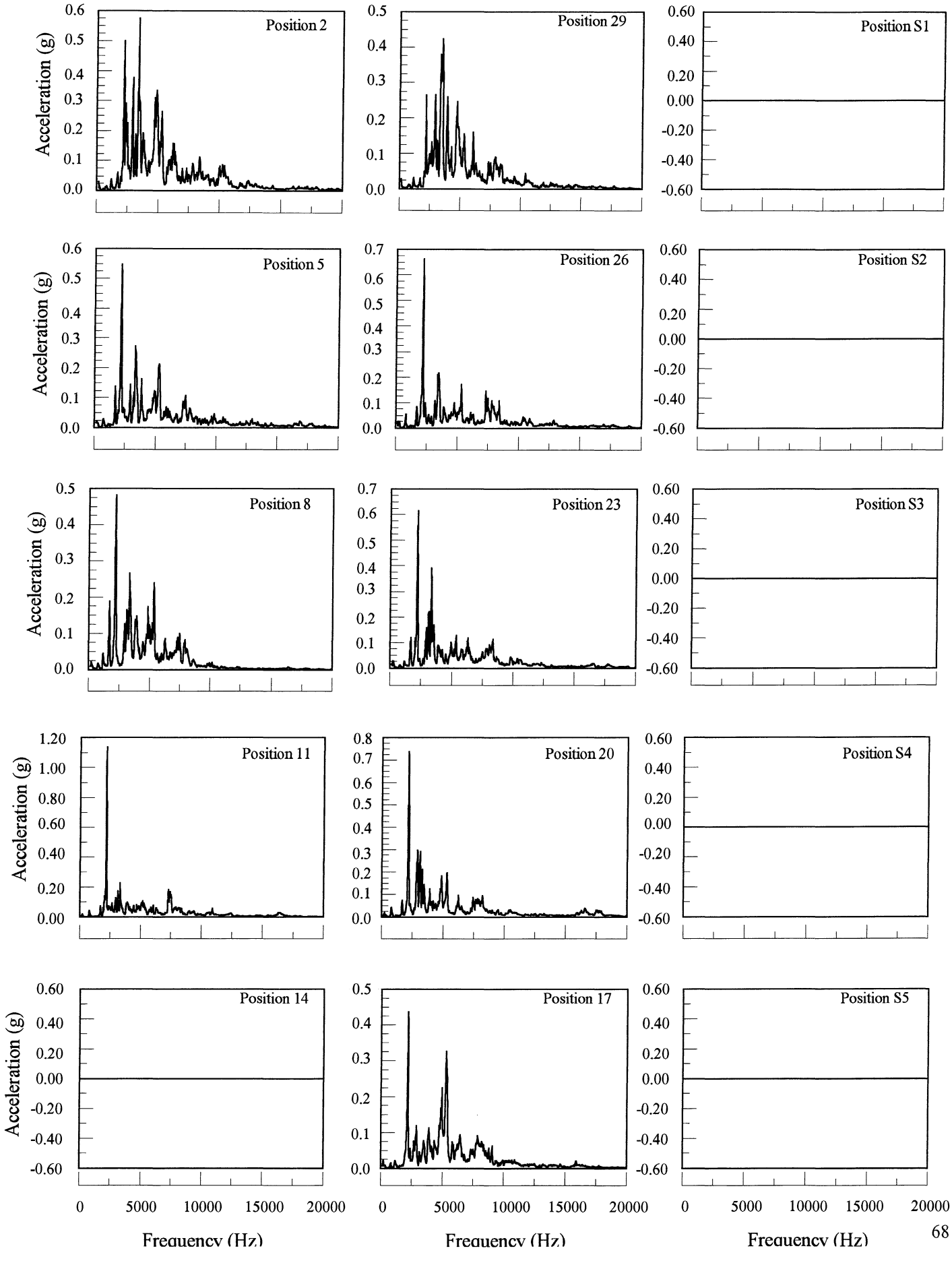

JA D6 R134a Test

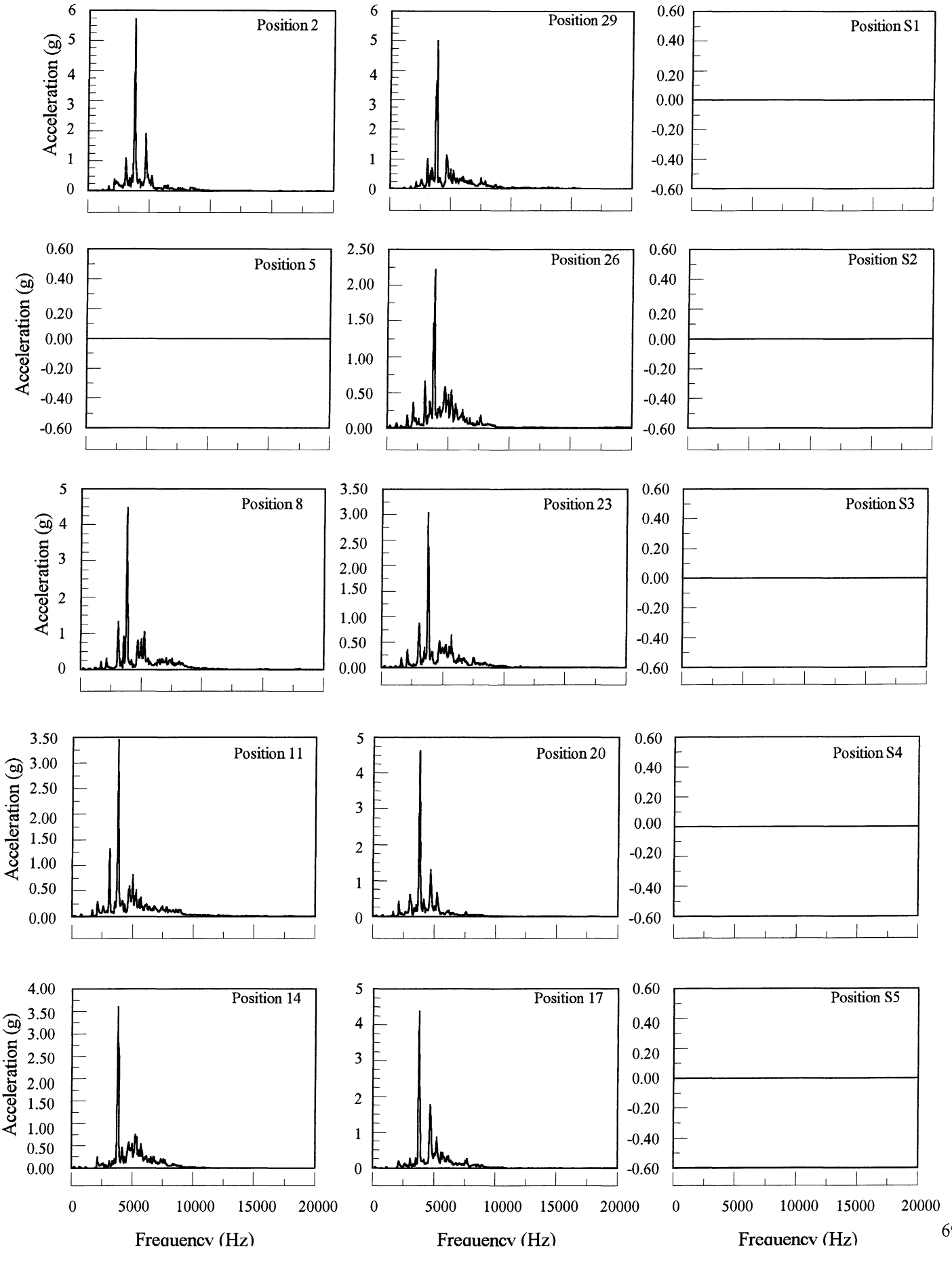

NSF-1 G1 R134a Test

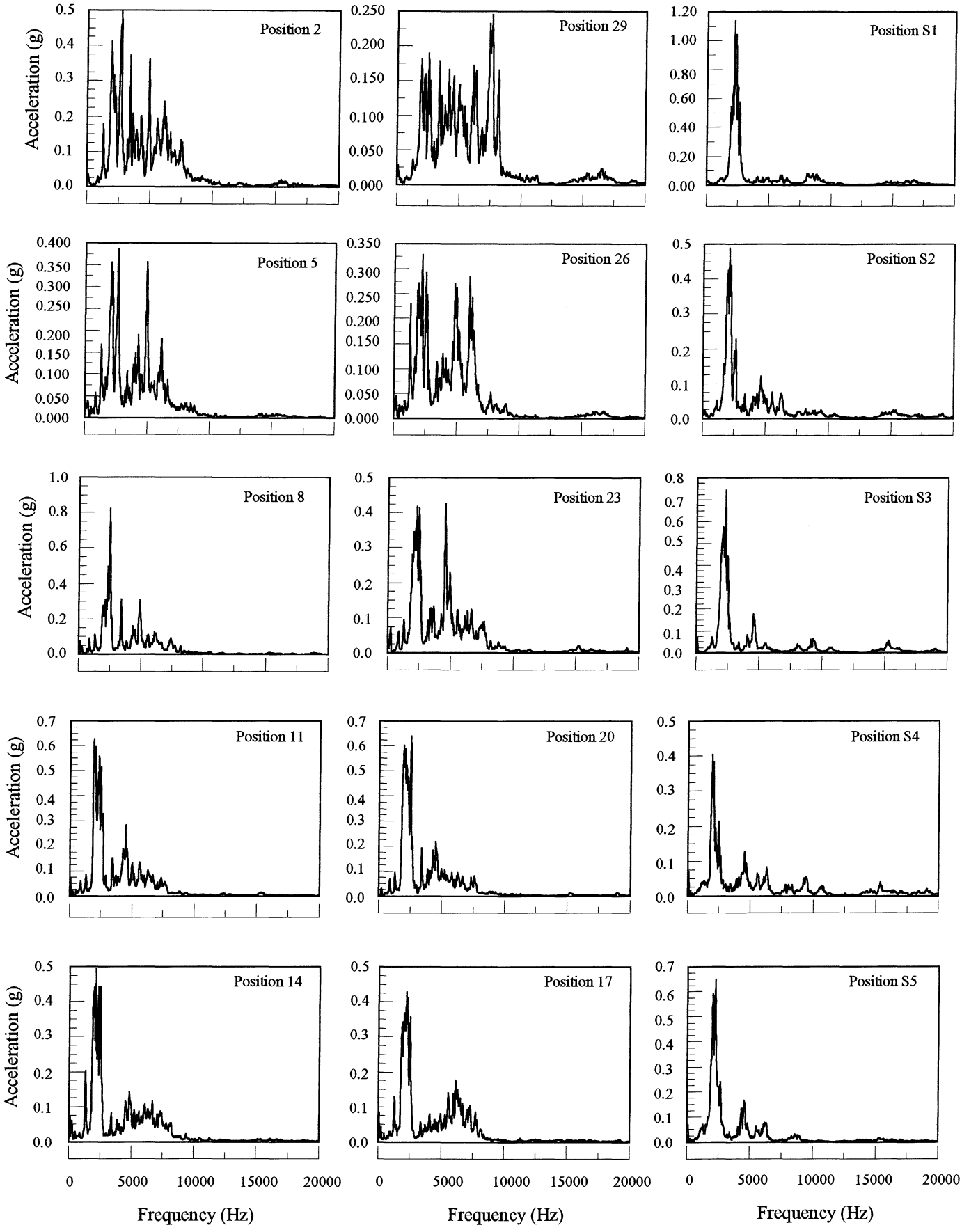

NSF-1 G2 R134a Test

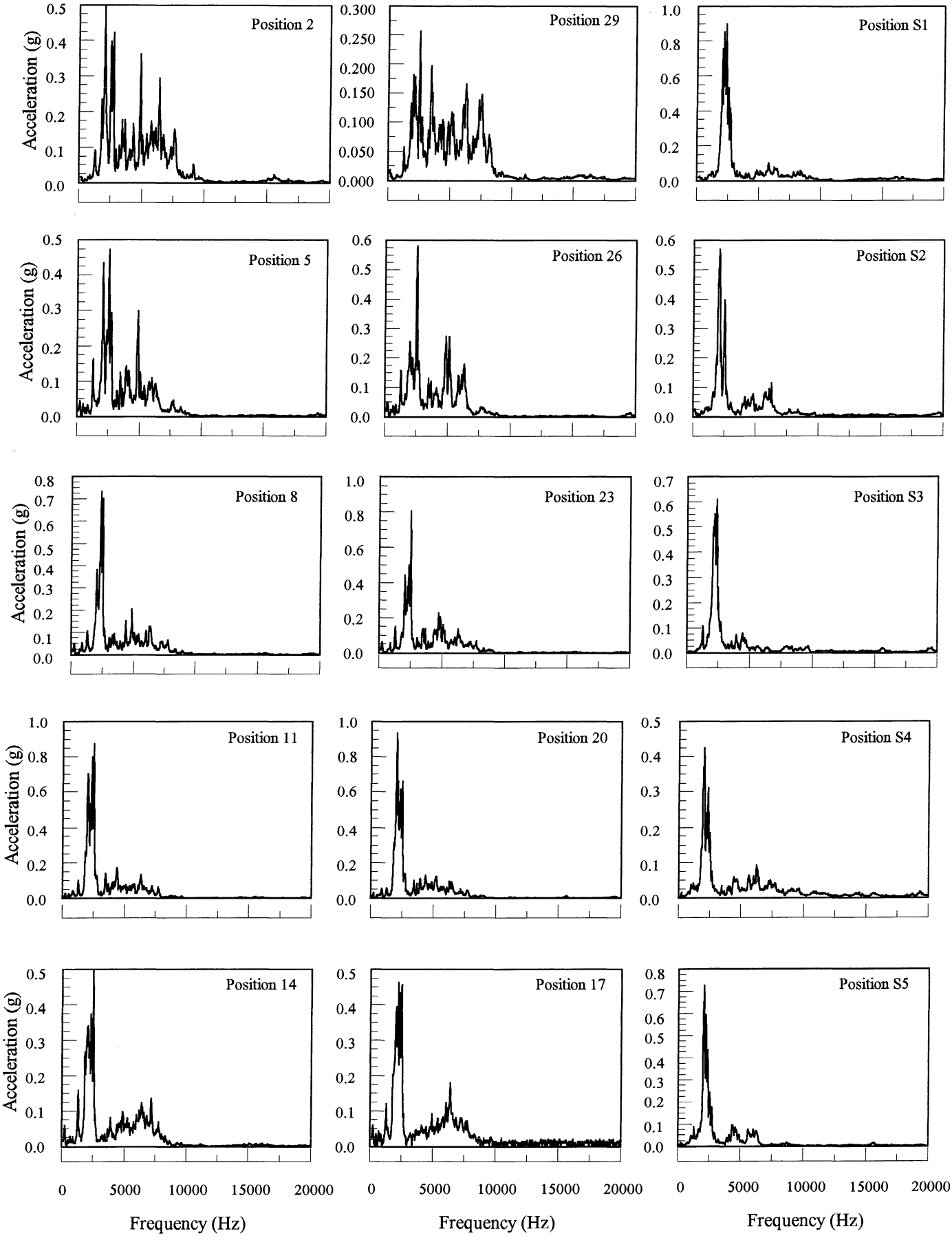

NSF-1 G3 R134a Test

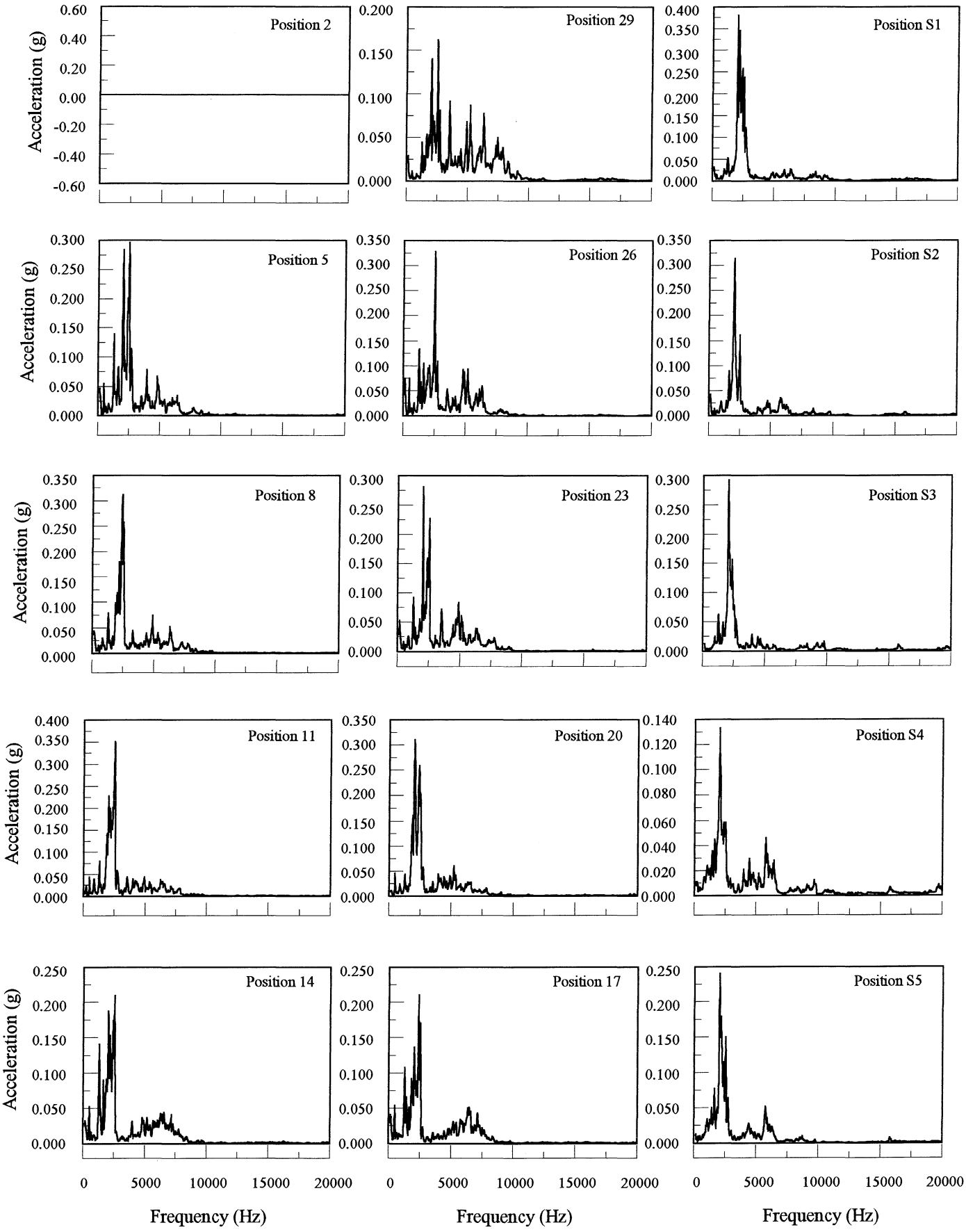

NSF-1 G4 R134a Test

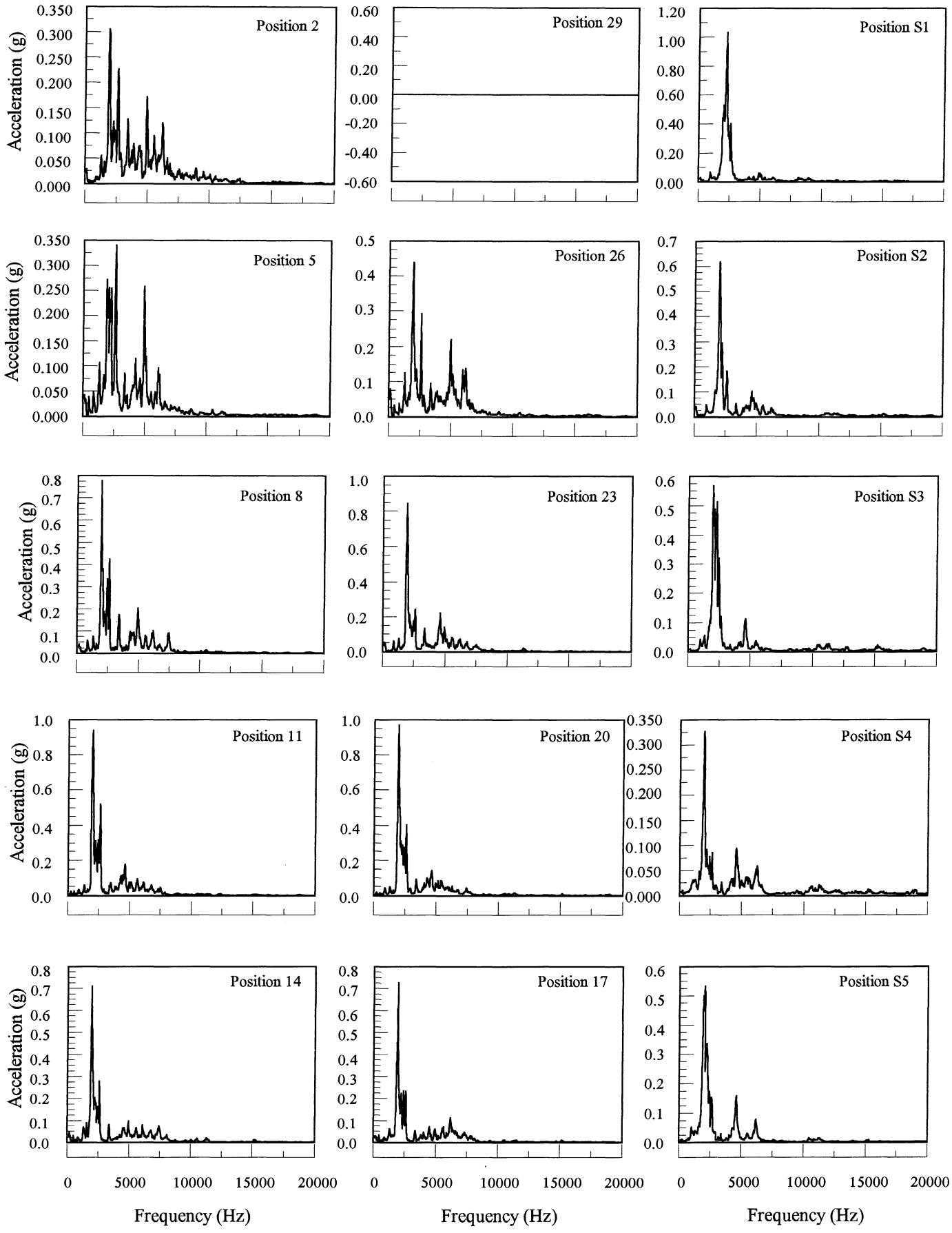

NSF-1 G5 R134a Test

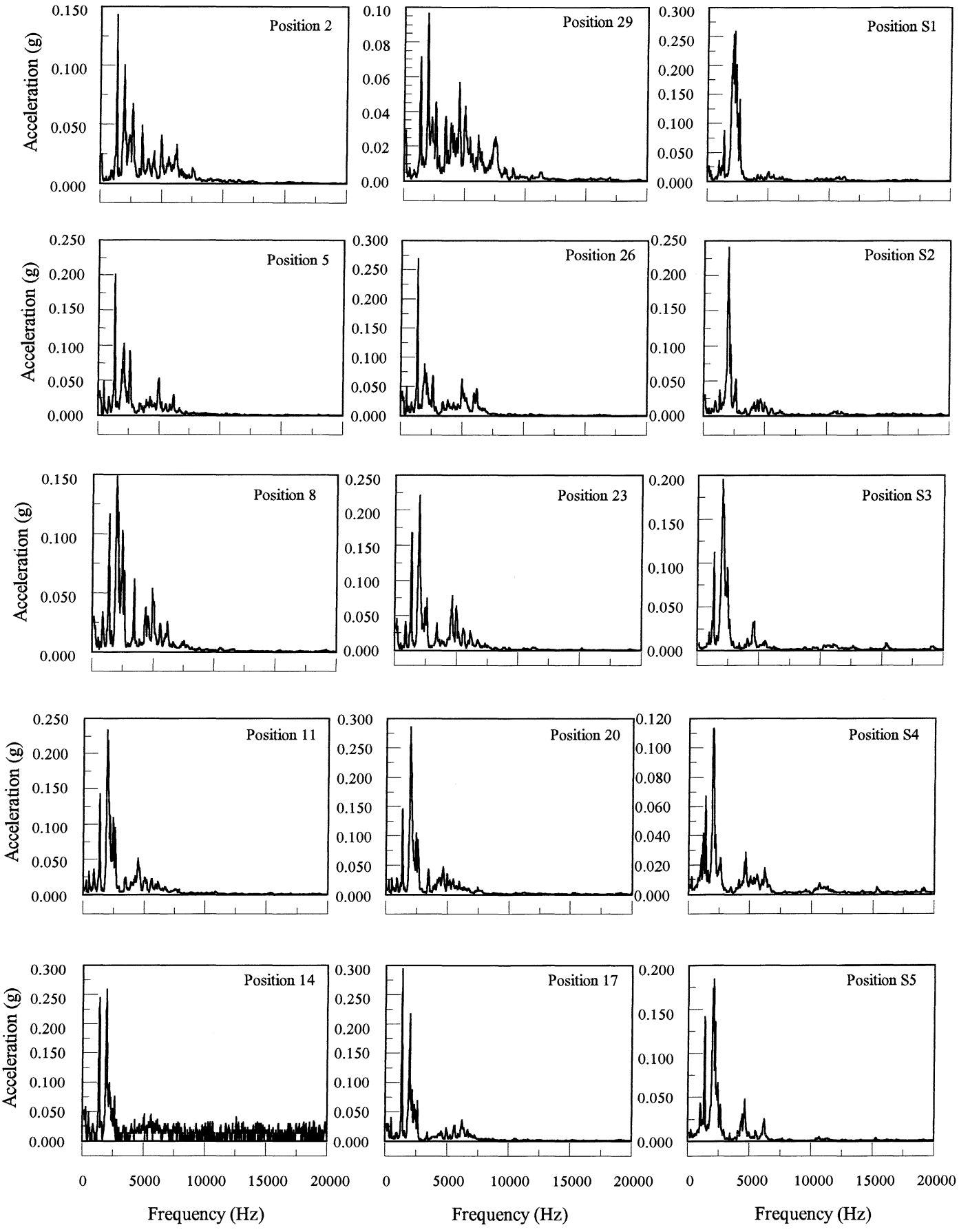

NSF-2 E1 R134a Test

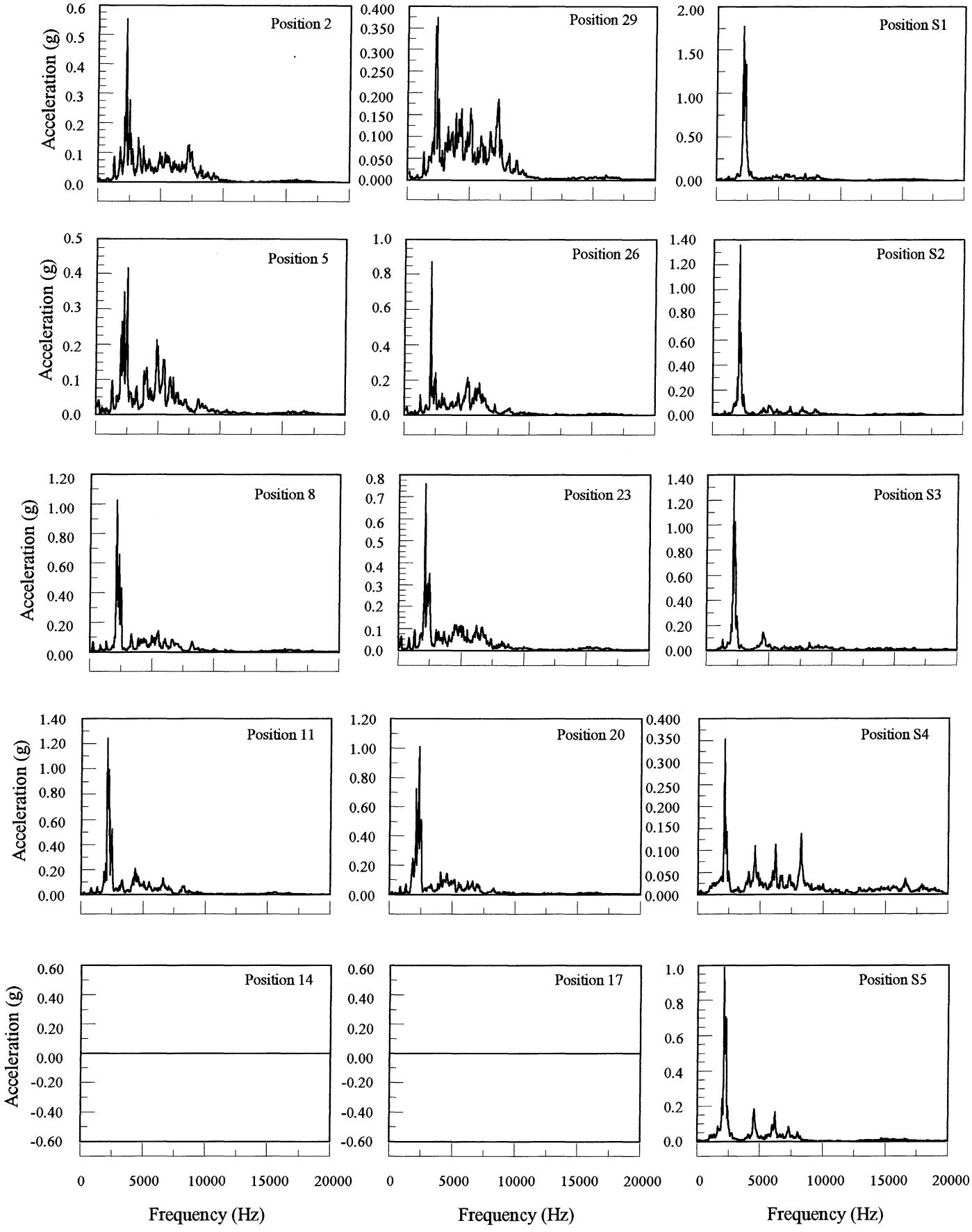

NSF-2 E2 R134a Test

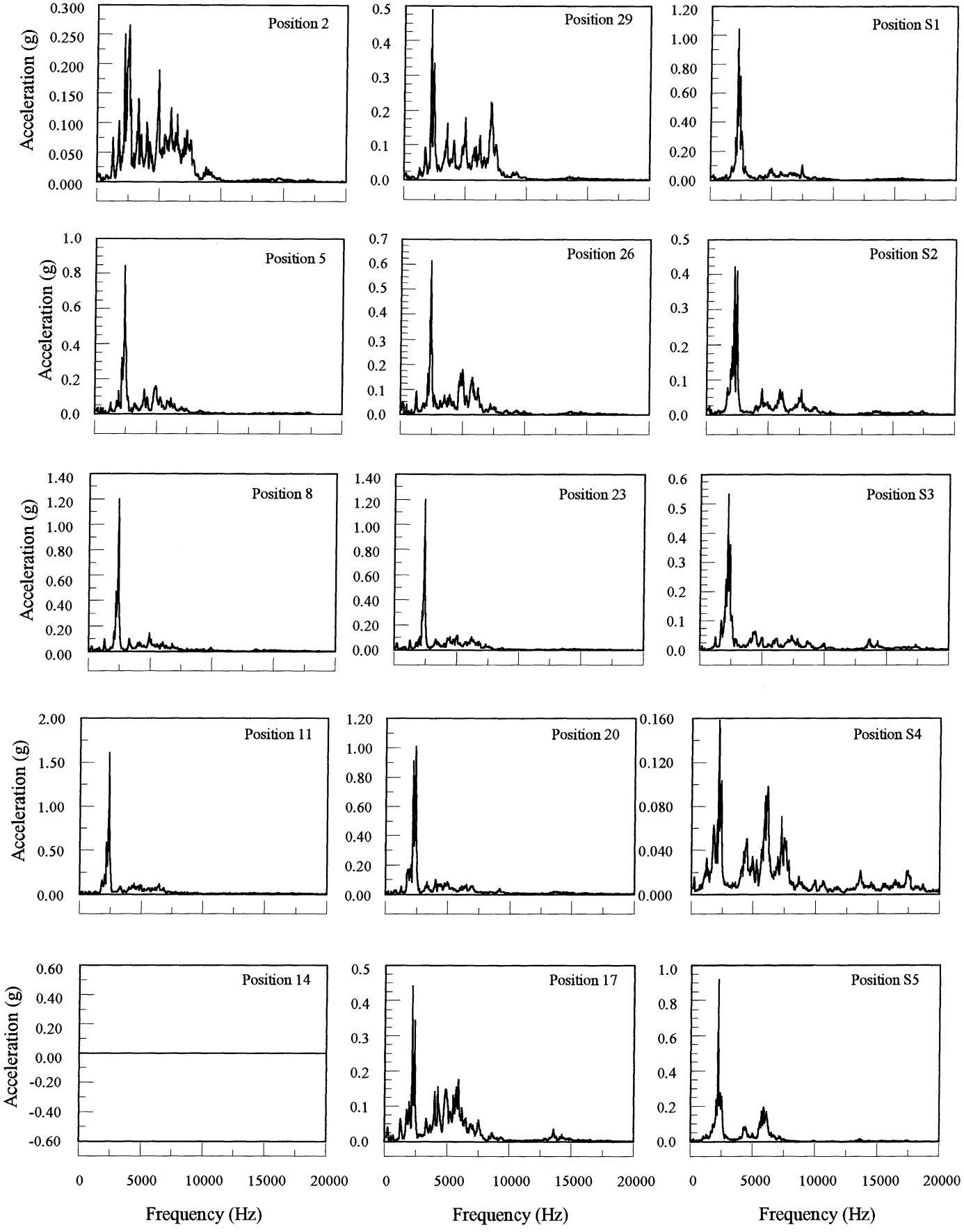

NSF-2 E3 R134a Test

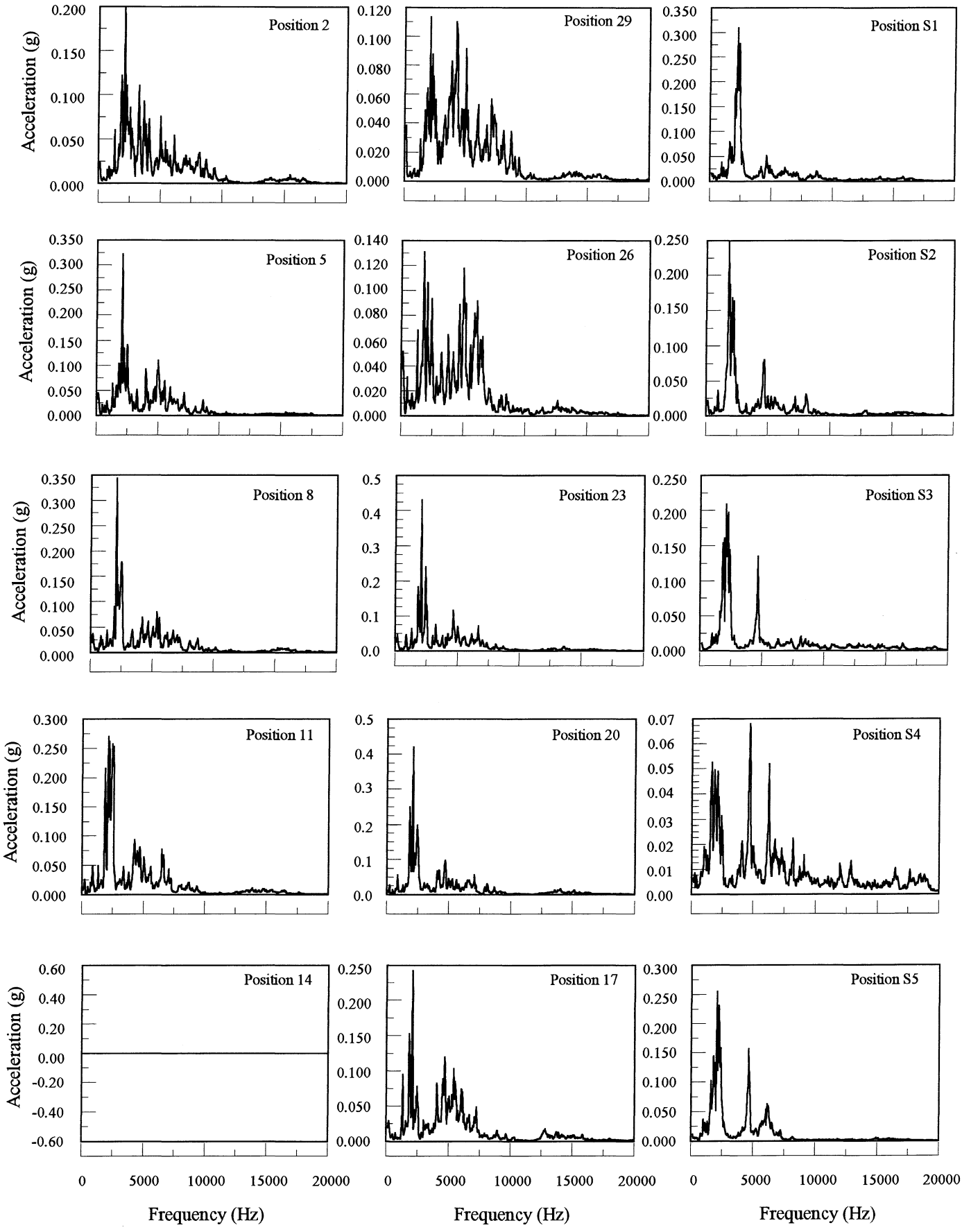

NSF-2 E4 R134a Test

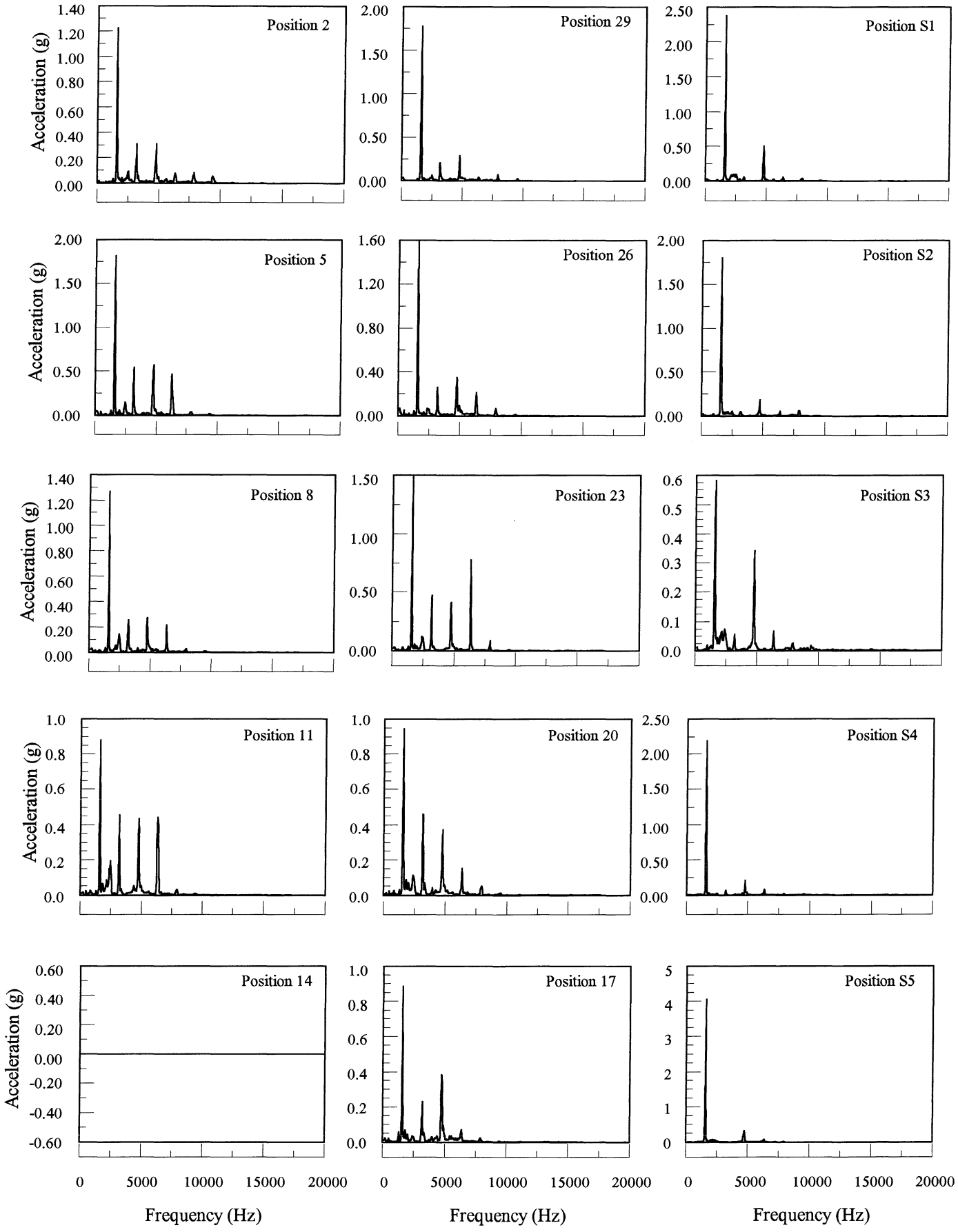

NSF-2 E5 R134a Test

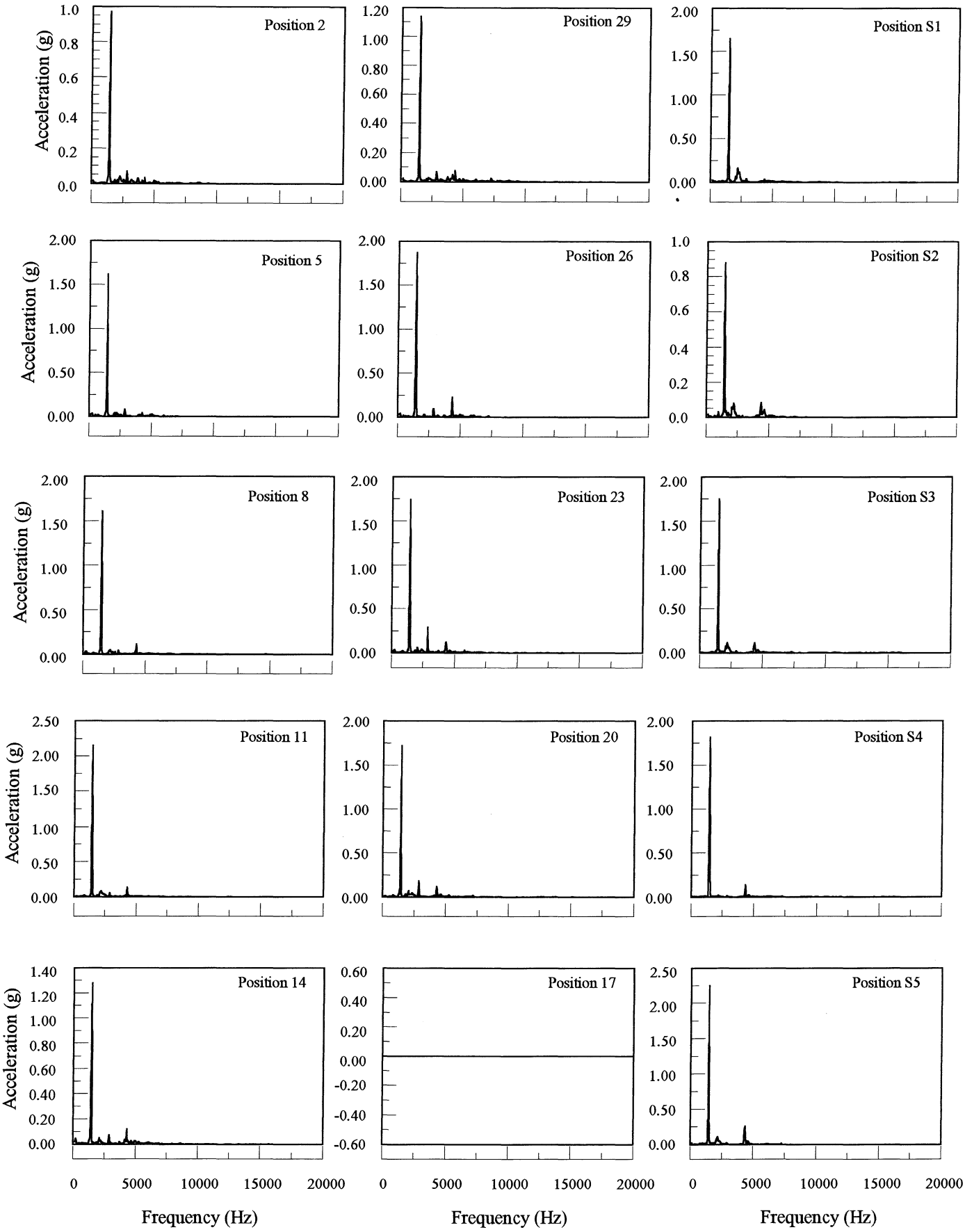

NSF-3 F1 R134a Test

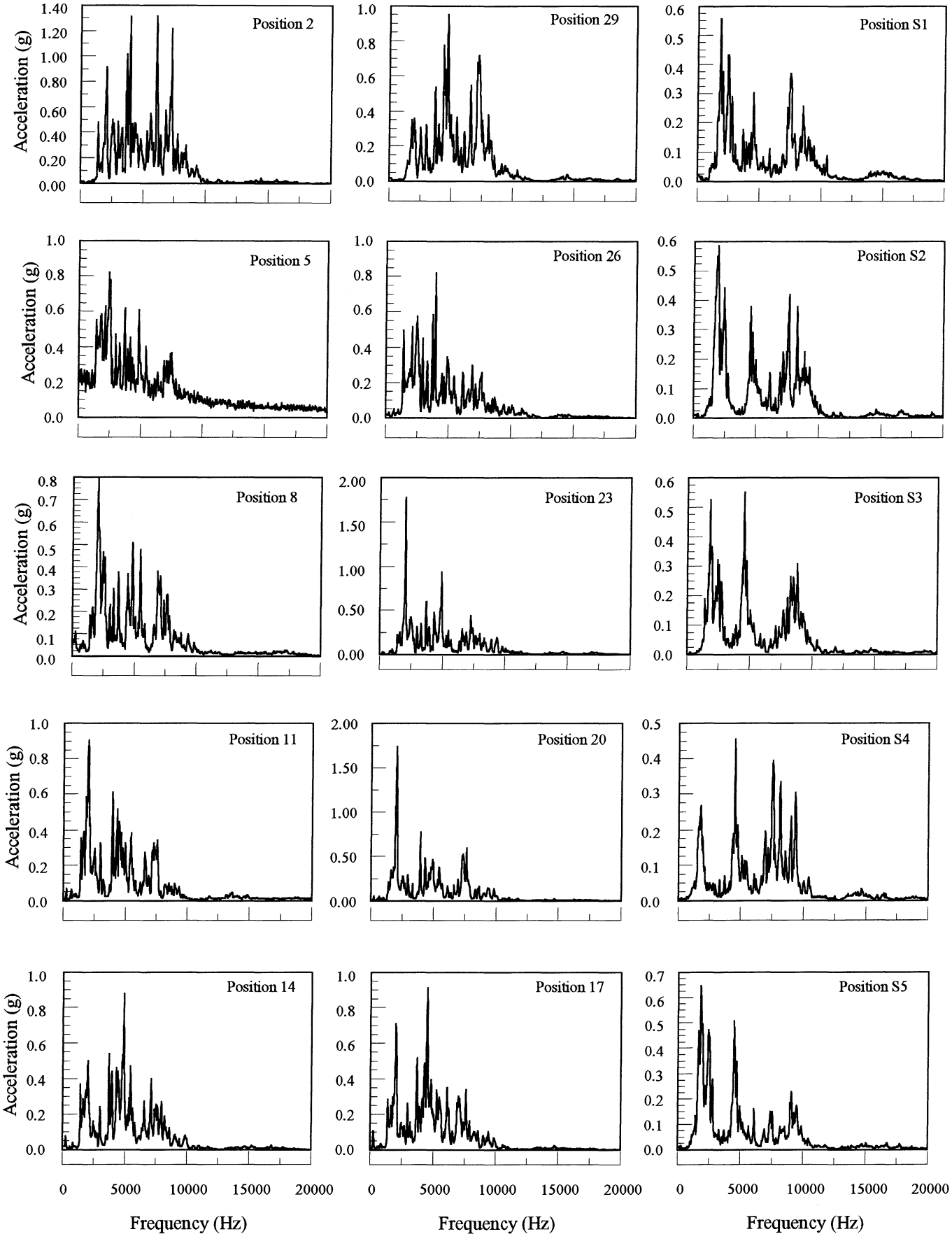

NSF-3 F2 R134a Test

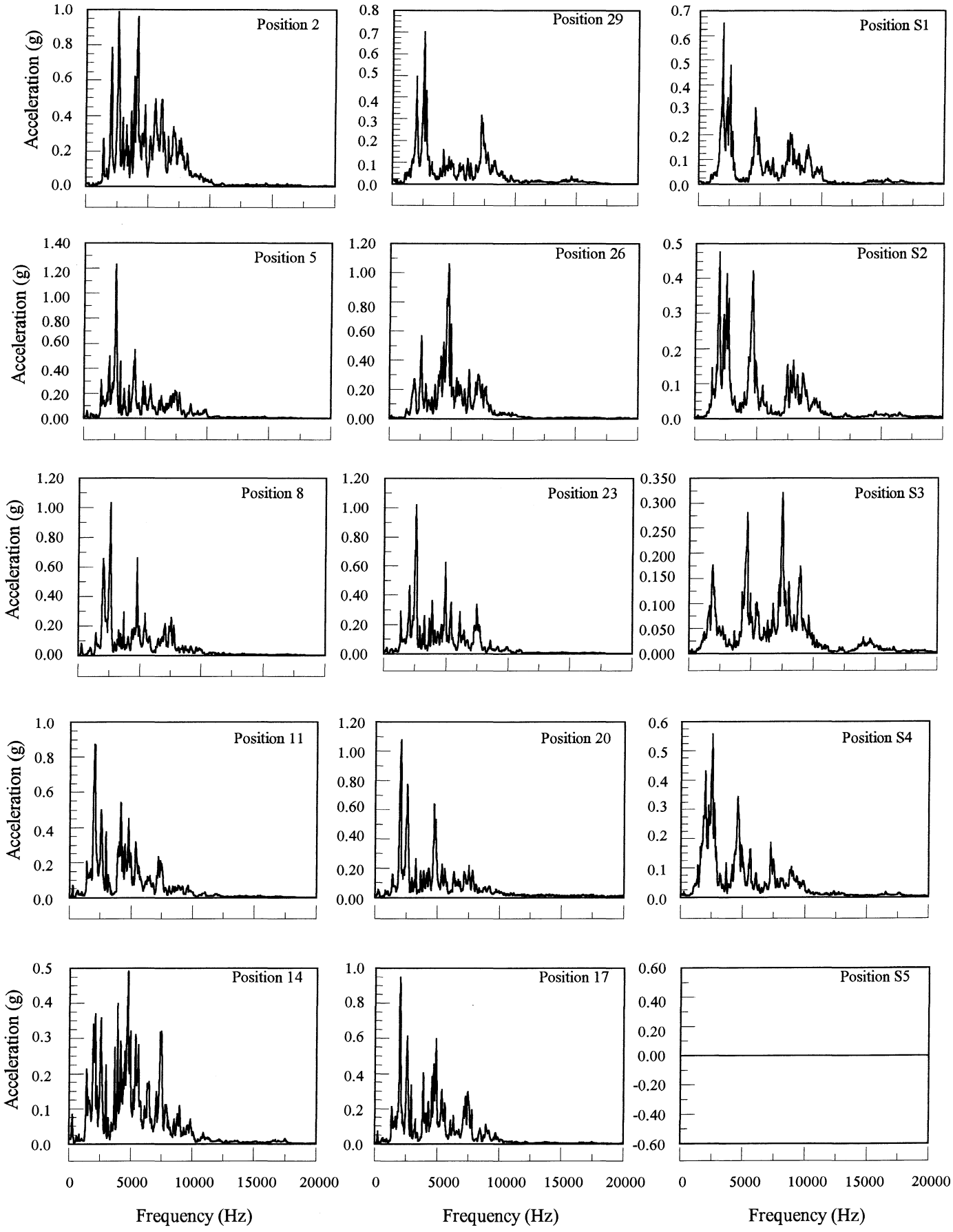

NSF-3 F3 R134a Test

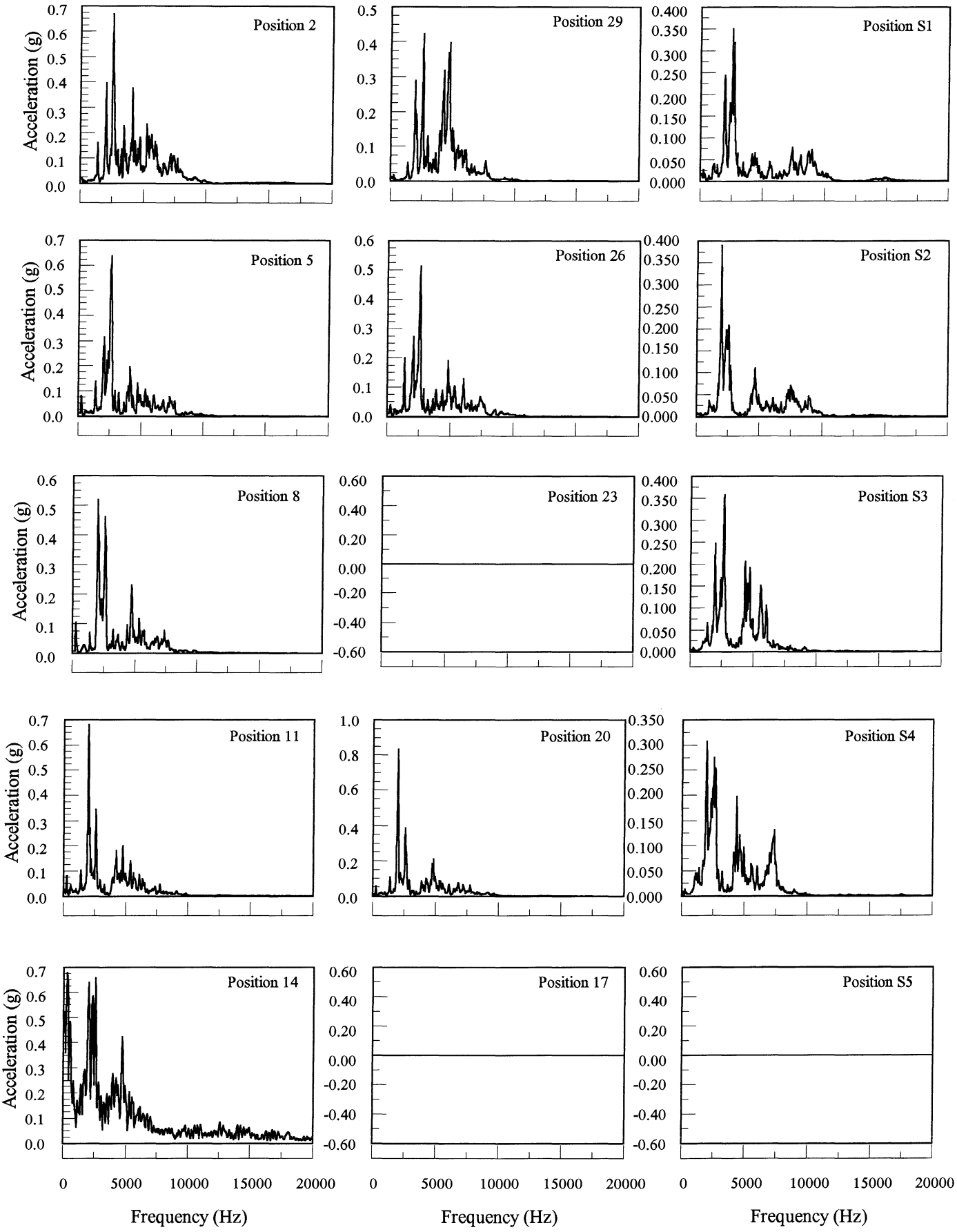

NSF-3 F4 R134a Test

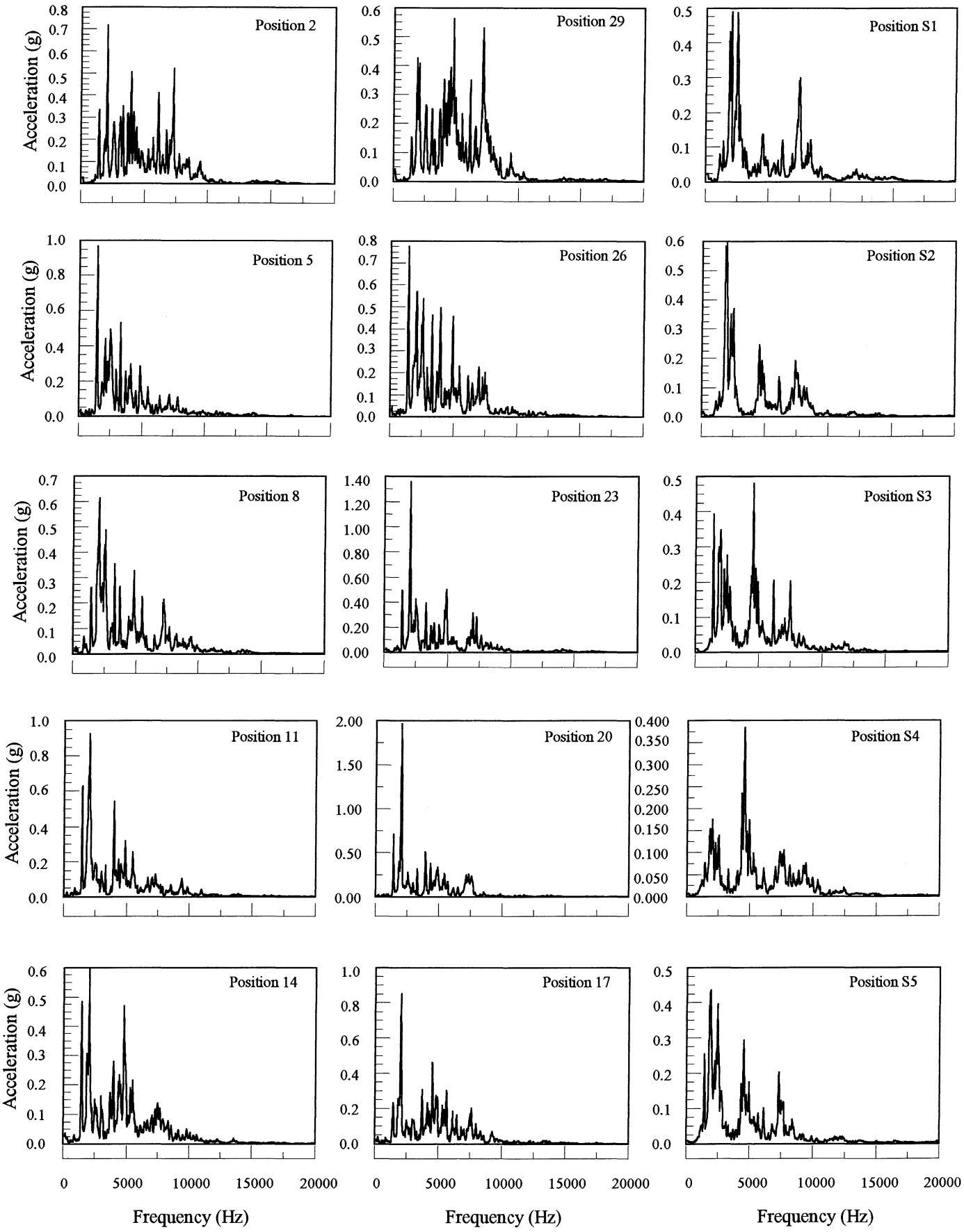

NSF-3 F5 R134a Test

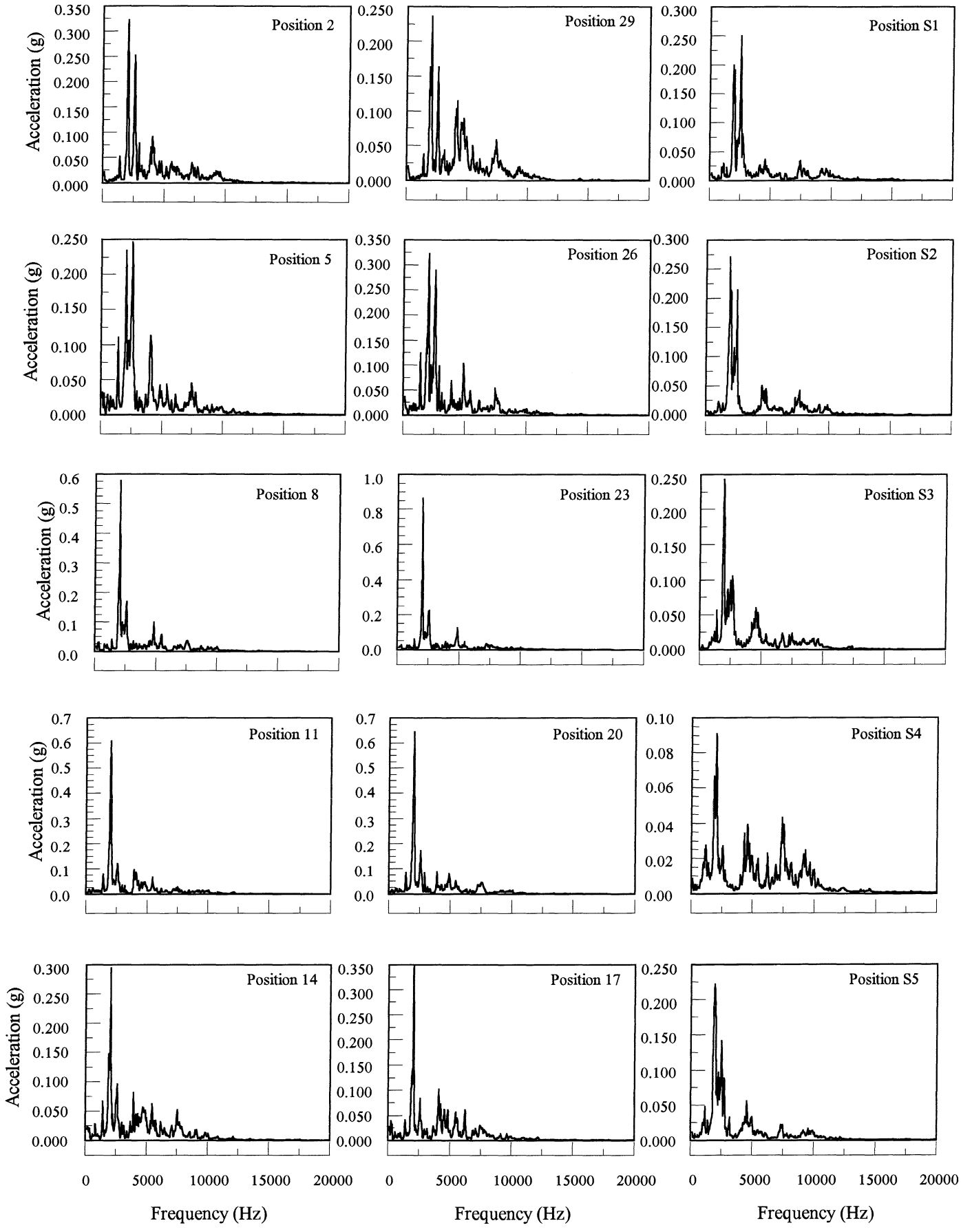

Appendix II

Acceleration Power Spectra, Nitrogen Tests

Acceleration Power Spectra AS/PL Evaporator N2 Test

Velocity at Cross Section

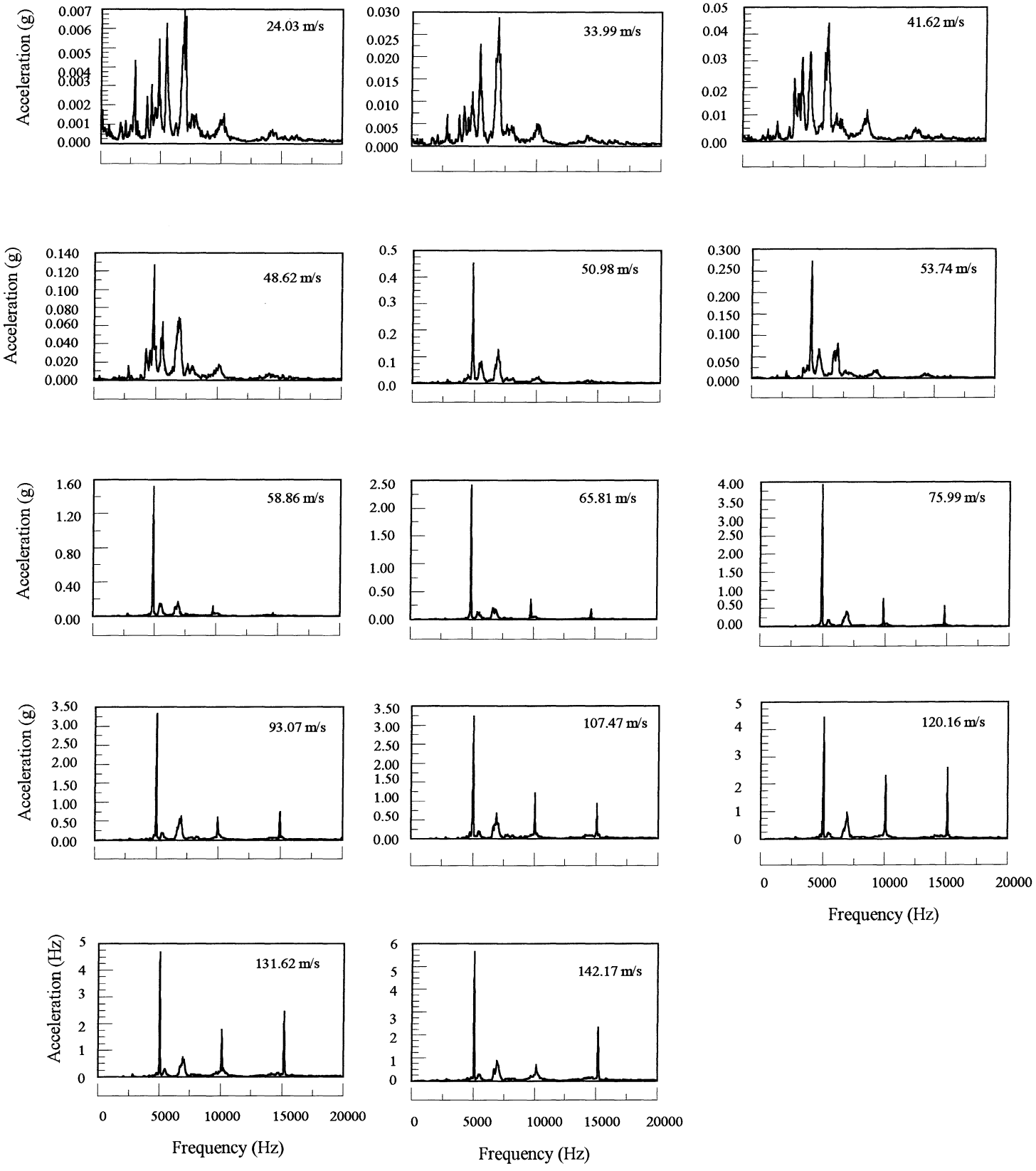

Acceleration Power Spectra AS/PL mod Evaporator

N2 Test

Velocity at Cross Section (without wire)

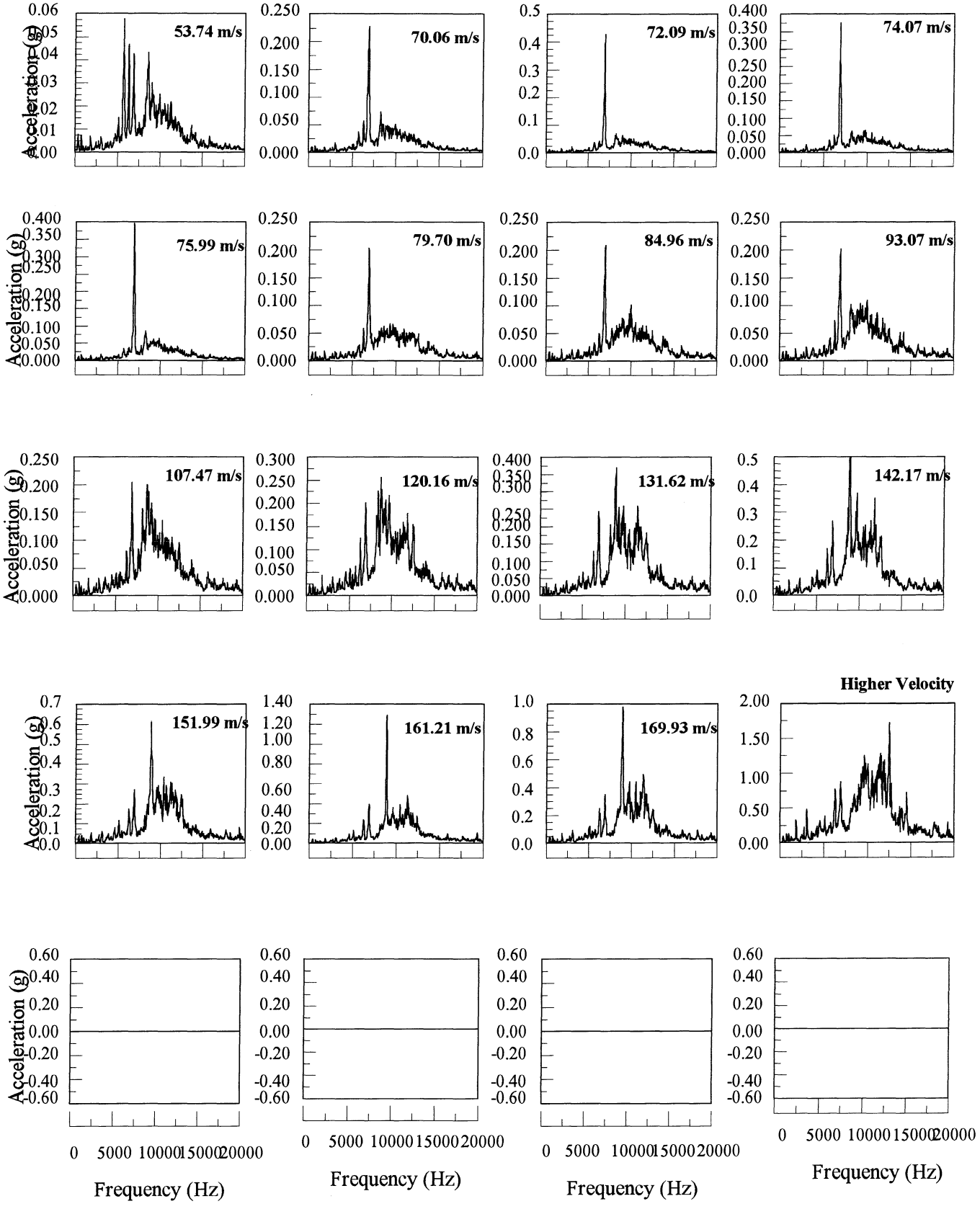

Acceleration Power Spectra LH Evaporator
1st Sample N2 Test
Velocity at Cross Section

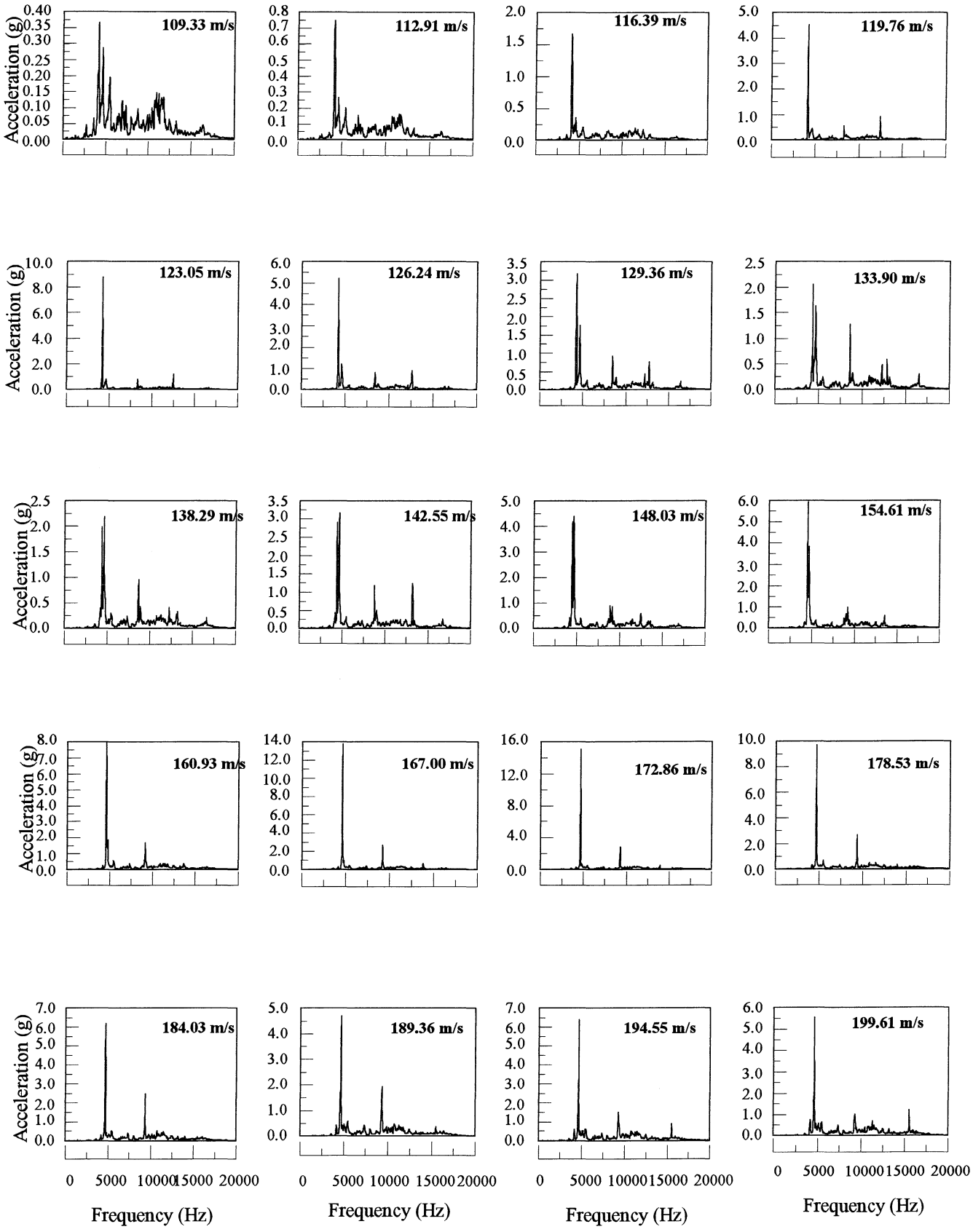

Acceleration Power Spectra LH Evaporator
2nd Sample N2 Test
Velocity at Cross Section

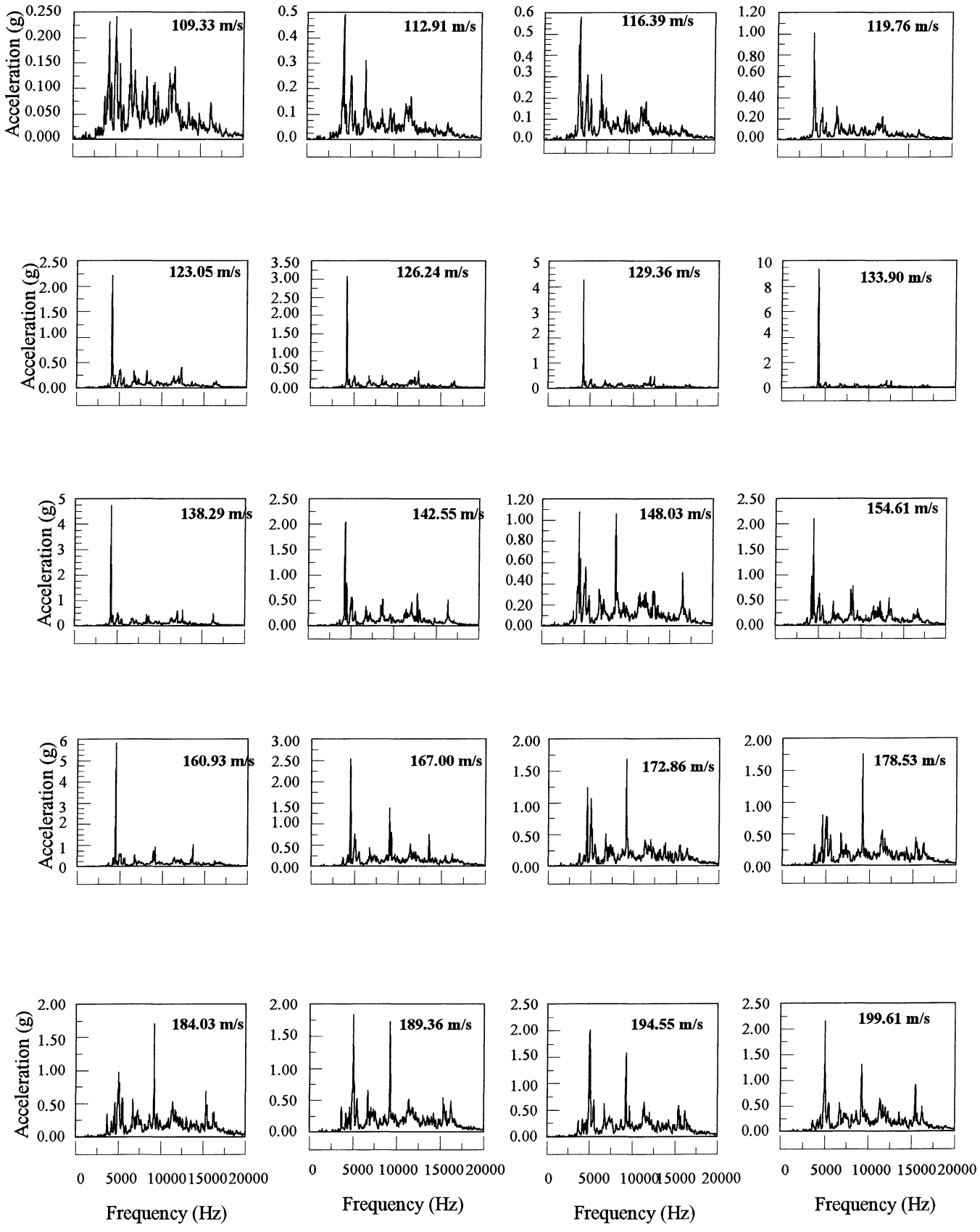

Acceleration Power Spectrum JA Evaporator
1st Sample N2 Test
Velocities at Cross Section

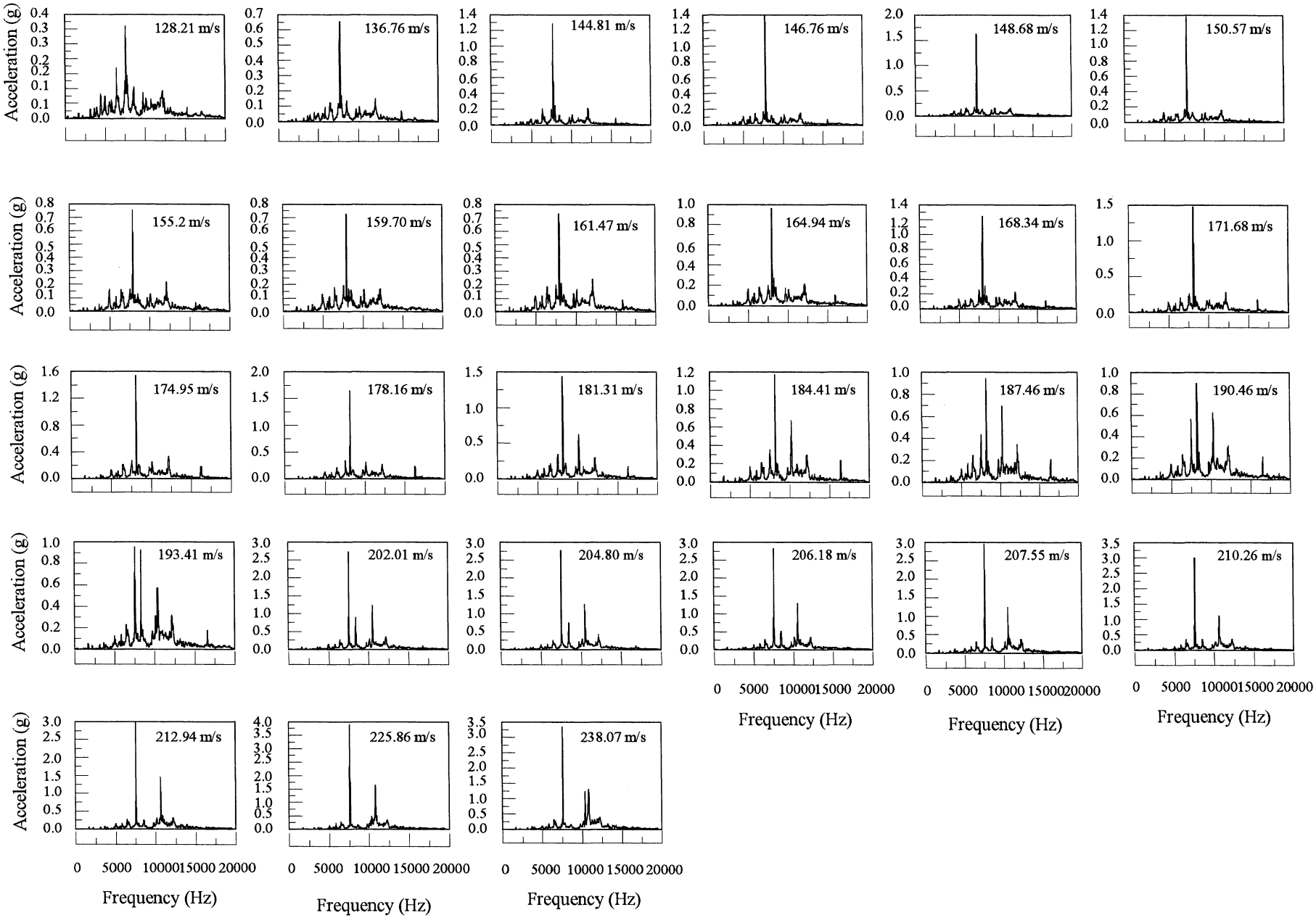

Acceleration Power Spectra JA Evaporator
2rd Sample N2 Test
Velocity at Cross Section

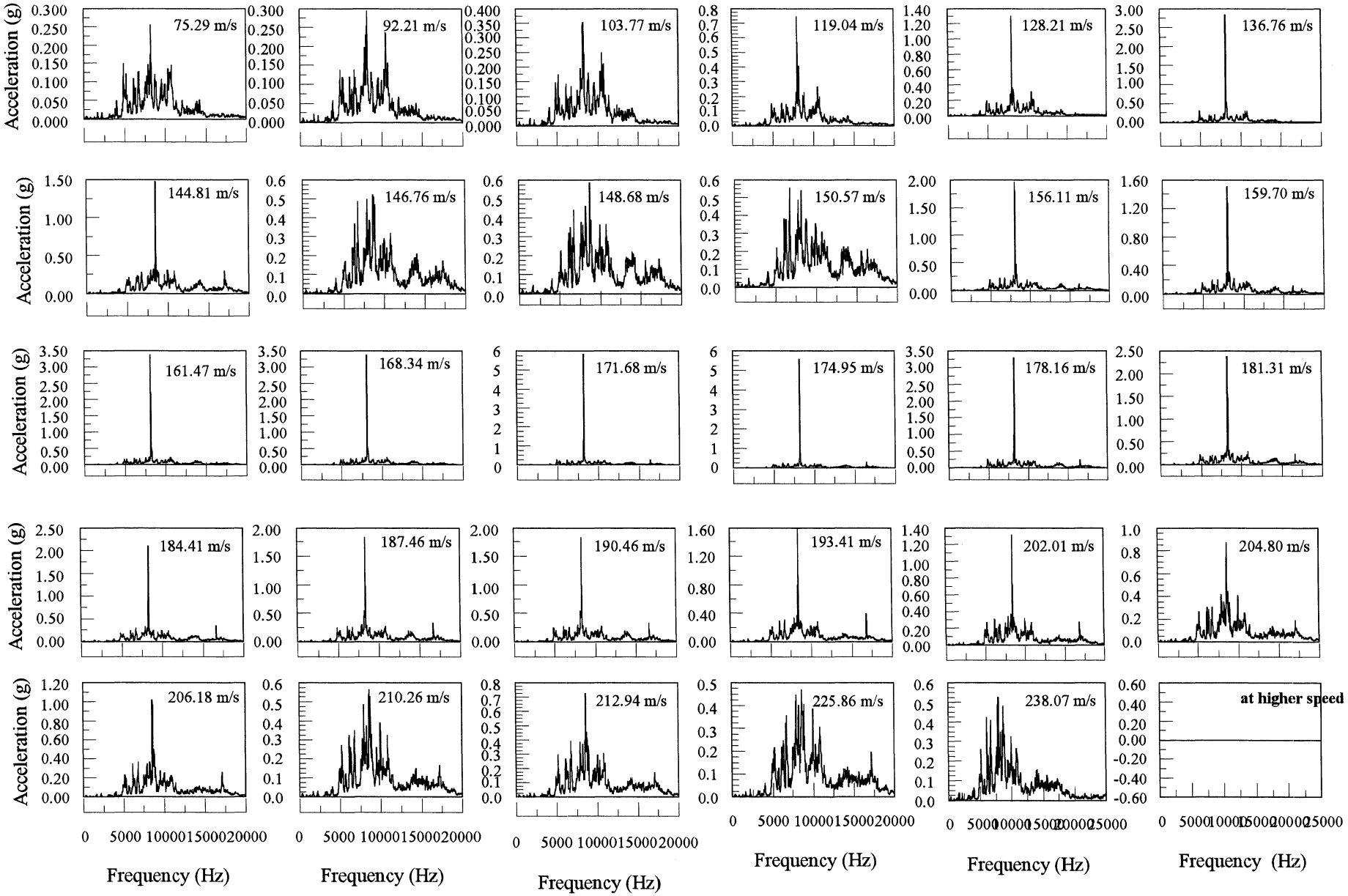

Acceleration Power Spectra JA Evaporator
3rd Sample N2 Test
Velocity at Cross Section

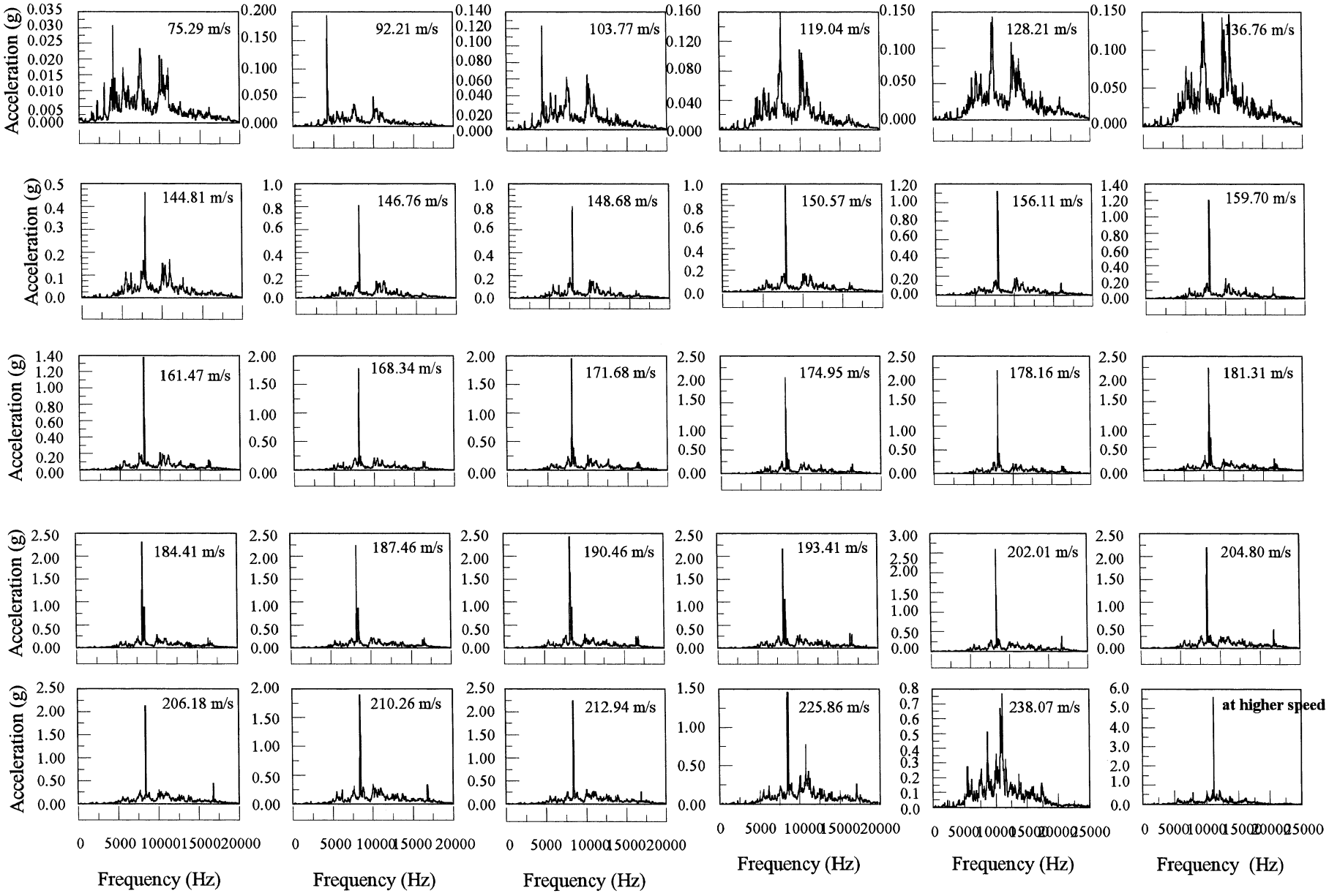

Acceleration Power Spectra NSF-1 Evaporator
N2 Test
Velocity at Cross Section

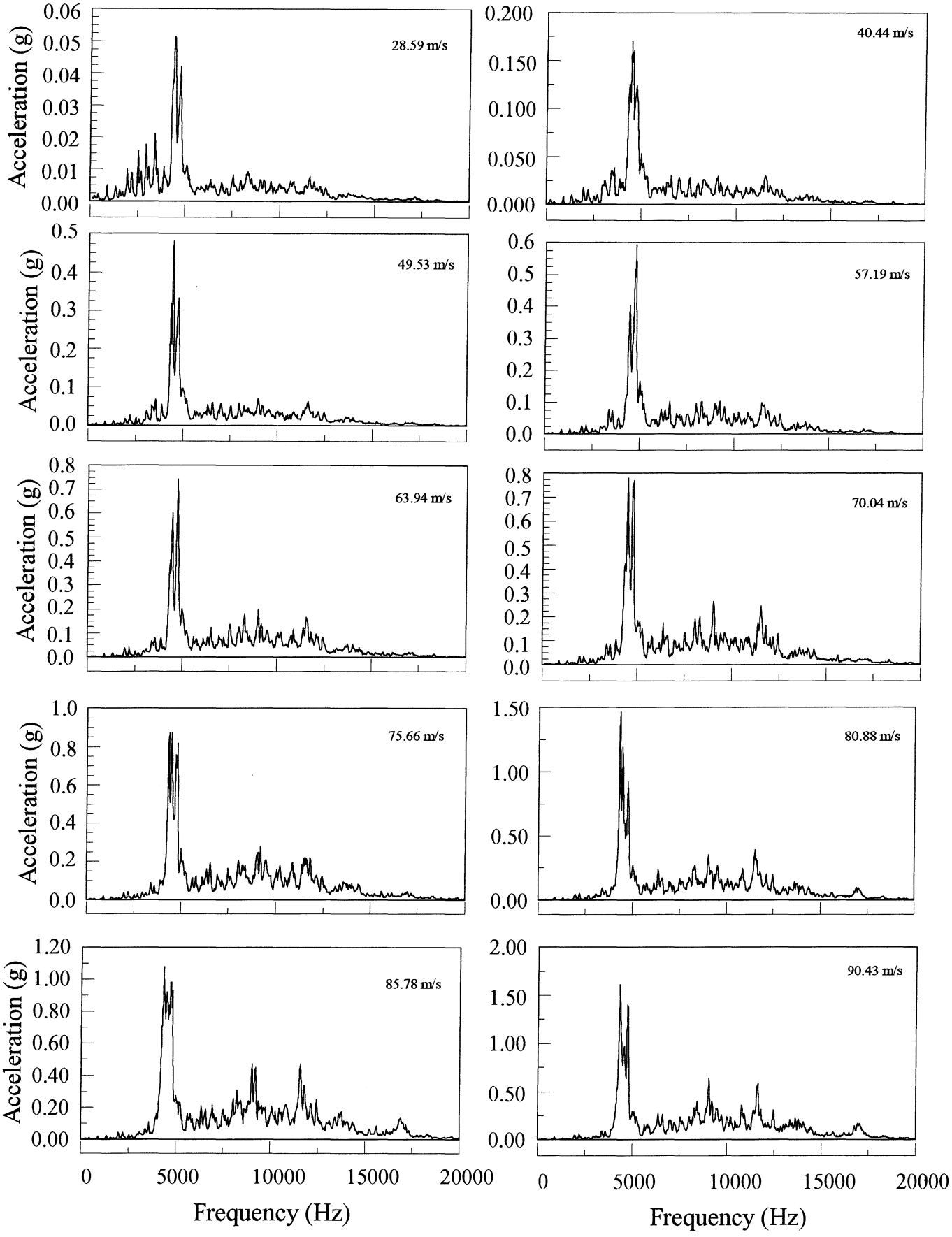

Acceleration Power Spectra NSF-2 Evaporator
N2 Test
Velocity at Cross Section

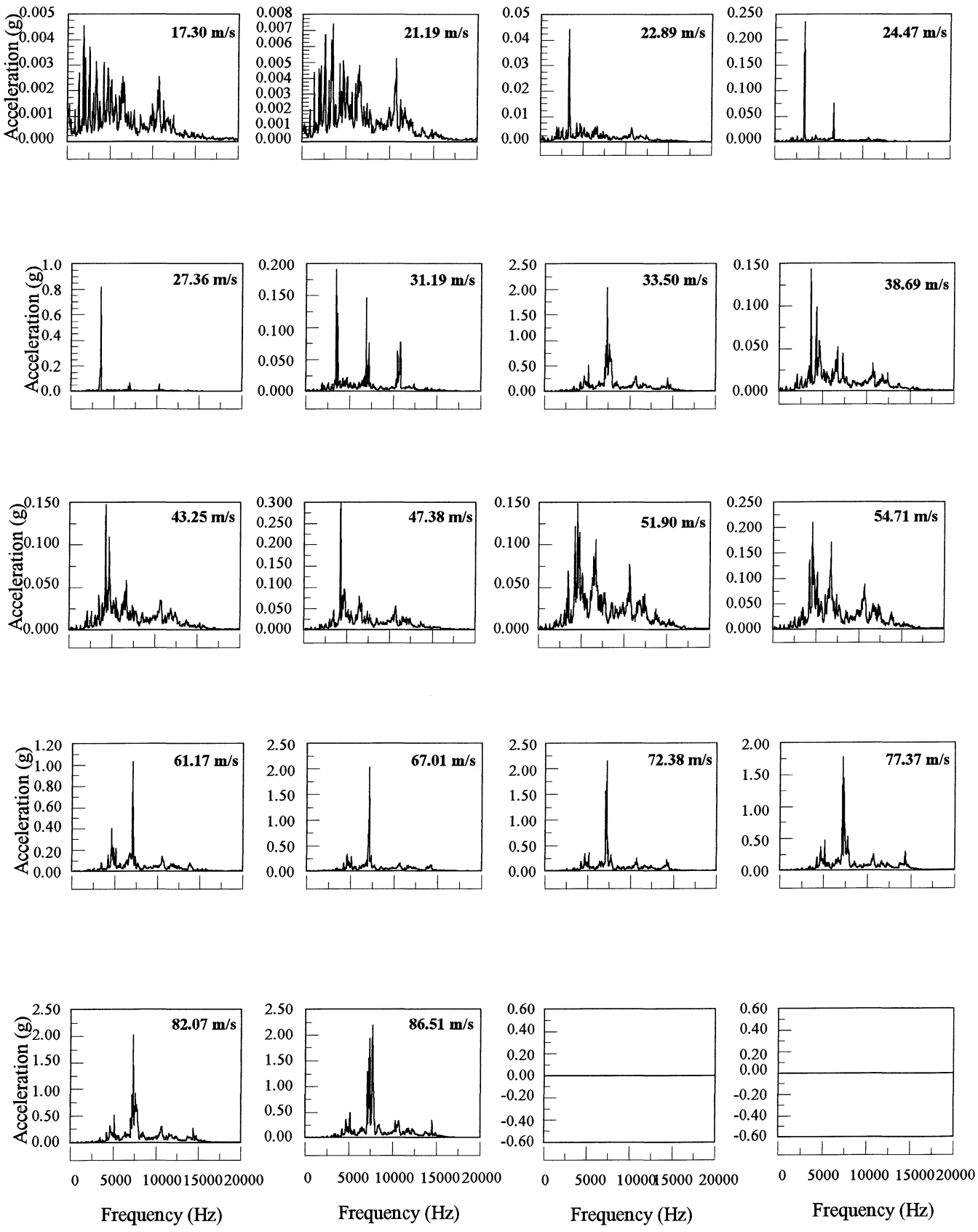

Acceleration Power Spectra NSF-3 Evaporator
N2 Test
Velocity at Cross Section

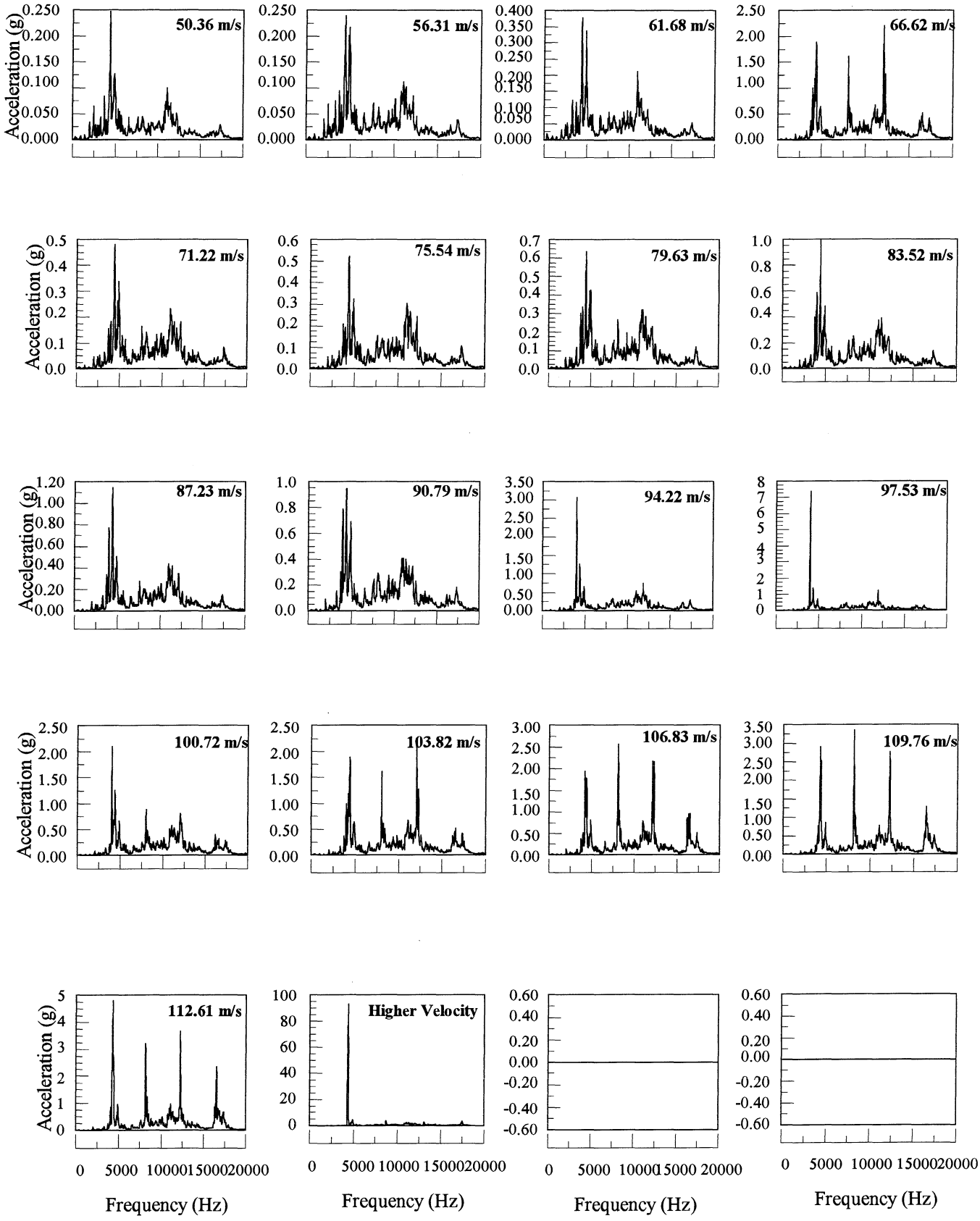

Appendix III

Sound Power Distribution Diagrams

Sound Power Distribution A1 Test

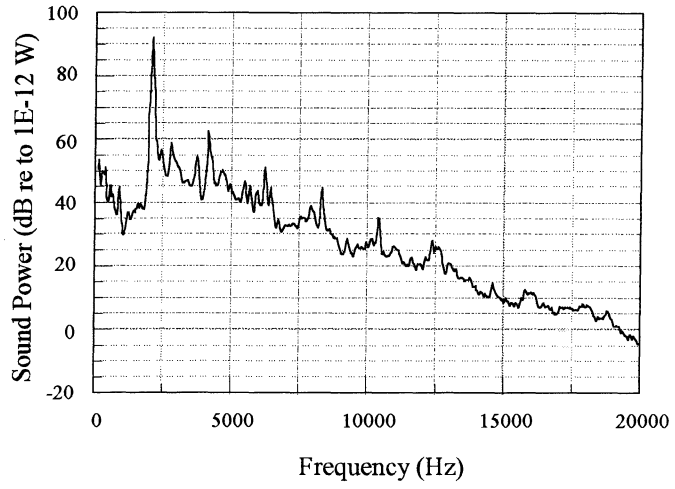

Sound Power Distribution A2 test

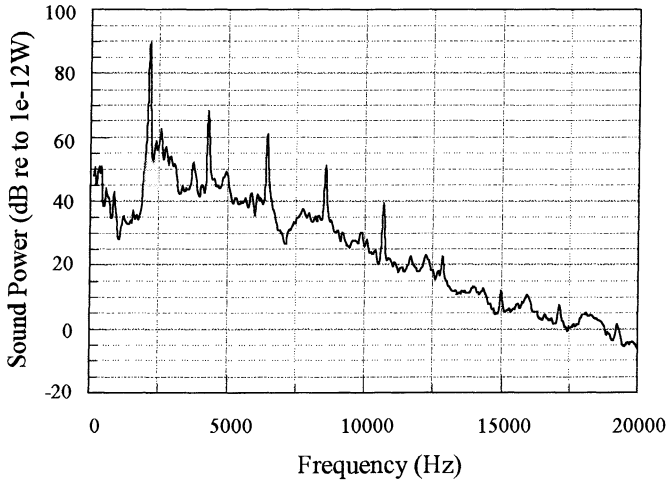

Sound Power Distribution A3 Test

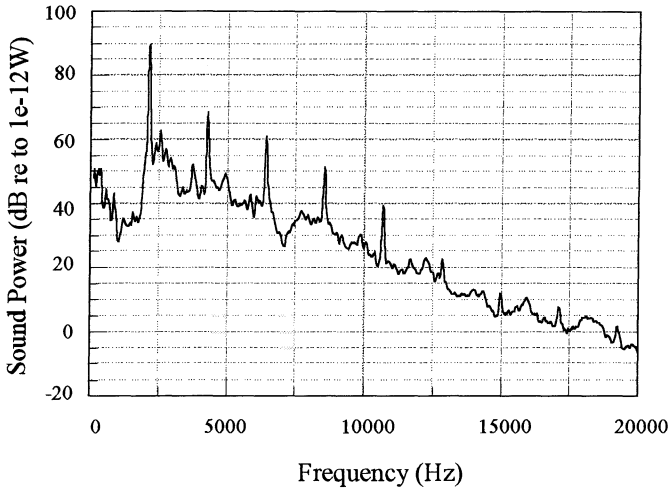

Sound Power Distribution A4 Test

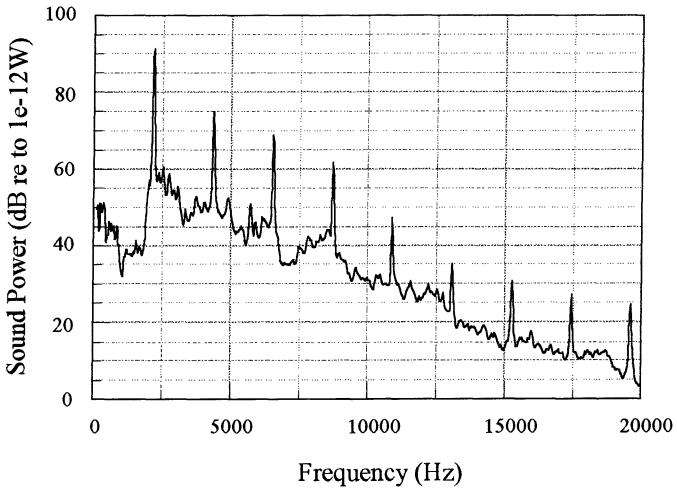

Sound Power Distribution A5 Test

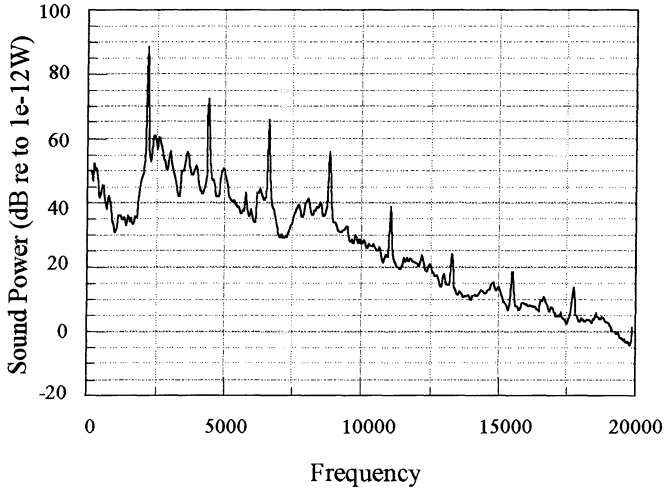

Sound Power Distribution A6 Test

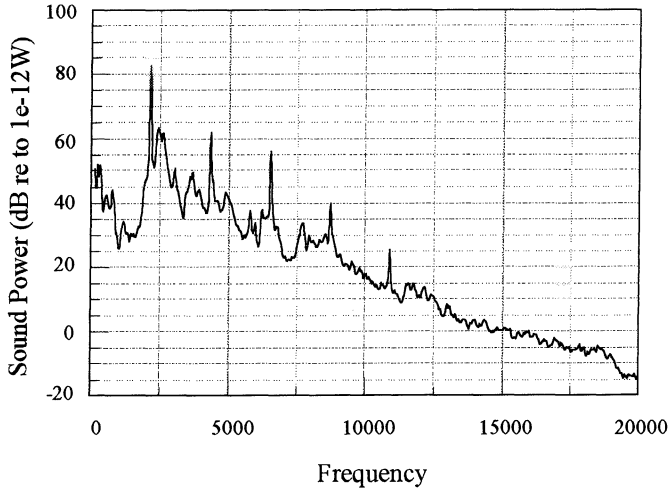

Sound Power Distribution C1 Test

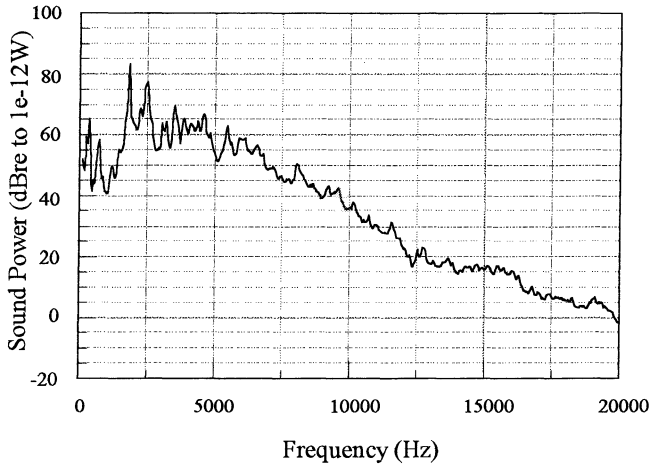

Sound Power Distribution C2 Test

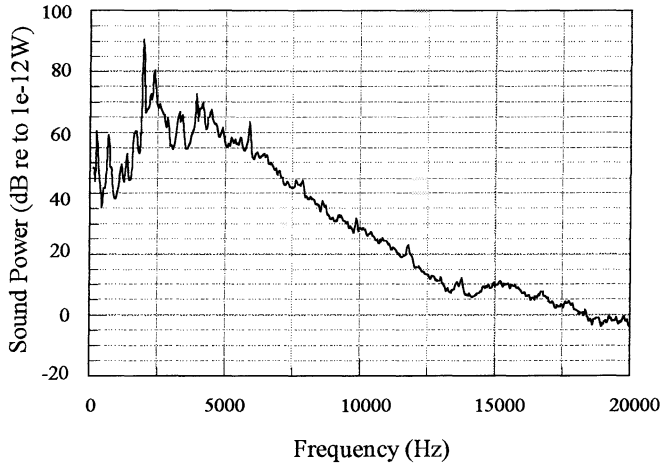

Sound Power Distribution C3 Test

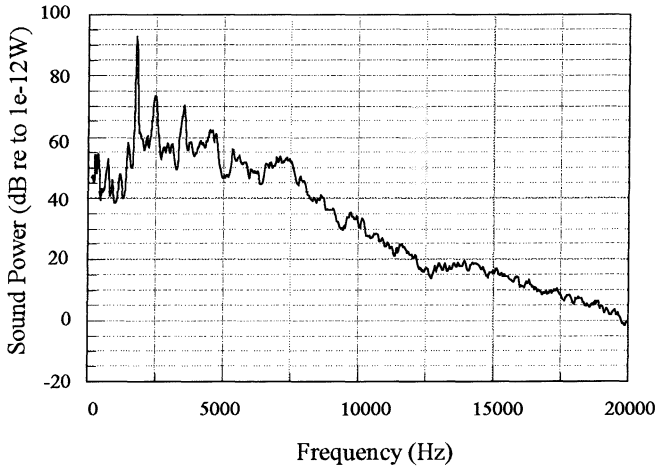

Sound Power Distribution D1 Test

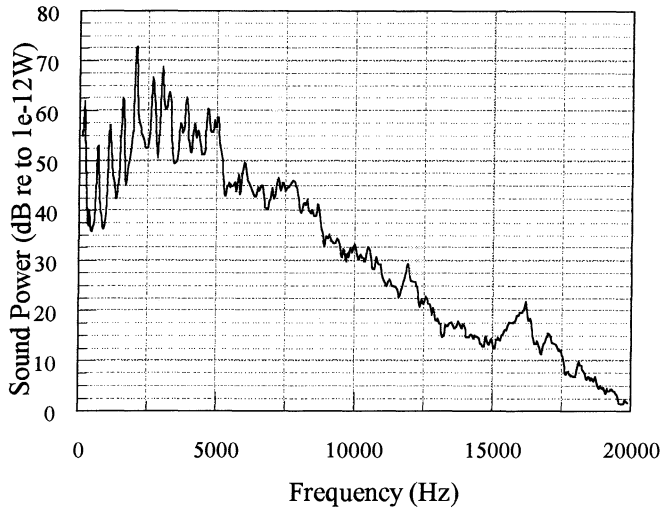

Sound Power Distribution D2 Test

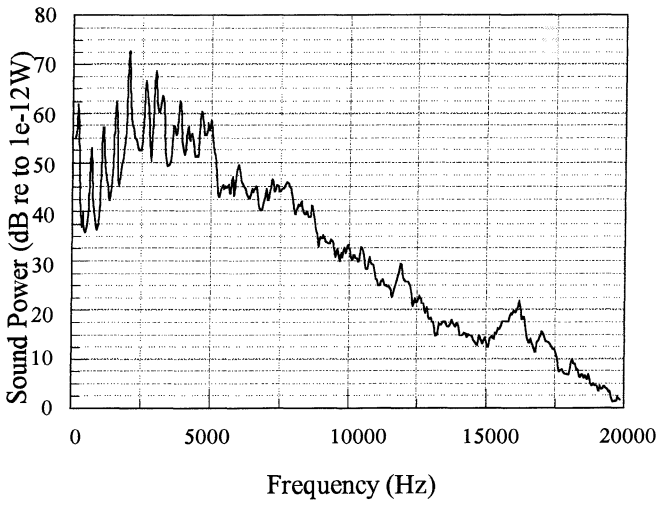

Sound Power Distribution D3 Test

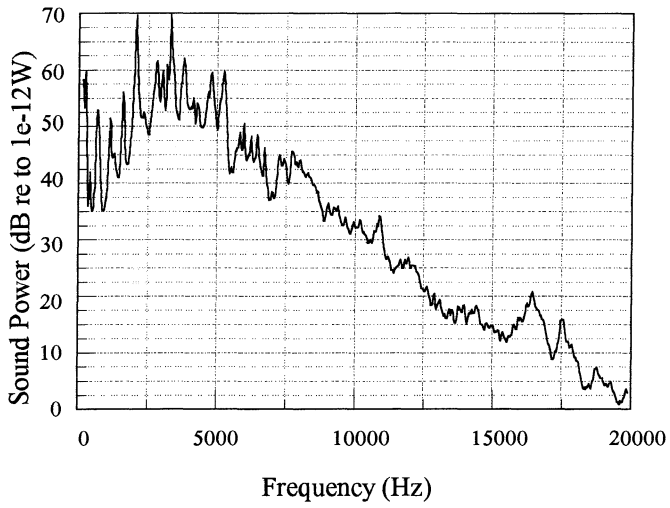

Sound Power Distribution D5 Tests

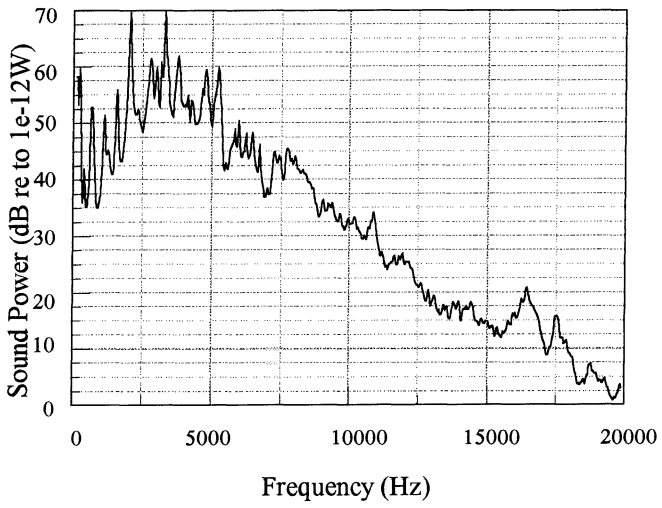

Sound Power Distribution D6 Test

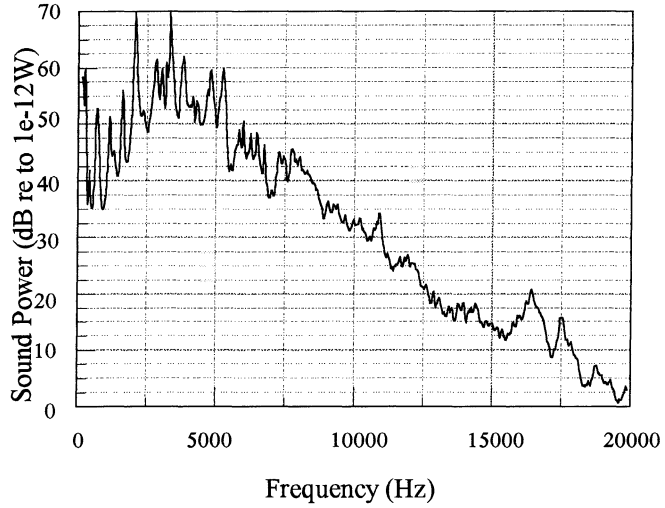

Sound Power Distribution G1 Test

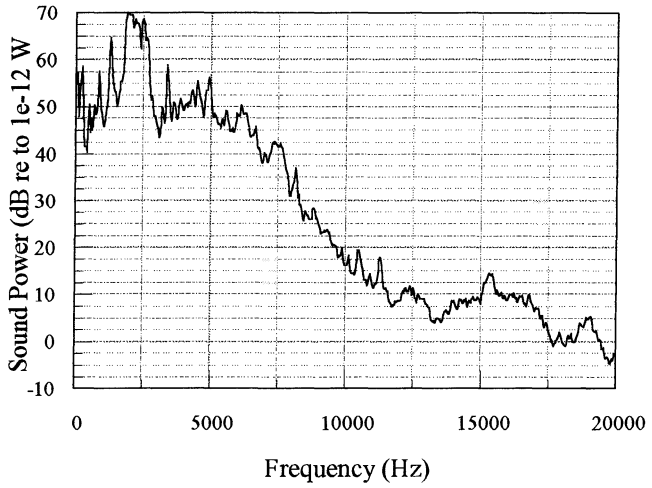

Sound Power Distribution G2 Test

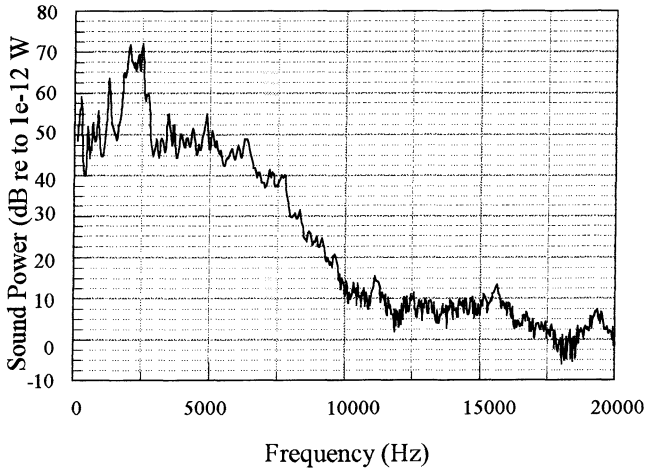

Sound Power Distribution G3 Test

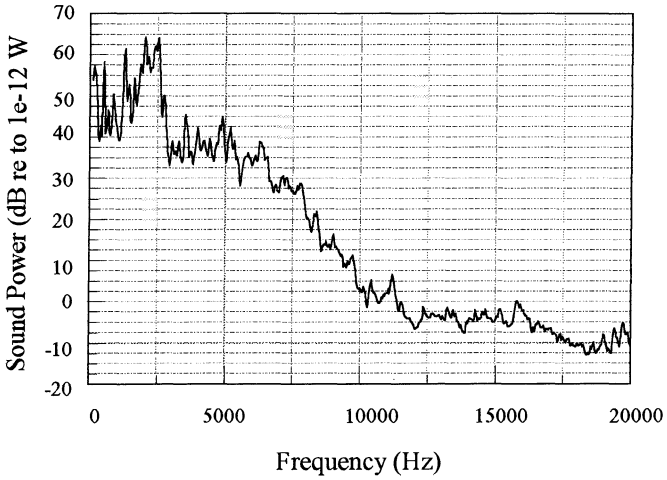

Sound Power Distribution G4 Test

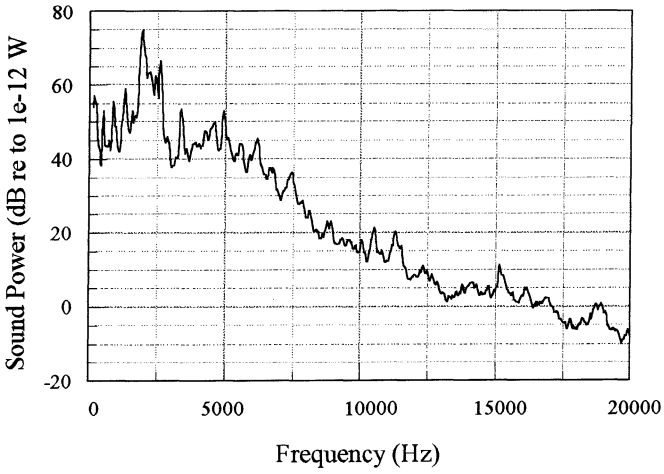

Sound Power Distribution G5 Test

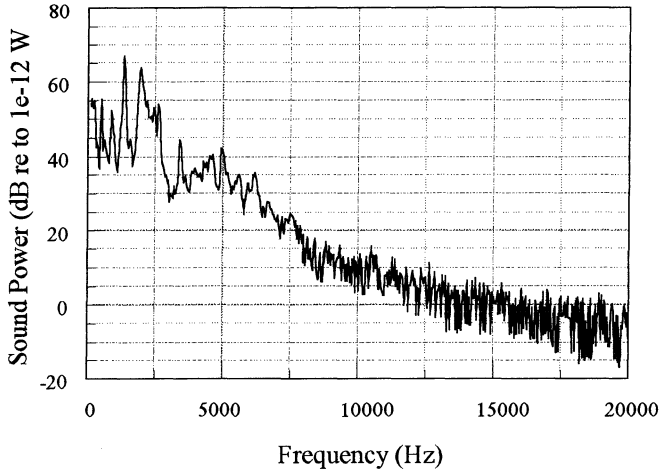

Sound Power Distribution E1 Test

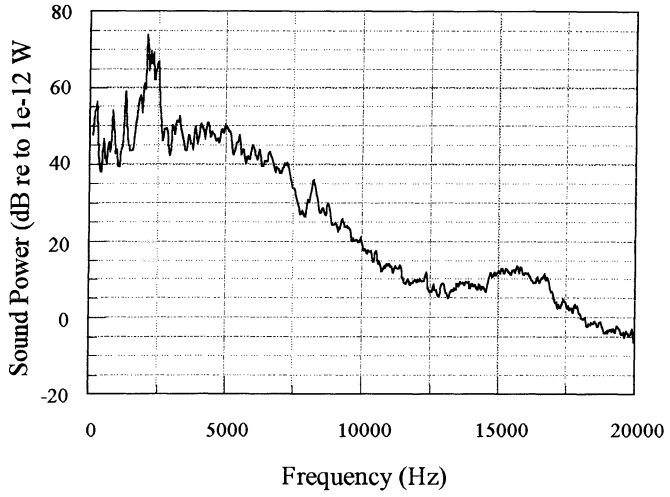

Sound Power Distribution E2 Test

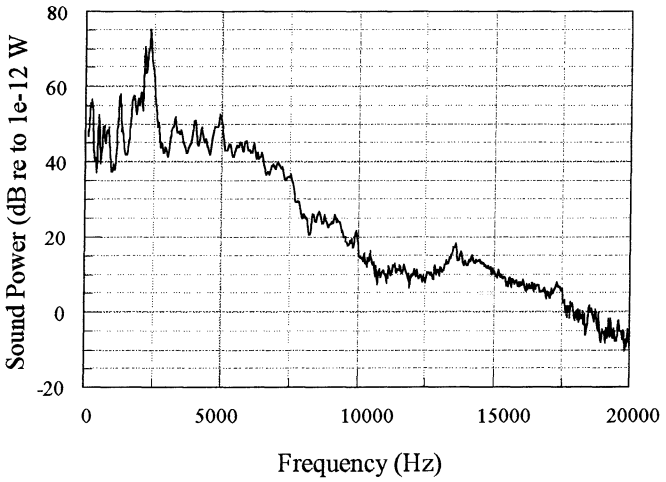

Sound Power Distribution E3 Test

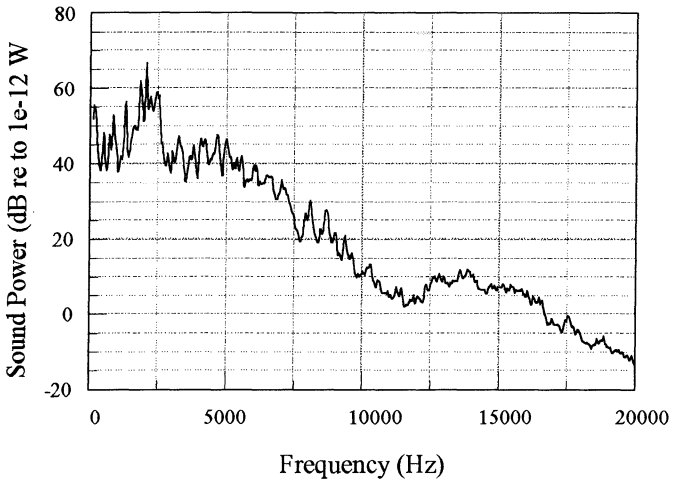

Sound Power Distribution E4 Test

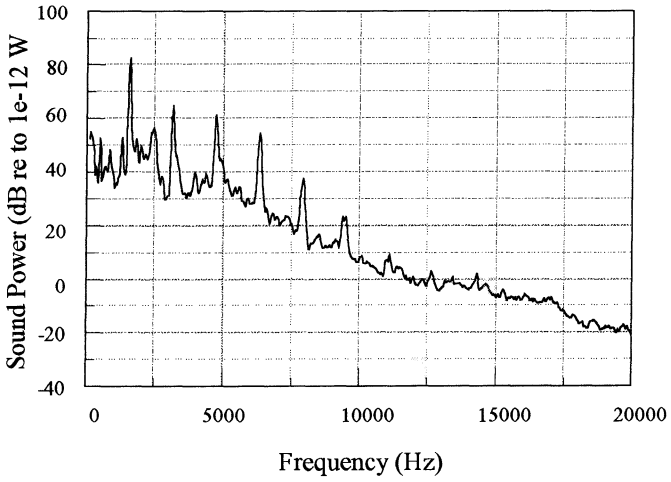

Sound Power Distribution E5 Test

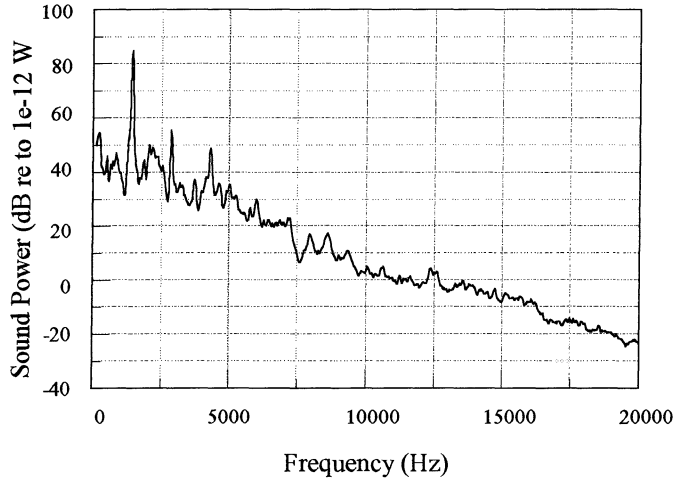

Sound Power Distribution F1 Test

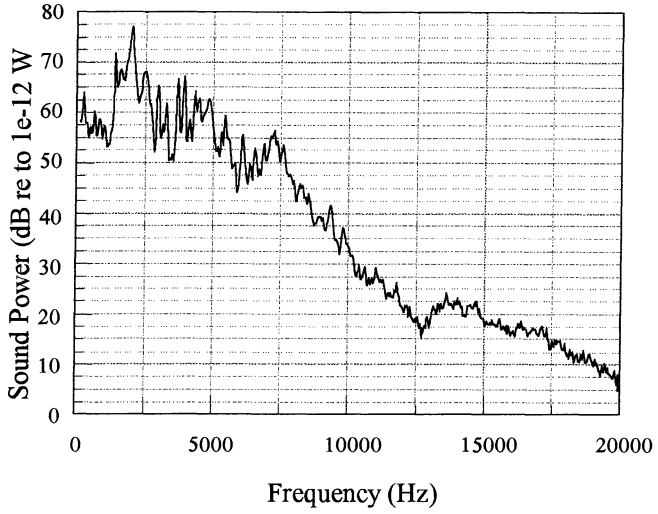

Sound Power Distribution F2 Test

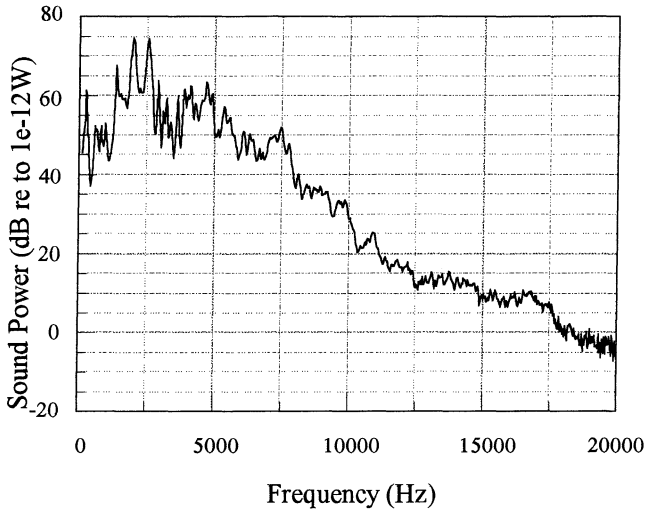

Sound Power Distribution F3 Test

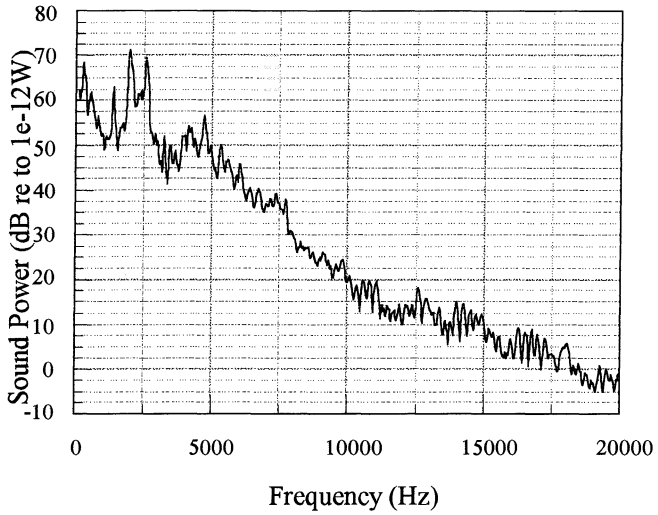

Sound Power Distribution F4 Test

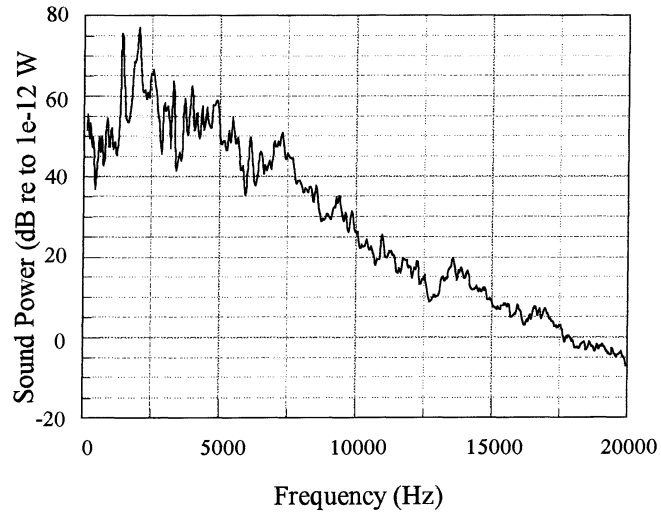

Sound Power Distribution F5 Test

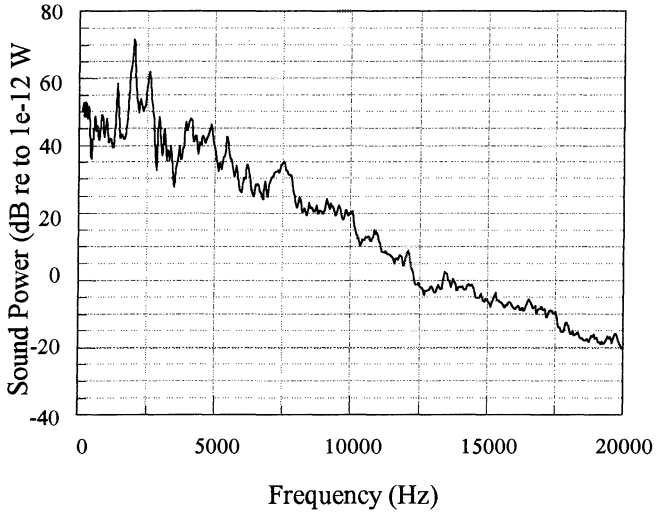

Appendix IV

Band Sound Power vs. Velocity Diagrams

AS/PL, LH, 104

JA, NSF-1, 105

NSF-2, NSF-3 , 106

Band Sound Power vs. Velocity diagrams

AS/PL Evaporator 95% Sound Power Divided by Frequency Band.

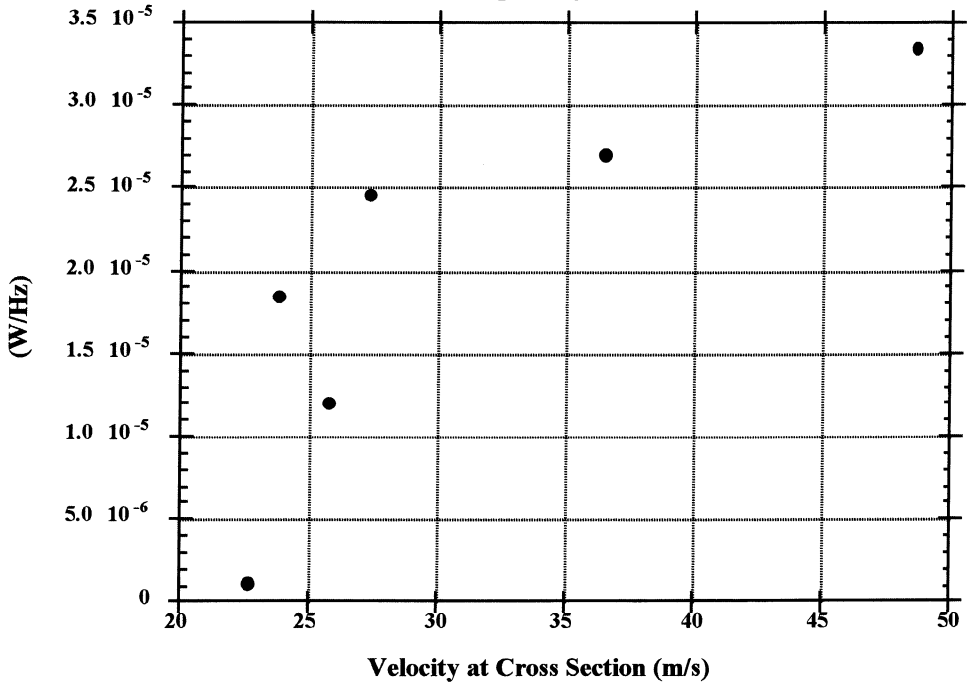

LH Evaporator 95 % Sound Power Divided by Frequency Band.

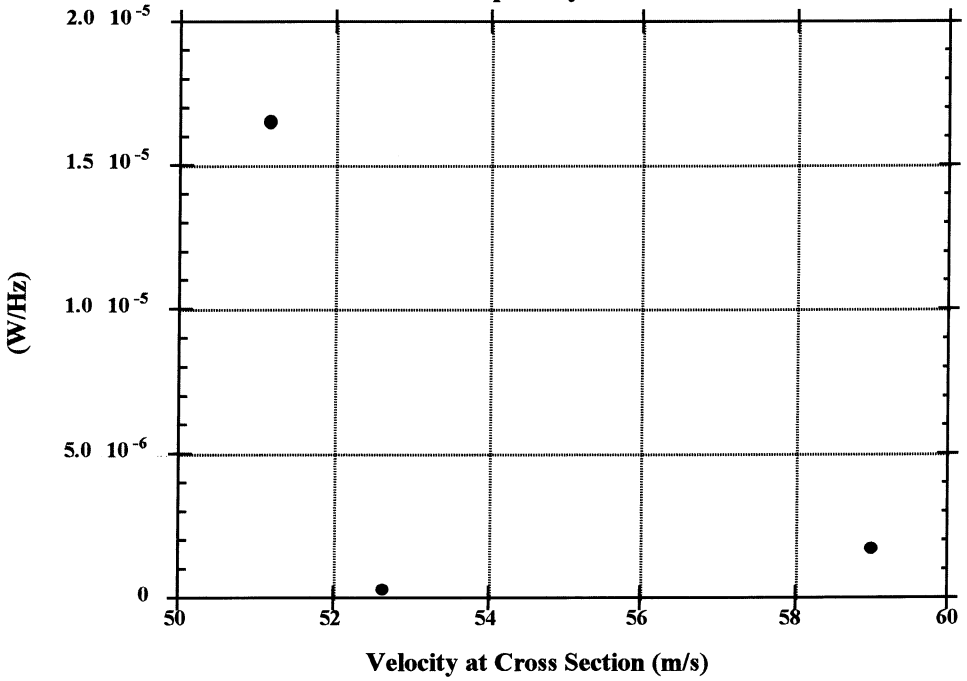

JA Evaporator 95% Sound Power Divided by Frequency Band.

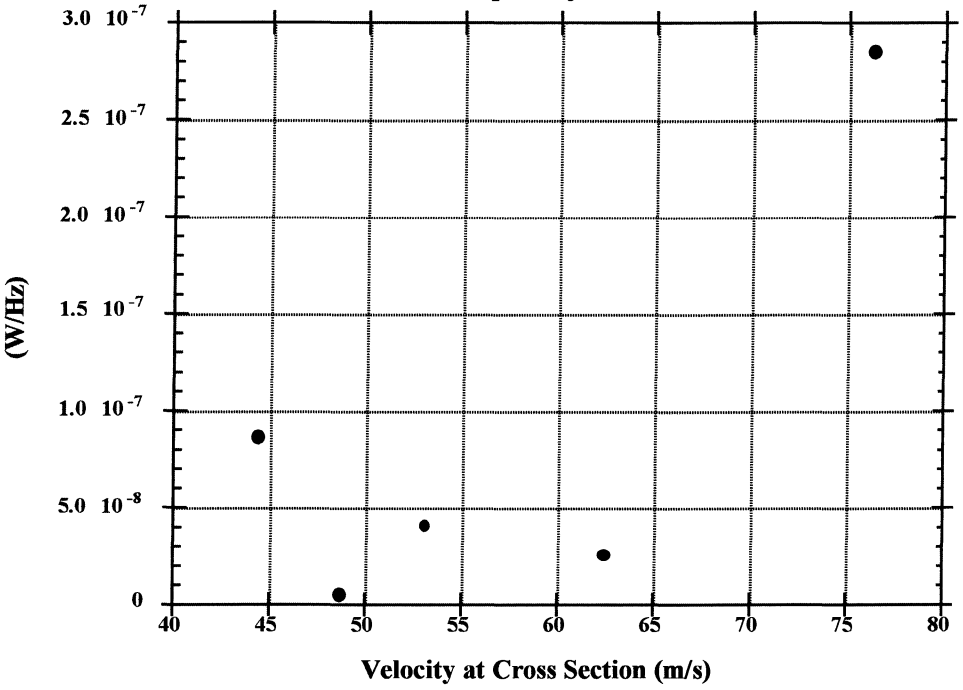

NSF-1 Evaporator 95% Sound Power Divided by Frequency Band.

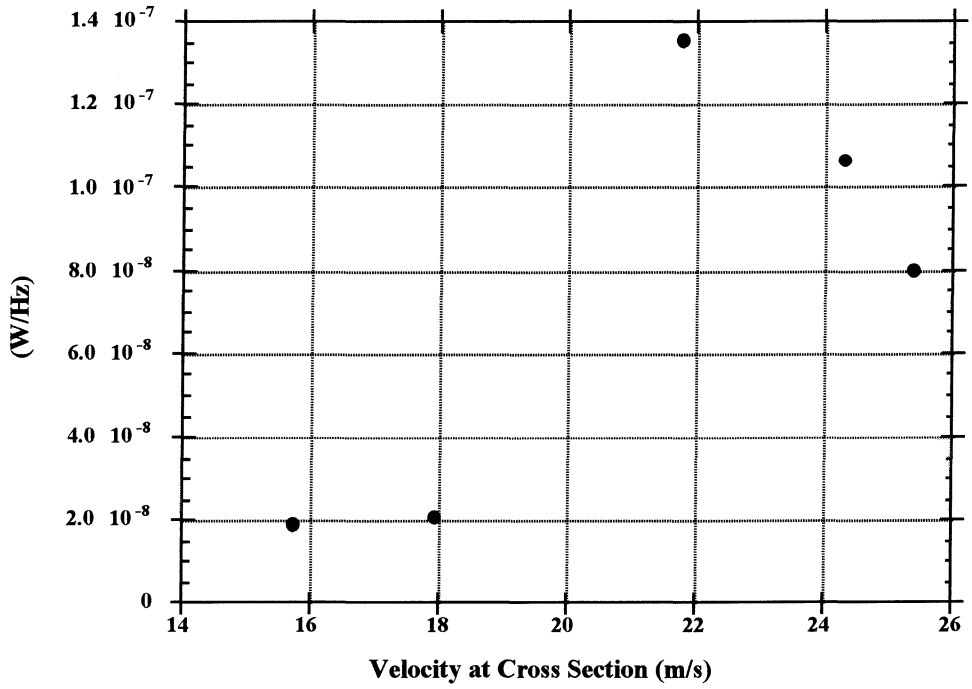

NSF-2 Evaporator 95% Sound Power Divided by Frequency Band.

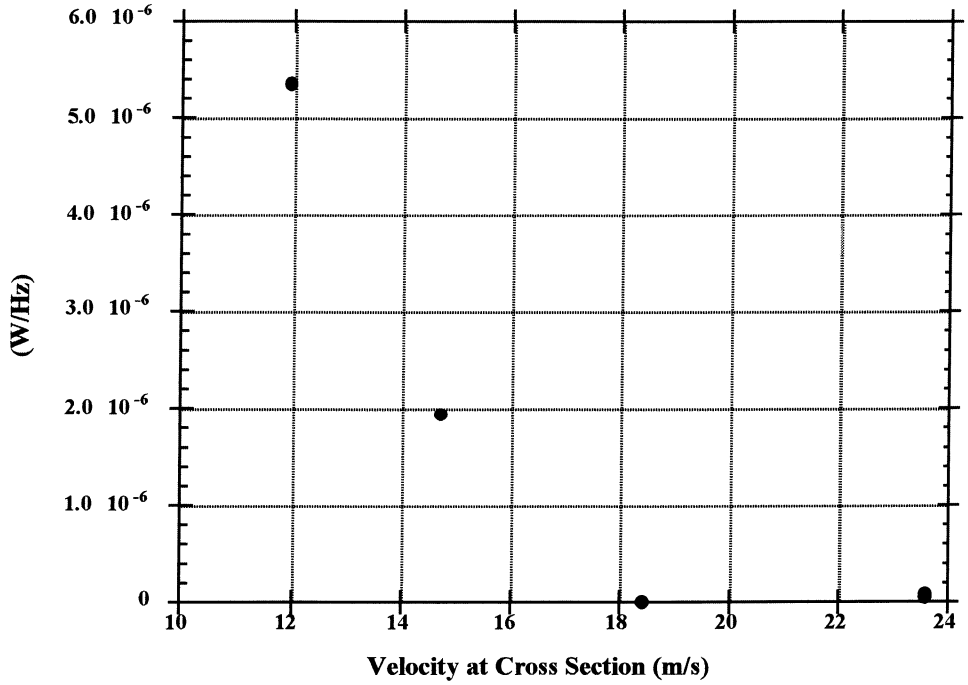

NSF-3 Evaporator 95% Sound Power Divided by Frequency Band.

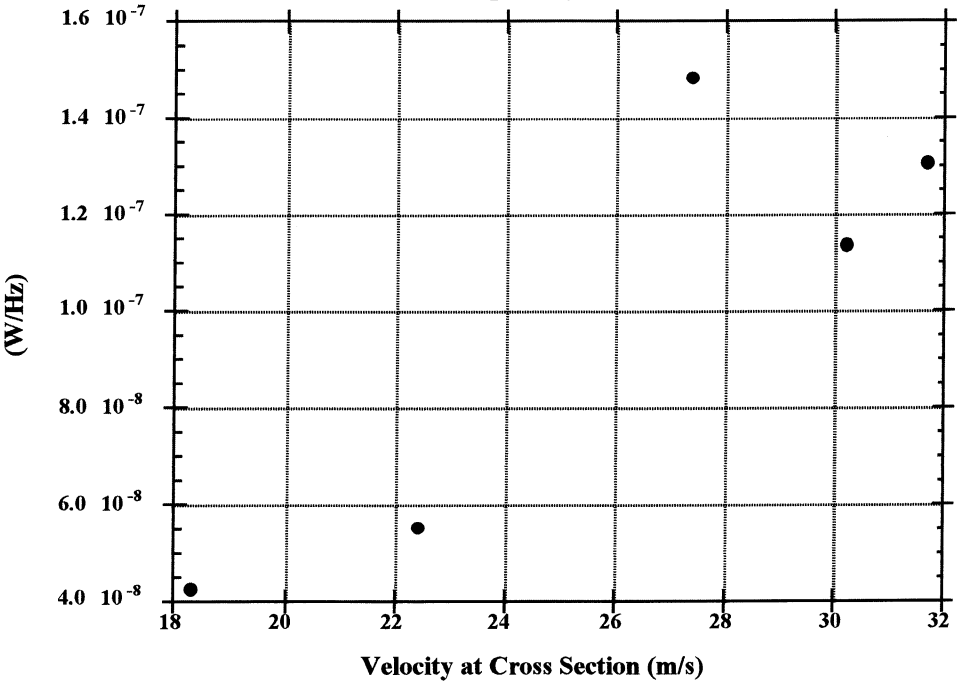

Appendix V

Auxiliary Tables

Refrigerant Tests Table

Evaporator	Test Name	Press. inlet Bars	Temp. inlet °C	P ress. outlet Bars	T emp. outlet °C	Mass Flow g/s	Superheat inlet °C	Superheat outlet °C	c inlet m/s	c outlet m/s	V at cross section m/s
AS/PL											
	A6	5.59	40.8	4.53	38.3	14.78	21.6	25.6	154.7	156.4	22.6
	A2	6.31	33.3	4.78	29.8	18.63	10.1	15.5	149.5	152.4	23.8
	A5	6.28	43.3	4.55	39.4	19.02	20.2	26.5	153.9	156.7	25.7
	A4	7.17	37.3	4.58	31.6	24.27	9.8	18.6	148.8	153.7	27.3
	A1	7.44	28.4	5.27	24.0	24.36	sat	6.7	143.6	148.4	36.5
	A3	6.90	24.9	4.08	18.7	24.92	sat	9.2	144.	150.	48.6
LH											
	C3	6.88	31.0	4.73	26.2	25.42	4.9	12.2	146.3	151.1	51.2
	C1	6.57	37.7	4.54	33.4	24.14	13.2	20.6	150.6	155.	52.6
	C2	8.57	74.0	5.69	69.0	29.74	40.2	49.2	161.2	165.	59.0
JA											
	D2	5.64	36.7	4.69	34.4	17.6	17.2	20.7	153.	155.	44.3
	D5	5.96	32.7	4.79	30.1	20.17	11.4	15.7	150.1	153.	48.7
	D1	8.21	31.4	5.61	27.6	26.61	sat	8.3	142.9	148.9	53.0
	D3	6.23	35.8	4.54	32.2	24.1	13.1	19.5	151.	154.	62.3
	D6	7.72	71.6	5.18	67.1	29.93	41.5	50.2	162.	165.2	75.0
NSF-1											
	G5	5.63	45.3	4.71	42.8	15.86	25.9	29.0	156.4	157.7	15.7
	G3	6.55	64.7	5.28	61.3	18.99	40.3	43.8	161.7	163.0	17.9
	G4	6.42	45.9	4.77	42.3	22.29	22.1	28.0	154.6	157.4	21.7
	G2	7.26	60.8	5.20	56.6	25.74	32.9	39.7	158.7	161.6	24.3
	G1	7.48	53.3	5.22	48.7	27.9	24.32	31.7	155.0	158.7	25.4
NSF-2											
	E5	6.94	31.9	6.22	30.3	18.38	5.5	7.5	146.5	148.	11.9
	E4	5.56	44.4	4.80	42.1	15.93	25.3	27.6	156.	157.2	14.7
	E3	6.06	31.7	4.94	29.3	21.81	9.8	14.0	149.	152.	18.4
	E2	6.71	57.2	5.13	53.7	26.05	32.0	37.2	158.	161.	23.6
	E1	7.11	42.7	5.35	38.9	29.17	15.5	21.1	151.2	154.6	23.6
NSF-3											
	F5	5.98	42.9	5.06	40.3	16.22	21.4	24.3	154.5	155.9	19.7
	F3	6.59	55.5	5.29	52.2	19.79	30.9	34.8	158.1	159.8	24.1
	F4	6.56	35.2	4.76	31.4	23.66	10.7	17.2	149.4	153.2	29.5
	F2	7.49	53.1	5.30	48.6	27.19	24.1	31.1	154.9	158.5	32.6
	F1	7.78	37.37	5.24	31.8	30.41	5.6	13.1	145.9	151.3	34.3

Sound Power Calculations Table

	Evaporator	Avg. Flow Velocity	Freq. at max. g's (at peak)	Bandwidth (Hz)	Percentage of Sound Power	Total Sound Power	95% of Sound Power	95 % sound power/freq. band	c inlet	c outlet	c average
		[m/s]	[Hz]	[Hz]		[W]	[W]	[W/Hz]	[m/s]	[m/s]	[m/s]
	AS-PL										
	A1	36.49	2078	125	0.963669727	0.00350165	0.00337443	2.6995E-05	sat	148	148
	A2	23.78	2143	93.75	0.96648487	0.00178827	0.00172834	1.8436E-05	149	152	151
	A3	48.59	2135	93.75	0.953412415	0.00328295	0.00313001	3.3387E-05	sat	150	150
	A4	27.25	2176	93.75	0.952556601	0.00241843	0.00230369	2.4573E-05	149	154	151
	A5	25.71	2220	93.75	0.951742181	0.00118313	0.00112603	1.2011E-05	154	157	155
	A6	22.59	2179	250	0.952668221	0.00030006	0.00028586	1.1434E-06	155	156	156
Averages	A1-A6	30.735		125	0.956755669	0.00207908	0.00199139	1.5931E-05	152	153	152
	LH										
	C1	52.64	1833	2812.5	0.950789149	0.0009256	0.00088005	3.1291E-07	151	155	153
	C2	59.01	1957	1312.5	0.951261204	0.00236199	0.00224687	1.7119E-06	161	165	163
	C3	51.15	1787	187.5	0.9516489	0.00325721	0.00309972	1.6532E-05	146	151	149
Averages	C1-C3	54.26667		1437.5	0.951233084	0.0021816	0.00207555	1.4439E-06	153	157	155
	JA										
	D1	53	2175	3312.5	0.951020436	0.00014218	0.00013522	4.082E-08	143	149	146
	D2	44.28	2241	1500	0.950177398	0.00013619	0.0001294	8.627E-08	153	155	154
	D3	62.34	3415	3687.5	0.950078968	0.00010065	9.5625E-05	2.5932E-08	151	154	153
	D5	48.69	2175	2593.75	0.95029704	1.4486E-05	1.3766E-05	5.3074E-09	150	153	152
	D6	76.3	3740	1593.75	0.950729521	0.00047848	0.00045491	2.8543E-07	162	165	164
Averages	D1-D6	56.922		2537.5	0.950460673	0.0001744	0.00016578	6.5333E-08	152	155	154
	NSF-1										
	G1	25.36	2295	2375	0.950658651	0.00019995	0.00019008	8.0035E-08	155	159	157
	G2	24.29	2487	1781.25	0.950712295	0.00019936	0.00018953	1.0641E-07	159	162	160
	G3	17.93	2014	1625	0.950490639	3.5568E-05	3.3807E-05	2.0804E-08	162	163	162
	G4	21.74	1893	1156.25	0.950329256	0.00016495	0.00015676	1.3557E-07	155	157	156
	G5	15.72	1923	1375	0.952067635	0.00002763	2.6306E-05	1.9131E-08	156	158	157
Averages	G1-G5	21.008		1662.5	0.950851695	0.00012549	0.0001193	7.1758E-08	157	160	158

	Evaporator	Avg. Flow Velocity	Freq. at max. g's (at peak)	Bandwidth (Hz)	Percentage of Sound Power	Total Sound Power	95% of Sound Power	95 % sound power/freq. band	c inlet	c outlet	c average
		[m/s]	[Hz]	[Hz]		[W]	[W]	[W/Hz]	[m/s]	[m/s]	[m/s]
	NSF-2										
	E1	23.6	2101	1937.5	0.950650857	0.0001177	0.00011189	5.7751E-08	151	155	153
	E2	23.57	2391	1375	0.950551207	0.0001324	0.00012585	9.1529E-08	158	161	160
	E3	18.41	2071	2718.75	0.950864405	0.00002655	2.5245E-05	9.2857E-09	149	152	151
	E4	14.73	1583	156.25	0.950386583	0.00031902	0.00030319	1.9404E-06	156	157	157
	E5	11.95	1443	93.75	0.980147712	0.00051206	0.00050189	5.3535E-06	147	148	147
Averages	E1-E5	18.452		1256.25	0.956520153	0.00022155	0.00021362	1.7004E-07	152	155	153
	NSF-3										
	F1	31.68	2016	3843.75	0.950197231	0.00052821	0.0005019	1.3058E-07	147	152	149
	F2	30.23	2016	2812.5	0.950043407	0.00033609	0.0003193	1.1353E-07	155	159	157
	F3	22.41	1982	2750	0.950551301	0.00016006	0.00015215	5.5326E-08	154	157	155
	F4	27.39	2015	2125	0.95031037	0.00033173	0.00031525	1.4835E-07	154	157	155
	F5	18.31	2012	1281.25	0.950951077	0.00005733	5.4518E-05	4.2551E-08	152	155	154
Averages	F1-F5	26.004		2562.5	0.950410677	0.00028268	0.00026862	1.0483E-07	152	156	154

Table of Cross Section Velocities as a function of Pressure Difference at Venturi Nitrogen Tests.

Delta P in H2O	Vdot=K*sqrt(2*deltap*vspecific) Volumetric flow (m^3/s)	AS-PL Dimples Vel. (m/s)	AS-PL Toenails Vel. (m/s)	JA Dimples Vel. (m/s)	JA Toenails Vel. (m/s)	JA Bottom pass Vel. (m/s)	LH Dimples Vel. (m/s)	LH Toenails Vel. (m/s)	LH Bottom pass Vel. (m/s)	E-large sausages Vel. (m/s)	F-Small dimples (1st section) Vel. (m/s)	F-Small dimples (2nd section) Vel. (m/s)	G-Large dimples Vel. (m/s)
0.00	0.00	0.00	0.00	0.00	0.00	0.00	0.00	0.00	0.00	0.00	0.00	0.00	0.00
0.10	0.0004571	16.99	24.84	23.81	28.39	22.97	19.96	20.87	34.89	8.65	12.13	11.26	9.04
0.20	0.00064644	24.03	35.13	33.67	40.15	32.48	28.23	29.52	49.35	12.23	17.16	15.93	12.79
0.30	0.00079172	29.43	43.03	41.24	49.18	39.78	34.57	36.15	60.44	14.98	21.01	19.51	15.66
0.40	0.0009142	33.99	49.68	47.61	56.78	45.94	39.92	41.74	69.79	17.30	24.26	22.52	18.09
0.50	0.00102211	38.00	55.55	53.23	63.48	51.36	44.63	46.67	78.02	19.34	27.13	25.18	20.22
0.60	0.00111966	41.62	60.85	58.32	69.54	56.26	48.89	51.13	85.47	21.19	29.71	27.58	22.15
0.70	0.00120937	44.96	65.73	62.99	75.12	60.77	52.81	55.22	92.32	22.89	32.10	29.79	23.92
0.80	0.00129287	48.06	70.26	67.34	80.30	64.97	56.46	59.04	98.69	24.47	34.31	31.85	25.58
0.90	0.0013713	50.98	74.53	71.42	85.17	68.91	59.88	62.62	104.68	25.95	36.39	33.78	27.13
1.00	0.00144548	53.74	78.56	75.29	89.78	72.64	63.12	66.00	110.34	27.36	38.36	35.61	28.59
1.10	0.00151603	56.36	82.39	78.96	94.16	76.18	66.20	69.23	115.73	28.69	40.23	37.35	29.99
1.20	0.00158344	58.86	86.06	82.47	98.35	79.57	69.15	72.30	120.87	29.97	42.02	39.01	31.32
1.30	0.0016481	61.27	89.57	85.84	102.37	82.82	71.97	75.26	125.81	31.19	43.74	40.60	32.60
1.40	0.00171031	63.58	92.95	89.08	106.23	85.95	74.69	78.10	130.56	32.37	45.39	42.14	33.83
1.50	0.00177034	65.81	96.21	92.21	109.96	88.96	77.31	80.84	135.14	33.50	46.98	43.62	35.02
1.60	0.0018284	67.97	99.37	95.23	113.57	91.88	79.84	83.49	139.57	34.60	48.52	45.05	36.17
1.70	0.00188467	70.06	102.43	98.16	117.06	94.71	82.30	86.06	143.87	35.67	50.02	46.43	37.28
1.80	0.00193931	72.09	105.40	101.01	120.45	97.45	84.69	88.55	148.04	36.70	51.47	47.78	38.36
1.90	0.00199245	74.07	108.29	103.77	123.75	100.12	87.01	90.98	152.10	37.71	52.88	49.09	39.42
2.00	0.00204421	75.99	111.10	106.47	126.97	102.72	89.27	93.34	156.05	38.69	54.25	50.36	40.44
2.10	0.00209469	77.87	113.84	109.10	130.11	105.26	91.47	95.65	159.90	39.64	55.59	51.61	41.44
2.20	0.00214399	79.70	116.52	111.67	133.17	107.74	93.62	97.90	163.66	40.58	56.90	52.82	42.41
2.30	0.00219217	81.49	119.14	114.18	136.16	110.16	95.73	100.10	167.34	41.49	58.18	54.01	43.37
2.40	0.00223932	83.25	121.70	116.63	139.09	112.53	97.79	102.25	170.94	42.38	59.43	55.17	44.30
2.50	0.0022855	84.96	124.21	119.04	141.96	114.85	99.80	104.36	174.47	43.25	60.66	56.31	45.21
2.60	0.00233076	86.65	126.67	121.39	144.77	117.12	101.78	106.43	177.92	44.11	61.86	57.42	46.11
2.70	0.00237516	88.30	129.08	123.71	147.53	119.35	103.72	108.45	181.31	44.95	63.03	58.52	46.99
2.80	0.00241874	89.92	131.45	125.98	150.23	121.54	105.62	110.44	184.64	45.77	64.19	59.59	47.85
2.90	0.00246156	91.51	133.78	128.21	152.89	123.70	107.49	112.40	187.91	46.59	65.33	60.64	48.70
3.00	0.00250364	93.07	136.07	130.40	155.51	125.81	109.33	114.32	191.12	47.38	66.44	61.68	49.53

Delta P in H2O	Vdot=K*sqrt(2*deltap*vspecific)	AS-PL Dimples	AS-PL Toenails	JA Dimples	JA Toenails	JA Bottom pass	LH Dimples	LH Toenails	LH Bottom pass	E-large sausages	F-Small dimples (1st section)	F-Small dimples (2nd section)	G-Large dimples
3.10	0.00254502	94.61	138.32	132.55	158.08	127.89	111.14	116.21	194.28	48.16	67.54	62.70	50.35
3.20	0.00258575	96.12	140.53	134.67	160.61	129.94	112.91	118.07	197.39	48.94	68.62	63.70	51.15
3.30	0.00262584	97.61	142.71	136.76	163.10	131.95	114.67	119.90	200.45	49.69	69.69	64.69	51.95
3.40	0.00266533	99.08	144.85	138.82	165.55	133.94	116.39	121.70	203.46	50.44	70.74	65.66	52.73
3.50	0.00270424	100.53	146.97	140.85	167.97	135.89	118.09	123.48	206.43	51.18	71.77	66.62	53.50
3.60	0.0027426	101.96	149.05	142.84	170.35	137.82	119.76	125.23	209.36	51.90	72.79	67.57	54.26
3.70	0.00278043	103.36	151.11	144.81	172.70	139.72	121.42	126.96	212.25	52.62	73.79	68.50	55.00
3.80	0.00281775	104.75	153.14	146.76	175.02	141.60	123.05	128.66	215.10	53.33	74.78	69.42	55.74
3.90	0.00285459	106.12	155.14	148.68	177.30	143.45	124.65	130.35	217.91	54.02	75.76	70.33	56.47
4.00	0.00289095	107.47	157.12	150.57	179.56	145.27	126.24	132.01	220.68	54.71	76.72	71.22	57.19
4.10	0.00292686	108.81	159.07	152.44	181.79	147.08	127.81	133.65	223.42	55.39	77.68	72.11	57.90
4.20	0.00296234	110.12	161.00	154.29	184.00	148.86	129.36	135.27	226.13	56.06	78.62	72.98	58.60
4.30	0.0029974	111.43	162.90	156.11	186.17	150.62	130.89	136.87	228.81	56.73	79.55	73.85	59.30
4.40	0.00303206	112.72	164.79	157.92	188.33	152.36	132.40	138.45	231.45	57.38	80.47	74.70	59.98
4.50	0.00306632	113.99	166.65	159.70	190.45	154.09	133.90	140.01	234.07	58.03	81.38	75.54	60.66
4.60	0.0031002	115.25	168.49	161.47	192.56	155.79	135.38	141.56	236.66	58.67	82.28	76.38	61.33
4.70	0.00313372	116.50	170.31	163.21	194.64	157.47	136.84	143.09	239.21	59.31	83.17	77.20	61.99
4.80	0.00316688	117.73	172.11	164.94	196.70	159.14	138.29	144.61	241.75	59.93	84.05	78.02	62.65
4.90	0.0031997	118.95	173.90	166.65	198.74	160.79	139.72	146.10	244.25	60.55	84.92	78.83	63.30
5.00	0.00323218	120.16	175.66	168.34	200.76	162.42	141.14	147.59	246.73	61.17	85.78	79.63	63.94
5.10	0.00326434	121.35	177.41	170.02	202.75	164.04	142.55	149.06	249.19	61.78	86.63	80.42	64.58
5.20	0.00329619	122.53	179.14	171.68	204.73	165.64	143.94	150.51	251.62	62.38	87.48	81.21	65.21
5.30	0.00332773	123.71	180.86	173.32	206.69	167.22	145.32	151.95	254.03	62.98	88.32	81.98	65.83
5.40	0.00335898	124.87	182.55	174.95	208.63	168.79	146.68	153.38	256.41	63.57	89.14	82.75	66.45
5.50	0.00338994	126.02	184.24	176.56	210.56	170.35	148.03	154.79	258.77	64.15	89.97	83.52	67.06
5.60	0.00342062	127.16	185.90	178.16	212.46	171.89	149.37	156.19	261.12	64.74	90.78	84.27	67.67
5.70	0.00345103	128.29	187.56	179.74	214.35	173.42	150.70	157.58	263.44	65.31	91.59	85.02	68.27
5.80	0.00348117	129.41	189.19	181.31	216.22	174.93	152.02	158.96	265.74	65.88	92.39	85.76	68.87
5.90	0.00351105	130.52	190.82	182.87	218.08	176.43	153.32	160.32	268.02	66.45	93.18	86.50	69.46
6.00	0.00354068	131.62	192.43	184.41	219.92	177.92	154.61	161.67	270.28	67.01	93.97	87.23	70.04
6.10	0.00357006	132.72	194.03	185.94	221.74	179.40	155.90	163.02	272.52	67.56	94.75	87.95	70.62
6.20	0.0035992	133.80	195.61	187.46	223.55	180.86	157.17	164.35	274.75	68.12	95.52	88.67	71.20
6.30	0.00362811	134.87	197.18	188.96	225.35	182.32	158.43	165.67	276.96	68.66	96.29	89.38	71.77
6.40	0.0036568	135.94	198.74	190.46	227.13	183.76	159.69	166.98	279.14	69.21	97.05	90.09	72.34
6.50	0.00368525	137.00	200.29	191.94	228.90	185.19	160.93	168.28	281.32	69.74	97.80	90.79	72.90
6.60	0.00371349	138.05	201.82	193.41	230.65	186.61	162.16	169.57	283.47	70.28	98.55	91.49	73.46
6.70	0.00374152	139.09	203.34	194.87	232.39	188.02	163.39	170.85	285.61	70.81	99.30	92.18	74.02

Delta P in H2O	Vdot=K*sqrt(2*deltap*vspecific)	AS-PL Dimples	AS-PL Toenails	JA Dimples	JA Toenails	JA Bottom pass	LH Dimples	LH Toenails	LH Bottom pass	E-large sausages	F-Small dimples (1st section)	F-Small dimples (2nd section)	G-Large dimples
6.80	0.00376934	140.12	204.86	196.32	234.12	189.41	164.60	172.12	287.74	71.33	100.04	92.86	74.57
6.90	0.00379695	141.15	206.36	197.76	235.84	190.80	165.81	173.38	289.84	71.86	100.77	93.54	75.11
7.00	0.00382437	142.17	207.85	199.19	237.54	192.18	167.00	174.63	291.94	72.38	101.50	94.22	75.66
7.10	0.00385159	143.18	209.33	200.60	239.23	193.55	168.19	175.87	294.01	72.89	102.22	94.89	76.19
7.20	0.00387862	144.19	210.79	202.01	240.91	194.91	169.37	177.11	296.08	73.40	102.94	95.56	76.73
7.30	0.00390546	145.18	212.25	203.41	242.58	196.25	170.54	178.33	298.13	73.91	103.65	96.22	77.26
7.40	0.00393212	146.18	213.70	204.80	244.23	197.59	171.71	179.55	300.16	74.42	104.36	96.87	77.79
7.50	0.0039586	147.16	215.14	206.18	245.88	198.92	172.86	180.76	302.18	74.92	105.06	97.53	78.31
7.60	0.0039849	148.14	216.57	207.55	247.51	200.25	174.01	181.96	304.19	75.41	105.76	98.17	78.83
7.70	0.00401103	149.11	217.99	208.91	249.13	201.56	175.15	183.15	306.19	75.91	106.45	98.82	79.35
7.80	0.00403699	150.07	219.40	210.26	250.74	202.86	176.29	184.34	308.17	76.40	107.14	99.46	79.86
7.90	0.00406279	151.03	220.80	211.60	252.35	204.16	177.41	185.52	310.14	76.89	107.82	100.09	80.37
8.00	0.00408842	151.99	222.20	212.94	253.94	205.45	178.53	186.69	312.09	77.37	108.50	100.72	80.88
8.10	0.0041139	152.93	223.58	214.27	255.52	206.73	179.65	187.85	314.04	77.86	109.18	101.35	81.38
8.20	0.00413921	153.87	224.96	215.58	257.09	208.00	180.75	189.01	315.97	78.33	109.85	101.98	81.88
8.30	0.00416437	154.81	226.32	216.89	258.66	209.27	181.85	190.15	317.89	78.81	110.52	102.60	82.38
8.40	0.00418939	155.74	227.68	218.20	260.21	210.52	182.94	191.30	319.80	79.28	111.18	103.21	82.88
8.50	0.00421425	156.66	229.04	219.49	261.75	211.77	184.03	192.43	321.70	79.75	111.84	103.82	83.37
8.60	0.00423897	157.58	230.38	220.78	263.29	213.01	185.11	193.56	323.59	80.22	112.50	104.43	83.86
8.70	0.00426354	158.50	231.71	222.06	264.82	214.25	186.18	194.68	325.46	80.69	113.15	105.04	84.34
8.80	0.00428797	159.40	233.04	223.33	266.33	215.48	187.25	195.80	327.33	81.15	113.80	105.64	84.83
8.90	0.00431227	160.31	234.36	224.60	267.84	216.70	188.31	196.91	329.18	81.61	114.44	106.24	85.31
9.00	0.00433643	161.21	235.68	225.86	269.34	217.91	189.36	198.01	331.02	82.07	115.09	106.83	85.78
9.10	0.00436045	162.10	236.98	227.11	270.84	219.12	190.41	199.11	332.86	82.52	115.72	107.43	86.26
9.20	0.00438434	162.99	238.28	228.35	272.32	220.32	191.46	200.20	334.68	82.97	116.36	108.02	86.73
9.30	0.00440811	163.87	239.57	229.59	273.80	221.51	192.49	201.28	336.50	83.42	116.99	108.60	87.20
9.40	0.00443174	164.75	240.86	230.82	275.26	222.70	193.53	202.36	338.30	83.87	117.62	109.18	87.67
9.50	0.00445525	165.62	242.13	232.04	276.72	223.88	194.55	203.44	340.10	84.32	118.24	109.76	88.14
9.60	0.00447864	166.49	243.40	233.26	278.18	225.06	195.57	204.50	341.88	84.76	118.86	110.34	88.60
9.70	0.00450191	167.36	244.67	234.47	279.62	226.23	196.59	205.57	343.66	85.20	119.48	110.91	89.06
9.80	0.00452505	168.22	245.93	235.68	281.06	227.39	197.60	206.62	345.42	85.64	120.09	111.48	89.52
9.90	0.00454808	169.07	247.18	236.88	282.49	228.55	198.61	207.68	347.18	86.07	120.70	112.05	89.97
10.00	0.00457099	169.93	248.42	238.07	283.91	229.70	199.61	208.72	348.93	86.51	121.31	112.61	90.43

REFERENCES

[1] Baird R.C., "Pulsation -Induced Vibration in Utility Steam Generation Units" Combustion, Vol. 25 (10), 1954, pp. 38-44

[2] Putman A.A., "Flow-Induced Noise in Heat Exchangers.", Journal of Engineering for Power Vol. 81, 1959, pp. 417-422.

[3] McDonough M. Personal communication.

[4] Blevins R.D., Bressler M.M., "Acoustic Resonance in Heat Exchanger Tube Bundles -Part I: Physical Nature of the Phenomenon", Journal of Pressure Vessel Technology, Vol. 109, Aug. 1987, pp. 275-281

[5] McDonough M.W. "Evaporator Whistle Root Cause Investigation: Plate Acoustic Resonance" Engineering Report, Chrysler Corporation, Dayton Thermal Products Division Feb/23/1995.

[6] Chen Y.N. "Flow-Induced Vibration and Noise in Tube-Bank Heat Exchangers Due to von Karman Streets" Journal of Engineering for Industry, Vol. 90, 1968, pp. 134-146

[7] Bies D.A. , Hansen C.H. "Engineering Noise Control ,theory and practice" 2nd Edition, 1996 pp. 216

[8] Chan C.M.P. , Anderton D. "Correlation between Engine Block Surface Vibration and Radiated Noise of In-Line Diesel Engines", Noise Control Engineering Vol. 2., 1974, No. 1 pp. 16

[9] Takatsubo J., Ohno S., Suzuki T. "Calculation of the Sound Pressure Produced by Structural Vibration Using the Results of Vibration Analysis" Bulletin of the JSME, Vol. 26, 1983, No. 221 pp. 1970-1976

[10] Blevins R.D. , Bressler M.M. "Experiments on Acoustic Resonance in Heat Exchanger Tube Bundles" Journal of Sound and Vibration, Vol. 164 (3), 1993, pp. 503-533.

[11] Blevins R.D., Bressler M.M " Acoustic Resonance in Heat Exchanger Tube Bundles - Part II: Prediction and Suppression of Resonance" Journal of Pressure Vessel Technology, ASME transactions, Vol. 109, Aug. 1987, pp. 282-288.

[12] Blevins R.D. "Acoustic Modes of Heat Exchanger Tube Bundles" Journal of Sound and Vibration, Vol. 109 (1), 1986, pp. 19-31.

[13] Chen Y.N. "Flow Induced Vibration and Noise in Tube-Bank Heat Exchangers Due to von Karman Streets" Journal of engineering for industry, transactions of the ASME, Feb. 1968.

[14] Blevins R.D. "Flow Induced Vibration" Second edition, Krieger publishing company. 1994.

[15] Blevins R.D., Bressler M.M " Acoustic Resonance in Heat Exchanger Tube Bundles - Part I: Physical Nature of the Phenomenon" Journal of Pressure Vessel Technology, ASME transactions, Vol. 109, Aug. 1987, pp. 275-281.

[16] White F.M. "Viscous Fluid Flow" Second Edition, McGraw-Hill company, 1991.

[17] Ziada S. Oengoren A. "Vorticity Shedding and Acoustic Resonance in an In-line Tube Bundle Part I: Vorticity Shedding, and part II: Acoustic resonance" Journal of fluids and Structures 1992, Vol. 6, pp. 271-309.

[18] Ziada S., Oengoren A. and Buhlmann E.T. "On Acoustical Resonance in Tube Arrays Part I: Experiments, Part II: Damping Criteria" Journal of Fluids and Structures 1989, Vol. 3, pp. 293-324.